



# **Development of Biomaterial for 3D Bio-printed Oviduct Model**

A thesis submitted for the award of degree of Master of Biotechnology at Flinders University  
of South Australia

**Hana Alanazi**

Submission: November 2018

Department of Medical Biotechnology College of Medicine and Public Health  
Flinders University, South Australia

**Supervisors:**

Dr. Anton Blencowe from University of South Australia

Assoc. Prof. Fiona Young

### **Declarations**

“I certify that this work does not incorporate without acknowledgment, any material previously submitted for a degree or diploma in any university; and that to the best of my knowledge and belief it does not contain any material previously published or written by another person except where due reference is made in the text. ”

Hana Alanazi

3/ 11/ 2018

## **Acknowledgement**

First, I would like to thank Assoc. Prof. Fiona Young, who suggested this project for me and she always supports me during my study. I also would like to express my sincere gratitude and appreciation to my primary supervisor Dr. Anton Blencowe from University of South Australia, who has been patient and supportive throughout my research. I feel privileged to have you as my supervisor, and his team, Applied Chemistry and Translational Biomaterials (ACTB) group, for their collaboration and synthesising the necessary materials for this research. Also, I want to thank Faruq Ahmed, Postdoctoral Research Associate who help me technically during my lab work. My deepest gratitude also goes to members of Department of Medical Biotechnology Flinders University; Asaduzzaman Mohammad, Figueroa Gonzalez Daniela, Ellen Kambanaros and Arinze Tochukwu Ezeobi for their help during this project. I would like to thank the Saudi Cultural Mission founded by the Saudi Arabia Government for their financial support. Finally, big thanks to my family for their emotional support and love throughout this journey.

## Table of Contents

<b>Abbreviation.....</b>	<b>vii</b>
<b>List of figures.....</b>	<b>viii</b>
<b>List of tables.....</b>	<b>xiii</b>
<b>Abstract.....</b>	<b>xiv</b>
<b>1 Literature review .....</b>	<b>1</b>
1.1 Overview of the larger project .....	1
1.1 Overview of Master’s Research project .....	1
1.2 Oviduct and fertilisation .....	1
1.2.1 Morphological Features of Oviduct .....	2
1.2.2 Differences between Mouse and Human Oviduct .....	3
1.2.3 Oviductal Fluid .....	4
1.3 Two Dimensional (2D) Cell Culture .....	5
1.3.1 Extracellular Matrix .....	6
1.3.2 In Vitro Cell Culture Substrate Preparation .....	7
1.4 Cell viability assays .....	9
1.4.1 Trypan blue exclusion assay .....	9
1.4.2 Tetrazolium reduction assays .....	10
1.4.3 ELISA: .....	11
1.5 3D-BioPrinting .....	12
1.5.1 Matrix in 3D bio-printer:.....	13
1.5.2 Different Matrices in 3D bio-printing .....	14
1.6 Project Aims.....	16
1.7 Hypothesis.....	16
<b>2 Method .....</b>	<b>17</b>
2.1 Cell Culture Reagents .....	17
2.2 Oviduct Disaggregation Reagents.....	17
2.3 Cell Viability Assay Reagents .....	18
2.3.1 Thiazolyl Blue Tetrazolium (MTT) Reagents .....	18
2.3.2 Preparation of Trypan Blue Dye .....	18

2.3.3	Preparation of Tetrazolium (MTS) Reagents:.....	18
2.4	<i>Matrix Preparation</i> .....	18
2.4.1	2%(w/v) Agarose Gel:.....	18
2.4.2	2% (w/v) Carboxylated Agarose Gel:.....	18
2.4.3	Collagen Solution.....	19
2.4.4	Fibronectin Solution.....	19
2.4.5	Matrix Preparation for Encapsulated Cells.....	19
2.5	<i>Cell Line Maintenance and Subculture</i> .....	20
2.6	<i>Cell Viability Assays</i> .....	20
2.6.1	Trypan Blue Exclusion Assay.....	20
2.6.2	MTT and MTS Assay Standard Curves.....	20
2.7	<i>Matrix Interference with MTT Assay</i> .....	22
2.7.1	Matrix Interference with SDS Dissolution of Formazan Crystals in MTT Assay.....	23
2.7.2	Matrix Interference Spectrophotometer Reading of 570 nm OD Readings.....	23
2.8	<i>Matrix Interference with MTS Assay</i> .....	25
2.8.1	Matrix Interference with MTS Includes Dissolution of Formazan Crystals.....	25
2.8.2	Matrix Interference Spectrophotometer Reading of 490 nm OD Readings.....	25
2.9	<i>Matrix Interference with ELISA</i> .....	27
2.10	<i>OVCAR Cell Viability and Behaviour on Matrix Surface After 24-hr and 48-hr Incubation period</i> .....	27
2.11	<i>Viability and Behaviour of Encapsulated OVCAR cells After 48-hr incubation</i> .....	29
2.11.1	ELISA to Measure Progesterone Secreted by Encapsulated OVCAR Cells:.....	29
2.12	<i>Viability and Morphology of Primary-Derived Oviduct Cells After 48hr Encapsulation</i> .....	30
2.12.1	Isolation of Primary-Derived Oviduct Cells:.....	30
2.12.2	Encapsulation of Primary-Derived Oviduct Cells in Matrix:.....	30
2.13	<i>Image analysis</i> .....	31
2.14	<i>Statistical Analysis</i> :.....	31
<b>3</b>	<b>Result</b> .....	<b>32</b>
3.1	<i>Matrix Interference with Different Assays</i> .....	32
3.1.1	Interference of Agarose gel and Carboxylated Agarose gel (CA) with MTT assay.....	33
3.1.2	Interference of Agarose gel and Carboxylated Agarose gel (CA) with MTS assay.....	35
3.1.3	Interference of Agarose gel and Carboxylate Agarose gel (CA) with ELISA assay.....	37
3.2	<i>Effect of different matrices on OVCAR cells viability</i> .....	38
3.3	<i>Encapsulation of OVCAR cells in Carboxylated Agarose gel (CA)</i> .....	41

3.3.1	P4 production by encapsulated OVCAR cells in matrices .....	45
3.4	<i>Encapsulation of Oviduct cells in matrices:</i> .....	45
3.4.1	Disaggregation of Primary-Derived Oviduct Cells.....	45
3.4.2	Encapsulation of Primary-Derived Oviduct Cells in CA ± Adherence Proteins .....	46
<b>4</b>	<b>Discussion</b> .....	<b>49</b>
4.1	<i>Interference of Different Matrices with Different Assays</i> .....	49
4.2	<i>Effect of different matrices on OVCAR cells viability:</i> .....	50
4.3	<i>Encapsulation of OVCAR cells in CA with or without adherence proteins.</i> .....	51
4.4	<i>Encapsulation of primary-derived oviduct cells in matrices:</i> .....	52
4.5	<i>Conclusion:</i> .....	53
4.6	<i>Future work:</i> .....	53

### Abbreviation

RO water	Reverse Osmosis water
RT	Room temperature
3D	Three dimensional
OVCAR cells	Human ovarian carcinoma cells
P <sub>4</sub>	Progesterone
E <sub>2</sub>	Oestrogen
2D	Two dimensional
ECM	Extracellular matrix
FA	Focal adhesion
RGD	arginine–glycine–aspartic acid
OVECs	Oviduct epithelium cells
MTT	3-(4,5-dimethylthiazol-2-yl)-2,5-diphenyltetrazolium bromide
ELISA	enzyme-linked immunosorbent assay
CAD	Computer-aided design
CA	Caroxylatead Agarose
NA	Native Agarose
FBS	Foetal bovine serum
ITS	Insulin-transferrin-selenium
PBS	Phosphate buffered saline
αMEM	Minimum Essential Medium Eagle
DMEM F12	Dulbecco's Modified Eagle's Medium/Nutrient Mixture F-12 Ham
SDS	Sodium dodecyl sulphate
NaCl	Sodium chloride

## List of Figures

FIGURE 1-1 A SCHEMATIC VIEW OF OVIDUCT TO SHOW SPERM-OOCYTE FERTILIZATION (FERRAZ ET AL., 2016).....	2
FIGURE 1-2 MOUSE REPRODUCTIVE SYSTEM (A) A SCHEMATIC DIAGRAM OF DISSECTED OVIDUCT. (B) <i>EX VIVO</i> MOUSE REPRODUCTIVE TRACT(C) UNCOILED MOUSE OVIDUCT (TREUTING ET AL., 2011). .....	2
FIGURE 1-3 EPITHELIAL CELLS OF THE BOVINE OVIDUCT UNDER SCANNING ELECTRON MICROSCOPY. TWO DIFFERENT TYPES OF CELLS WERE IDENTIFIED—THE CILIATED CELLS(CI) AND THE SECRETORY CELLS(SC) (AVILÉS ET AL., 2015).....	3
FIGURE 1-4 SHOWING MORPHOLOGICAL FEATURES OF HUMAN OVIDUCT (COY ET AL., 2012).....	4
FIGURE 1-5 ROLE OF OVIDUCTAL SECRETIONS ON SPERM FUNCTIONS. (+) AND (-) REPRESENT STIMULATORY OR INHIBITORY IMPACTS RESPECTIVELY.....	5
FIGURE 1-6 A SCHEMATIC VIEW SHOWS THE FACTORS THAT INCLUDE IN CELL ADHESION(KHALILI AND AHMAD, 2015).....	7
FIGURE 1-7 THE DIFFERENCE OF CELLS GROWING IN 2D AND 3D ENVIRONMENT .....	9
FIGURE 1-8 PRINCIPAL OF MTT ASSAY, REACTION IN MITOCHONDRIA, REACTION OF MTT CHANGE INTO FORMAZAN (46). .....	11
FIGURE 1-9 THE MAIN PRINCIPLE OF ELISA ASSAY .....	12
FIGURE 2-1 A 96-WELL PLATE LAYOUT FOR MTT AND MTS ASSAY STANDARD CURVE .....	21
FIGURE 2-2 MTS(A) AND MTT(B) STANDARD CURVES FOR OVCAR CELLS. OVCAR CELLS WERE INCUBATED FOR 24H TO ALLOW CELL ADHERENCE IN A 96-WELL PLATE. AFTER INCUBATION TIME MTT OR MTS WAS APPLIED AS DESCRIBED IN (MTT, 2.6.3 SECTION; MTS, 2.6.4 SECTION). MEAN ± STANDARD DEVIATION OF OPTICAL DENSITY FOR 6 REPLICATE WELLS/EXPERIMENT (N=3) SHOWN. ....	22
FIGURE 2-3 A 96-WELL PLATE LAYOUT FOR MATRICES INTERFERENCE WITH MTT/MTS ASSAY. ....	23
FIGURE 2-4 A SCHEME OF MTT ASSAY TO EXPLAIN AT WHICH STAGE THE MATRIX WAS ADDED .....	24
FIGURE 2-5 A SCHEME OF MTS ASSAY TO EXPLAIN AT WHICH STAGE THE MATRIX WAS ADDED. ....	26
FIGURE 2-6 A 96-WELL PLATE LAYOUT FOR 2% AGAROSE GEL (PLATE 1) 2% CARBOXYLATED AGAROSE GEL (PLATE 2) COATING WITH DIFFERENT PROTEINS. ....	28
FIGURE 2-7 OVCAR CELLS WERE INCUBATED ON DIFFERENT SURFACE SUBSTRATES WITH/WITHOUT ADHESION PROTEIN.....	28
FIGURE 2-8 A 96-WELL PLATE LAYOUT FOR 2% CA GEL WITH OR WITHOUT ADHESION PROTEINS MIXED WITH OVCAR CELLS.....	29
FIGURE 2-9 A 96-WELL PLATE LAYOUT FOR 2% CARBOXYLATED AGAROSE GEL WITH OR WITHOUT ADHESION PROTEINS MIXED WITH OVIDUCT CELLS.....	30
FIGURE 3-1 A SCHEME OF MTT AND MTS ASSAYS PROCEDURE TO SHOW AT WHICH STAGE THE MATRIX WAS ADDED IN THE INTERFERENCE INVESTIGATION. (A) INTERFERENCE OF MATRICES	



WITHOUT CELLS WITH MTT OR MTS ASSAY (B) INTERFERENCE OF MATRICES WITH MTT ASSAY IN TWO STEPS (C) INTERFERENCE OF MATRICES WITH MTS ASSAY IN TWO STEPS. .... 32

FIGURE 3-2 INTERFERENCE OF MATRICES WITHOUT CELLS WITH MTT ASSAY. AGAROSE GEL AND CA GEL (50 mL) WERE PLATED IN 96-WELL PLATE AND SOLIDIFIED WITHIN 2H. COMPLETE RPMI MEDIA (100 mL) WAS ADDED ON TOP OF MATRICES, MEDIA ONLY (150 mL) WAS USED AS A NEGATIVE CONTROL. MTT WAS APPLIED AFTER 2 HRS OF INCUBATING THE MEDIA WITH MATRICES. THE EXPERIMENT WAS REPEATED IN THREE SEPARATE OCCASIONS (N=3). MEAN ± STANDARD DEVIATION ARE SHOWN. ANALYSING DATA WAS DONE BY A ONE-WAY ANOVA WITH THE TUKEY-KRAMER POST-HOST TEST. THE SIGNIFICANT DIFFERENCE WAS ASSIGNED ATP < 0.0001(\*\*\*) AND NO SIGN AT NO SIGNIFICANCE DIFFERENCE (P > 0.05). .... 33

FIGURE 3-3 INTERFERENCE OF MATRICES WITH DISSOLVING FORMAZAN CRYSTALS IN MTT ASSAY. A 96-WELL PLATE WAS SEEDED WITH 20 ×10<sup>3</sup>/WELL OF OVCAR CELLS AND INCUBATED FOR 24 HRS AT 37 °C AND 5 % CO<sub>2</sub> TO ALLOW CELL ADHERENCE. MTT WAS ADDED FOR 24H INCUBATION, THEN SDS SOLUTION WAS ADDED TO DISSOLVE FORMAZAN CRYSTALS AND PRODUCE PURPLE COLOUR. MATRICES (AGAROSE GEL AND CA GEL; 50 mL) WERE ADDED IN THE SAME TIME AS SDS SOLUTION. THE EXPERIMENT WAS REPLICATED ON THREE SEPARATE OCCASIONS (N=3). MEAN ± STANDARD DEVIATION ARE SHOWN. A ONE-WAY ANOVA WITH THE TUKEY-KRAMER POST-HOST TEST WAS USED TO ANALYSE DATA. NO SIGN INDICATES NO SIGNIFICANT DIFFERENCE (P > 0.05). .... 34

FIGURE 3-4 INTERFERENCE OF MATRICES WITH SPECTROPHOTOMETER READING (AT 570 NM). A 96-WELL PLATE WAS SEEDED WITH 20 ×10<sup>3</sup>/WELL OF OVCAR CELLS AND INCUBATED FOR 24H AT 37 °C AND 5 % CO<sub>2</sub> TO ALLOW CELL ADHERENCE. MTT ASSAY WAS APPLIED AND DIRECTLY BEFORE READING, MATRICES (AGAROSE GEL AND CA GEL; 50 mL) WERE ADDED. THE EXPERIMENT WAS REPLICATED ON THREE SEPARATE OCCASIONS (N=3). MEAN ± STANDARD DEVIATION ARE PRESENTED. DATA WAS ANALYSED USING A ONE-WAY ANOVA WITH THE TUKEY-KRAMER POST-HOST TEST. NO SIGN AT NO SIGNIFICANCE DIFFERENCE (P > 0.05)..... 34

FIGURE 3-5 INTERFERENCE OF MATRICES WITHOUT CELLS WITH MTS ASSAY. AGAROSE GEL AND CA GEL (50 mL ) WERE PLATED IN 96-WELL PLATE AND SOLIDIFIED WITHIN 2H COMPLETE RPMI MEDIA (100 mL) WAS ADDED ON TOP OF MATRICES, MEDIA ONLY (150 mL) WAS USED AS A NEGATIVE CONTROL. MTS WAS APPLIED AFTER 2 HRS OF INCUBATING THE MEDIA WITH MATRICES. THE EXPERIMENT WAS REPLICATED ON THREE SEPARATE OCCASIONS (N=3). MEAN ± STANDARD DEVIATION ARE PRESENTED. DATA WAS ANALYSED USING A ONE-WAY ANOVA WITH THE TUKEY-KRAMER POST-HOST TEST. THE SIGNIFICANT DIFFERENCE WAS ASSIGNED AT P < 0.0001(\*\*\*)..... 35

FIGURE 3-6 INTERFERENCE OF MATRICES WITH MTS INCLUDES DISSOLUTION OF FORMAZAN CRYSTALS. A 96-WELL PLATE WAS SEEDED WITH 20 ×10<sup>3</sup> CELLS/WELL OF OVCAR CELLS AND INCUBATED FOR 24H AT 37 °C AND 5 % CO<sub>2</sub> TO ALLOW CELL ADHERENCE. MTS REAGENT (30

mL) WAS ADDED TO THE WELLS AND IN THE SAME TIME MATRICES (AGAROSE GEL AND CA GEL; 50 mL) WERE ADDED. READINGS WERE OBTAINED AFTER 2H. MEAN ± STANDARD DEVIATION OF THREE SEPARATED EXPERIMENTAL REPLICATIONS (N=3) ARE PRESENTED. A ONE-WAY ANOVA WITH THE TUKEY-KRAMER POST-HOST TEST WAS USED TO ANALYSE DATA. THERE WAS NO SIGNIFICANT DIFFERENCE ( P > 0.05) IN OD OF AGAROSE GEL AND CA GEL COMPARED TO NEGATIVE CONTROL (20 ×10<sup>3</sup>/WELL OF OVCAR CELLS WITH RPMI MEDIA ONLY)..... 36

FIGURE 3-7 INTERFERENCE OF MATRICES WITH SPECTROPHOTOMETER READING (AT 490 NM). A 96-WELL PLATE WAS SEEDED WITH 20 ×10<sup>3</sup>/WELL OF OVCAR CELLS AND INCUBATED FOR 24H AT 37 °C AND 5 % CO<sub>2</sub> TO ALLOW CELL ADHERENCE. MTS ASSAY WAS APPLIED AND DIRECT BEFORE READING, MATRICES (AGAROSE GEL AND CA GEL; 50 mL) WERE ADDED. MEAN ± STANDARD DEVIATION OF THREE SEPARATED EXPERIMENTAL REPLICATIONS (N=3) ARE REPRESENT. A ONE-WAY ANOVA WITH THE TUKEY-KRAMER POST-HOST TEST WAS USED TO ANALYSE DATA. THE SIGNIFICANT DIFFERENCE WAS ASSIGNED AT P < 0.0001(\*\*\*)..... 36

FIGURE 3-8 MATRICES INTERFERENCE WITH P<sub>4</sub> ELISA ASSAY. TRIPPLICATE WELLS OF A 96 WELL PLATE WAS COATED WITH 50 µL MATRICES; RPMI MEDIA (CONTROL), AGAROSE AND CA AND WAS INCUBATED WITH 100 µL MEDIA AND CONDITIONED MEDIA WAS COLLECTED AFTER 24, 48 AND 72 HOURS. PROGESTERONE IN THE CONDITIONED MEDIA WAS ASSESSED IN A COMPETITIVE PROGESTERONE EIA IN WHICH PROGESTERONE CONCENTRATION (PG/M<sub>L</sub>) WAS CALCULATED BY COMPARING WITH A STANDARD CARVE (R<sup>2</sup>=0.97). MEAN±SD OF THREE REPLICATE EXPERIMENTS SHOWN. DATA WERE SUBJECTED TO TWO-WAY ANOVA WITH BONFERRONI POST-TEST, P>0.05 COMPARED TO CONTROL (MEDIA) AT SAME INCUBATION TIME. .... 37

FIGURE 3-9 COMPARISON OF THE EFFECT OF DIFFERENT MATRICES WITH OR WITHOUT ADHERENCE PROTEINS ON OVCAR CELLS AFTER 24 AND 48H. CELL VIABILITY WAS ASSESSED BY MTT ASSAY, IN WHICH CELL NUMBER WAS OBTAINED BY USING MTT STANDARD CURVE AND THE MATRICES INTERFERENCE WAS REMOVED BY SUBTRACTING OD OF MATRICES ONLY. THE EXPERIMENT WAS REPLICATED ON THREE SEPARATE OCCASIONS (N=3). MEAN ± STANDARD DEVIATION ARE PRESENTED. DATA WAS ANALYSED USING A ONE-WAY ANOVA WITH THE TUKEY-KRAMER POST-HOST TEST. THE SIGNIFICANT DIFFERENCE WAS ASSIGNED AT P < 0.0001(\*\*\*) COMPARED TO POSITIVE CONTROL AT THE SAME INCUBATION PERIOD..... 39

FIGURE 3-10 COMPARISON OF THE EFFECT OF DIFFERENT MATRICES WITH/WITHOUT ADHERENCE PROTEINS ON OVCAR CELLS AFTER 24 AND 48H. CELL VIABILITY WAS ASSESSED BY MTS ASSAY, IN WHICH CELL NUMBER WAS OBTAINED BY USING MTS STANDARD CURVE THE MATRICES INTERFERENCE WAS REMOVED BY SUBTRACTING OD OF MATRICES ONLY. THE EXPERIMENT WAS REPLICATED ON THREE SEPARATE OCCASIONS (N=3). MEAN ± STANDARD DEVIATION ARE PRESENTED. DATA WAS ANALYSED USING A ONE-WAY ANOVA WITH THE TUKEY-KRAMER POST-HOST TEST. THE SIGNIFICANT DIFFERENCE WAS ASSIGNED AT P < 0.0001(\*\*\*) COMPARED TO POSITIVE CONTROL AT THE SAME INCUBATION PERIOD..... 39

FIGURE 3-11 MORPHOLOGY OF OVCAR CELLS ATTACHED TO SURFACE OF DIFFERENT MATRICES WITH/WITHOUT ADHERENCE PROTEINS. OVCAR CELLS ( $20 \times 10^3$ ) WERE CULTURED ON 96-WELL PLATE OR MATRIX-COATED 96-WELL PLATE FOR 24 AND 48 HRS AT 37 °C AND 5 % CO<sub>2</sub> (A) WITHOUT MATRIX AS A POSITIVE CONTROL, (B) CA, (C) CA+5% COLLAGEN, (D) CA+10MG/ML FIBRONECTIN, AND (E) WELL CONTAINING AGAROSE AND UNATTACHED CELLS, (F) WELL CONTAINING AGAROSE AFTER ASPIRATION OF UNATTACHED CELLS. IMAGES WERE TAKEN USING A LIGHT MICROSCOPE. REPRESENTED IS ONE OF N=3 EXPERIMENTS AT EACH TIME POINT. SCALE BAR =100 MM. .... 40

FIGURE 3-12 VIABILITY OF CA ENCAPSULATED OVCAR CELL COMBINED WITH ADHERENCE PROTEINS. OVCAR CELLS ( $25 \times 10^3$ ) WERE ENCAPSULATED IN CA WITH/WITHOUT ADHERENCE PROTEINS FOR 48 H AT 37 °C AND 5 % CO<sub>2</sub>. CELL VIABILITY WAS ASSESSED BY MTS ASSAY, IN WHICH CELL NUMBER WAS OBTAINED BY USING MTS STANDARD CURVE. THE EXPERIMENT WAS REPEATED THREE TIME SEPARATELY (N=3). MEAN ± STANDARD DEVIATION ARE SHOWN. A ONE-WAY ANOVA WITH THE TUKEY-KRAMER POST-HOST TEST WAS USED TO ANALYSE THE DATA. THE SIGNIFICANT DIFFERENCE WAS ASSIGNED AT  $P \leq 0.05$  (\*)  $P \leq 0.01$  (\*\*) AND  $P < 0.0001$  (\*\*\*)... 42

FIGURE 3-13 OVCAR CELL MORPHOLOGY AFTER ENCAPSULATION IN CA MATRIX WITH OR WITHOUT ADHERENCE PROTEINS. OVCAR CELLS ( $25 \times 10^3$ ) WERE ENCAPSULATED IN (B) CA ONLY, (C) CA+ 5%COLLAGEN, (D) CA+10MG/ML FIBRONECTIN (E) CA+ 5% COLLAGEN AND 10MG/ML FIBRONECTIN AND (A) POSITIVE CONTROL (CULTURED IN 96-WELL PLATE) FOR 48H AT 37 °C AND 5 % CO<sub>2</sub>. IMAGES WERE TAKEN USING A LIGHT MICROSCOPE AT 24H AND 48H. REPRESENTED IS ONE OF EXPERIMENTS (N=3) AT EACH TIME POINT. SCALE BAR =100 MM. BLUE ARROW= FLATTENED CELLS, BLACK ARROW= ROUND CELLS. .... 44

FIGURE 3-14 PROGESTERONE (P<sub>4</sub>) PRODUCED BY ENCAPSULATED OVCAR CELLS. OVCAR CELLS ( $25 \times 10^3$ ) WERE ENCAPSULATED IN CA WITH/WITHOUT ADHERENCE PROTEINS FOR 48H AT 37 °C AND 5 % CO<sub>2</sub>. CONDITIONED MEDIA FROM THREE SEPARATE EXPERIMENTS (N=3) WERE THEN SUBJECTED TO ELISA TO MEASURE PROGESTERONE PRODUCTION PER 10,000 OVCAR CELLS. THE MEAN ± STANDARD DEVIATION ARE PRESENTED AND ONE-WAY ANOVA WITH THE TUKEY-KRAMER POST-HOST TEST WAS APPLIED..... 45

FIGURE 3-15 DISSECTED OVIDUCTS. PHOTO WAS TAKEN DIRECTLY AFTER DISSECTING OVIDUCT FROM FEMALE MOUSE. REPRESENTATIVE OF THREE SEPARATE EXPERIMENTS (N=3). SCALE BAR = 1.5 MM. .... 46

FIGURE 3-16 CELL VIABILITY OF PRIMARY-DERIVED OVIDUCT CELLS ENCAPSULATED IN DIFFERENT MATRICES. PRIMARY-DERIVED OVIDUCT CELLS ( $10 \times 10^3$ ) WERE ENCAPSULATED IN CA WITH/WITHOUT ADHERENCE PROTEINS FOR 48H AT 37 °C AND 5 % CO<sub>2</sub> BEFORE APPLYING AN MTS ASSAY. A ONE-WAY ANOVA WITH THE TUKEY-KRAMER POST-HOST TEST WAS USED TO ANALYSE THE DATA. MEAN ± SD ARE SHOWN (N=3);  $P < 0.0001$  (\*\*\*) COMPARED WITH POSITIVE CONTROL. .... 47

FIGURE 3-17 MORPHOLOGICAL FEATURES OF PRIMARY-DERIVED OVIDUCT CELLS ENCAPSULATED IN CA MATRIX WITH OR WITHOUT ADHERENCE PROTEINS. OVCAR CELLS ( $25 \times 10^3$ ) WERE ENCAPSULATED IN (A) POSITIVE CONTROL (NO MATRIX WELL), (B) CA ONLY AND (C) CA+ 5% COLLAGEN AND 10MG/ML FIBRONECTIN FOR 48 HRS AT 37 °C AND 5 % CO<sub>2</sub>. IMAGES WERE TAKEN USING A LIGHT MICROSCOPE AT 3 AND 48H. REPRESENTED IS ONE OF THE EXPERIMENTS (N=3). SCALE BAR IS WRITTEN ON THE FIGURES. BLACK ARROW= CILIATED CELLS, BLUE ARROW= ROUND CELLS. .... 48

FIGURE 4-1 SCANNING ELECTRON MICROGRAPH OF SPERM BOUND TO CILIA ON THE EPITHELIUM OF THE OVIDUCTAL ISTHMUS.(BAR = 10 MM; (LEFEBVRE ET AL., 1997))..... 56

FIGURE 4-2 SCHEMATIC VIEW OF THE OVIDUCT AND SPERM JOURNEY INSIDE IT. .... 57

FIGURE 4-3 PASSIVE *IN VITRO* CELL ADHESION STAGES (KHALILI AND AHMAD, 2015). .... 60

## List of Tables

TABLE 3-1 NUMBERS OF VIABLE CELLS DETERMINED BY IMAGE ANALYSIS, MTT ASSAY AND MTS ASSAY. AFTER 24H AND 48H INCUBATION PERIOD AT 37 °C AND 5 % CO <sub>2</sub> , AN IMAGEJ SOFTWARE WAS USED TO COUNT THE NUMBER OF CELLS IN 4 PHOTOS/WELL, THEN ADJUSTED TO INDICATE THE TOTAL NUMBER OF CELLS IN THE WELL. MTT AND MTS ASSAY WERE APPLIED AFTER 24H AND 48H SEPARATELY. MEAN ± STANDARD DEVIATION ARE SHOWN. THE EXPERIMENT WAS REPEATED ON THREE SEPARATE OCCASIONS (N=3). DATA WAS ANALYSED USING A ONE-WAY ANOVA WITH THE TUKEY-KRAMER POST-HOST TEST. THERE WAS NO SIGNIFICANCE DIFFERENCE BETWEEN CELL NUMBERS OBTAINED BY IMAGE ANALYSIS, MTT AND MTS ASSAY AT 24 AND 48H FOR EACH SUBSTRATE TYPE ( P > 0.05). .....	41
TABLE 3-2 COMPARISON BETWEEN THE PERCENTAGE OF DIFFERENT CELLS ENCAPSULATED IN CA+ ADHERENCE PROTEINS BASED ON MORPHOLOGY FEATURES. OVCAR CELLS (25 ×10 <sup>3</sup> ) ENCAPSULATED IN CA+5% COLLAGEN AND 10µg/ML FIBRONECTIN FOR 48 HRS AT 37 °C AND 5 %. PERCENTAGE OF DIFFERENT CELL MORPHOLOGY WAS CALCULATED RELATIVELY TO THE TOTAL CELLS IN ONE FIGURE WHICH WERE COUNTED MANUALLY BY USING IMAGEJ. THIS DATA WAS OBTAINED FROM THE SAME EXPERIMENTS THAT DONE IN PREVIOUS FIGURES (N=3). THE MEAN ± STANDARD DEVIATION ARE SHOWN (6 FIGURES/ EXPERIMENT). .....	42
TABLE 3-3 OVIDUCT CELLS YIELD. OVIDUCTS FROM 2 MICE/ EXPERIMENT; N=6 ANIMALS WERE DISAGGREGATED BY 1% COLLAGENASE TYPE 1. TRY PAN BLUE ASSAY WAS UTILISED TO OBTAIN CELL YIELD FOR EACH OVIDUCT.....	46

## Abstract

There is a continued need, particularly in developing countries, for safe, reliable and cheap contraceptives. Development of new contraceptives is very expensive and time consuming, and requires extensive animal testing. *In vitro* models offer a potential alternative for the early stage high-throughput screening of contraceptive candidates. The introduction of 3D bioprinting has provided a platform for the rapid manufacture of such models, however, there is still much research that needs to be conducted to identify suitable matrices that can be printed and provided an optimal environment for cells and tissues. Therefore, the aim of this study was to identify hydrogel matrices that could be used for 3D bioprinting and support the viability and function of primary-derived oviduct cells harvested from mouse oviducts. The matrices chosen for this study were agarose and carboxylated agarose (CA) hydrogels, as these gels are compatible with extrusion printing, have a high water content like the natural extracellular matrix, and are considered bioinert. Whilst this latter characteristic makes the gels cytocompatible, it also limits protein adhesion which can lead to poor cell attachment. Therefore, the gels were combined with varying amounts of the adherence proteins collagen and fibronectin to assess the effect of these biofactors on cell adhesion, viability and function when in contact with the gel surface and when encapsulated within the gel. The cytotoxicity of the candidate matrices, and their ability to support oviduct cell viability and proliferation, were initially examined using human ovarian carcinoma (OVCAR) cell lines. OVCAR cells were cultured on the surface of these gels to test their viability and ability to attach on the candidate gel surface. Whereas CA gels with or without adherence proteins supported OVCAR cell attachment and viability, no attachment was noted for any of the agarose-based gels. Subsequently, OVCAR cells were encapsulated inside the CA gels. For CA, CA+collagen and CA+fibronectin gels there was a statistically significant decrease in cell viability to ~70-80 % compared to the controls. However, CA+collagen+fibronectin gels supported OVCAR cells with > 80% viability and evidence of cell attachment. Interestingly, all CA-based gels supported the production of progesterone (P<sub>4</sub>) from the encapsulated OVCAR gels. The optimised CA+collagen+fibronectin gel was then used to successfully encapsulate primary-derived oviduct cells, which remained viable after 48 h and displayed morphological characteristics. Whilst these results suggest that CA+collagen+fibronectin gels may be promising candidates for use in a 3D bioprinted oviduct model, further work is required to identify the individual cells types present in the mixed cell population disaggregated from murine oviduct and to assess the encapsulated primary-derived oviduct cells functionality.

# 1 Literature review

## 1.1 Overview of the larger project

Ways to limit experience of the global population include the provision of safe contraceptive methods (world health organization, 2018). Since 2000, the Bill and Melinda Gates Foundation has focused on enhancing healthcare and reducing extreme poverty globally (Bill & Melinda Gates Foundation, 2018, conserve energy future, 2018). They recognised that the need for a research model that allows the development and testing of effective contraceptives quickly and efficiently. The foundation funded a project to three dimensional (3D) Bio-print a model of the oviduct (fallopian tube) that facilitates sperm capacitation; a physiological process that sperm has to complete before it is able to fertilise an egg (Okabe, 2018). In the future, this *in vitro* model will be used to test the ability of different molecules to prevent sperm capacitation. Molecules with anti-capacitation activity may be developed into new contraceptives. This 9-month Master's research project will contribute to the main project.

## 1.1 Overview of Master's Research project

The main objective of this 9 month Master research project is to identify matrices with the potential to be used for 3D Bioprinting and which maintain the viability and morphology of primary-derived cells harvested from mouse oviducts. The cytotoxicity of candidate matrices will initially be examined using human ovarian carcinoma (OVCAR) transformed cell lines to optimise and identify the 'best' matrix which will then be tested with primary-derived oviduct cells.

## 1.2 Oviduct and fertilisation

The ability of sperm to fertilise an oocyte can only be realised after passage through the oviduct tract (**Figure 1-1**) during which the sperm undergo a process of capacitation (De Jonge, 2005, Suarez, 2016) (Okabe, 2018); sperm capacitation is described in appendix. 2). The site of fertilisation in the oviduct is the ampulla (**Figure 1-1**). To arrive at the ampulla, the sperm travels through the isthmus where capacitation occurs. The infundibulum portion of the oviduct facilitates the movement of the oocyte to the ampulla, where it is fertilised by the capacitated sperm (Besenfelder et al., 2012). *In vitro* culture of sperm in the presence of oviductal cells has shown improvements in cell motility and survival, which indicates the significance of interactions with the oviduct environment to sperm fertilisation capacity (De Jonge, 2005).

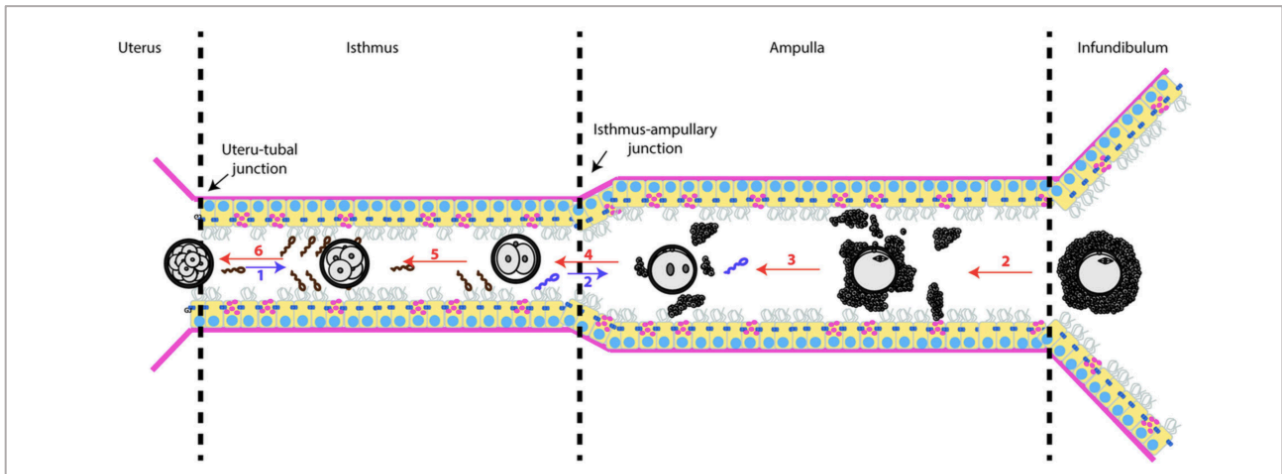


Figure 1-1 A schematic view of oviduct to show sperm-oocyte fertilization (Ferraz et al., 2016).

### 1.2.1 Morphological Features of Oviduct

The oviduct plays a critical role in sperm capacitation, fertilization and early embryonic growth. Structurally, the oviduct has four sections including utero-tubal junction, isthmus, ampulla and infundibulum as shown in Figure 1-2 (Dirksen, 1974). The junction that connects uterus and oviduct is termed as utero-tubal junction (Treuting et al., 2011). The blood supply to the oviduct derives from branches of the ovarian and uterine arteries (Leese, 1988).

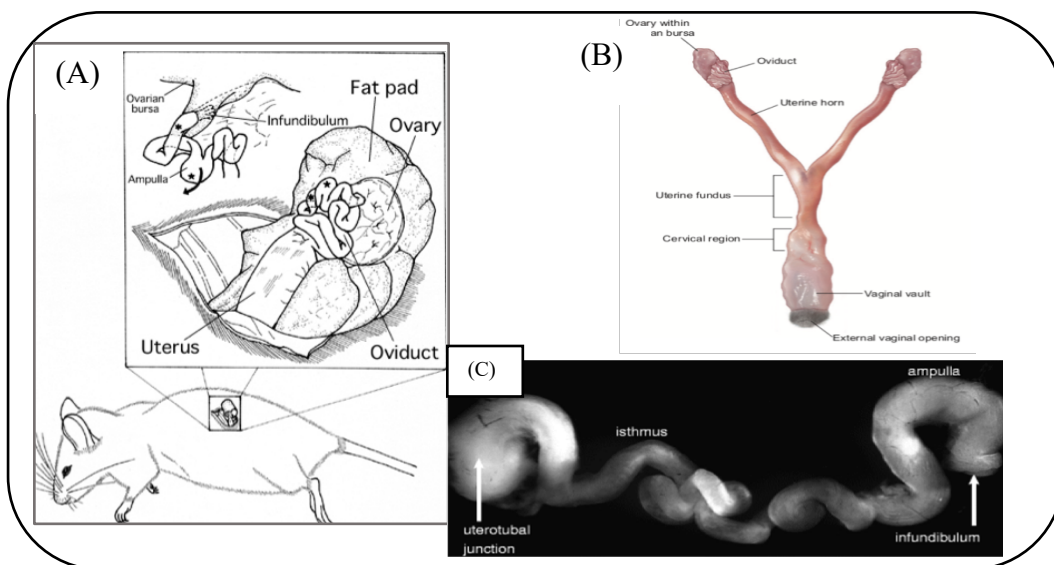


Figure 1-2 Mouse reproductive system (A) a schematic diagram of dissected oviduct. (B) *Ex vivo* mouse reproductive tract (C) Uncoiled mouse oviduct (Treuting et al., 2011).



The oviduct is comprised of a single layer of epithelial cells with a columnar shape. There are two kinds of epithelial cells in the oviduct, surface ciliated and interspersed non-ciliated cells (**Figure 1-3**). The ciliated cells present in the oviduct act to transport gametes, whereas the non-ciliated cells have a secretory function (Abe and Oikawa, 1991). Ciliated and secretory cell function is regulated by hormones Progesterone (P4) and Oestrogen (E2), which maintain ciliary beat frequency to facilitate the movement of fluid in the oviduct (Li and Winuthayanon, 2017). The oviduct cells are closely packed together and epithelial cells are connected by tight junctions (Nielsen et al., 2012).

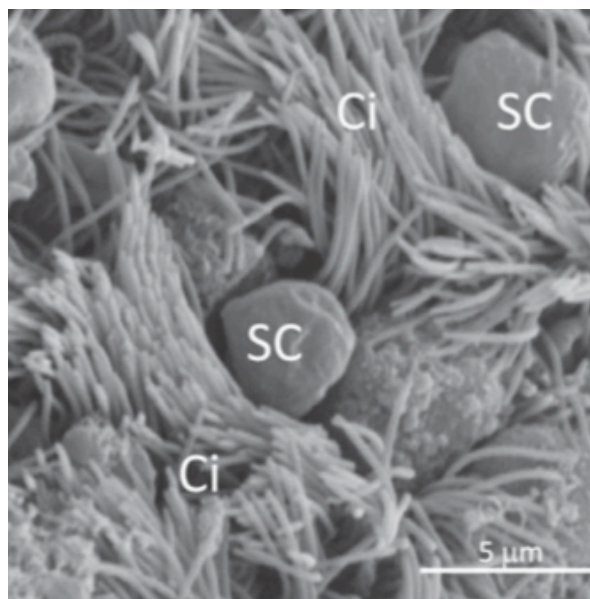


Figure 1-3 Epithelial cells of the bovine oviduct under scanning electron microscopy. Two different types of cells were identified—the ciliated cells(Ci) and the secretory cells(SC) (Avilés et al., 2015).

The infundibulum, or fimbria in humans contains a large proportion of ciliated cells, as does the adjoining ampulla (Dirksen, 1974). As well as regulating oviduct fluid movement, the ciliated cells also facilitate movement of the oocyte to the site of fertilisation in the ampulla. The isthmus ,however, contains a majority of secretory cells that produce fluid to support sperm capacitation transit through the oviduct to meet the oocyte (Li and Winuthayanon, 2017). The role that oviduct plays in sperm capacitation is described in appendix. 3.

### 1.2.2 Differences between Mouse and Human Oviduct

Difficulties in obtaining human oviduct tissues have led to the use of animal models to study the structure and function of the oviduct. Although there are variations in morphologic appearance of the oviduct, which are the result of different hormonal influences during the

oestrus cycle in mice, and the menstrual cycle in humans, the mouse oviduct has a length of 1.8cm and is a tightly coiled tube, while the human oviduct is larger at 12cm long, with a less tightly coiled structure(see **Figure 1-2 and 1-4** ) (Li and Winuthayanon, 2017). Despite these dissimilarities in oviduct morphology, both humans and mice feature an oviduct with three distinct segments. The primary difference in oviduct segmentations is that in humans the ampulla possesses a fimbriated end that opens to the peritoneal cavity adjacent to the ovary, while in mice it opens into the periovarian space. Both mouse and human oviducts have densely ciliated infundibulum and ampulla regions, and this prevalence of ciliated cells decreases in the tract toward the uterus. The ampulla and infundibulum mucosa in both species are comprised of tall columnar epithelium with motile cilia, while the isthmus features low pseudostratified columnar cells with variable quantities of cilia (Treuting et al., 2011).

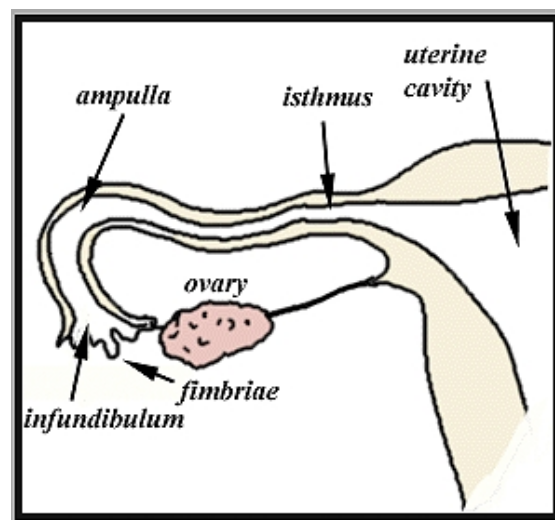


Figure 1-4 Showing morphological features of human oviduct (Coy et al., 2012).

### 1.2.3 Oviductal Fluid

Secretory cells of the oviduct are responsible for the generation of fluid in the tube (Abe and Oikawa, 1991). Bishop's (1956) investigations into oviductal fluid composition under various hormonal states characterised the complex mixture as a combination of plasma-derived components and specific proteins supplied by the oviduct epithelium (Leese, 1988). Electrolytes and ions from calcium potassium, sodium and chloride feature in the oviductal fluid, as well as bicarbonate that is thought to maintain pH in the range of 7.1-8.0, with fluctuations during phases of the reproductive cycle. By far, water is the largest constituent of oviductal fluid, which is transported thorough changes in osmotic gradients due to the

movement of ions. Oviductal fluid also contains the non-electrolytes such as glucose, pyruvate, lactate and amino acids, which are present to support gamete and embryo metabolism. The plasma components of the oviductal fluid are protein macromolecules albumin and immunoglobulin G (Leese, 1988). Also present is the oviduct-secreted protein (OSP) that has a role in enhancing sperm binding and penetration of oocytes. There is a growing body of research into the identification and characterisation of OSPs and the mechanisms of their interactions with gametes (**Figure 1-5**). Additionally, there are other factors present in the oviduct microenvironment including regulatory molecules such as protease inhibitors, growth factors, cytokines, binding proteins and enzymes (Buhi et al., 2000).

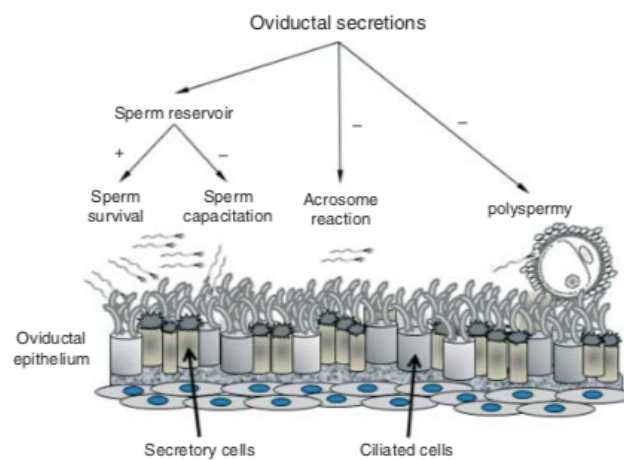


Figure 1-5 Role of oviductal secretions on sperm functions. (+) and (-) represent stimulatory or inhibitory impacts respectively.

### 1.3 Two Dimensional (2D) Cell Culture

Cell culture is defined as process during which cells are removed from an *in vivo* environment and seeded into an artificial environment *in vitro* (Cooke et al., 2008). Optimisation of the culture environment is essential to enable cells to grow *in vitro* and variables include growth media and culture substrate. The nature of the cell culture surface has an important role in cell attachment, proliferation, and function. Extracellular matrix (ECM) components are often used to coat culture surfaces to enhance cell attachment *in vitro*. Indeed, each cell type needs components that more accurately mimic their native environment (Cooke et al., 2008). Monolayer cultivation, a 2D cell culture method of cells that is applied widely in biomedicine requires an artificial substrate that is correctly charged and treated, to facilitate

cell adhesion and proliferation. Appropriateness of the substrate is critical as poor adhesion and overcrowding inhibit cell proliferation (Khoruzhenko, 2011). Most mammalian cells need to be adherent to suitable surfaces which can mediate anchorage-dependent viability and function, and the absence of this element often causes cell death (Jammalamadaka and Tappa, 2018). Common substrate materials used in two-dimensional cell culture are polystyrene or polyvinylchloride. As synthesized, polystyrene is hydrophobic and is unable to provide appropriate surface for attachment of cells. Therefore, the tissue culture plastics are treated by electrical discharge, or gamma irradiation to make wettable active surface. An alternative to the use of these single-use plastics is glass but this is expensive (Freshney, 2010).

Cells *in vivo* are imbedded in the ECM which works as a supporting scaffold for the living cells and guides cellular architecture at the tissue level. ECM organization is complicated and varies between tissues within a living organism, so it is not easy to be mimicked *in vitro*. However, understanding how the cell adheres to the ECM *in vivo* helps to build the knowledge to improve cell culture, either 2D or 3D, in term of cell adherence and migration within different scaffolds (Even-Ram and Yamada, 2005).

### **1.3.1 Extracellular Matrix**

Cell matrix adhesion causes cells to impart intracellular or extracellular forces at the localized sites of extracellular framework. These sites are mediated by integrin which acts as an adhesion anchor between cells or matrix (**Figure 1-6**). The integrins and adhesion cells links the extracellular matrix to the actin filaments of the cytoskeleton by the process of focal adhesion (FA) (cell adhesion process *in vitro* are described in appendix. 4). ECM enhances cells-to-cell communication, cell adhesion and differentiation. It also contains a mixture of growth factors, polysaccharide and proteins such as collagen, fibronectin, elastin and laminin. Cell shape is strongly connected to the role of the cell in the body, and is consequently determined by ECM mechanics and components (Li and Kilian, 2015). Collagen is a triple-helical protein that functions as the major constituent of the ECM of almost all tissues, constituting over 30% of the total proteins of which the majority percentage is for Collagen type I (Theocharis et al., 2016). Gelatin is obtained by the partial hydrolysis of collagen. The use of both collagen and gelatin in cell culture has increased recently. Within one type of tissue, a heterogeneous mix of different types of collagen fibers are generally produced with predomination of one type of collagen (Frantz et al., 2010). The fibronectin found in the ECM is a large glycoprotein that can be present in two forms; as plasma fibronectin and cellular fibronectin (Hynes, 1990). Fibronectin

is composed of two approximately 250 kDa subunits and is ubiquitously found in ECM. It has been implicated in many essential cell processes including adhesion and migration (**Figure 1-6**). Fibronectin is a very large molecule which explains the impact of its conformation on its biological functions (Zollinger and Smith, 2017). The Fibronectin sequence contains an arginine–glycine–aspartic acid (RGD) cell binding motif which promotes efficient cell adhesion (Tasiopoulos et al., 2018). Cell adhesion to ECM provides tissue architecture and is responsible for most of the biological processes by triggering signals between cells. The cell adhesion to ECM components is primarily facilitated by integrin receptors. Integrins are transmembrane linkers between the extracellular matrix proteins and the cytoskeleton in the cells. Integrin receptors also consist of noncovalently associated  $\alpha$  and  $\beta$  subunits, which interact with the actin cytoskeleton in cells. This interaction causes signalling to the cell nucleus during adhesion to initiate cell proliferation (Freshney, 2010).

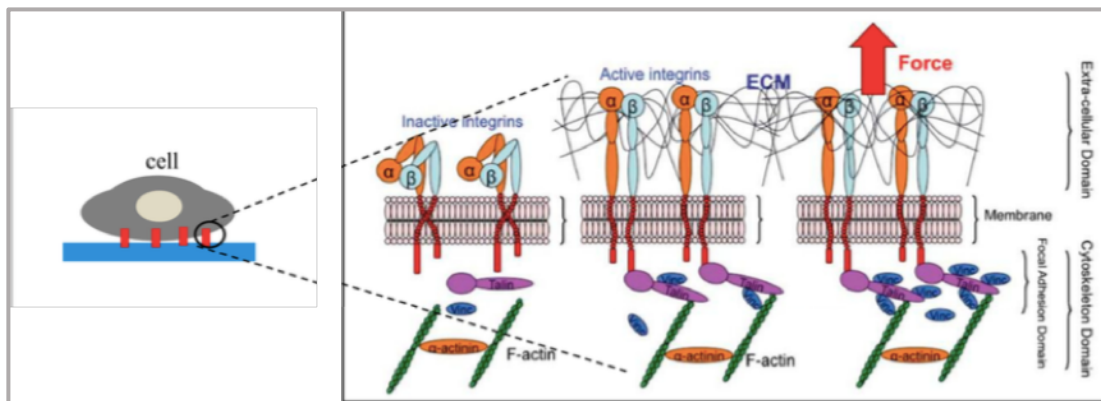


Figure 1-6 A schematic view shows the factors that are involved in cell adhesion(Khalili and Ahmad, 2015).

### 1.3.2 *In Vitro* Cell Culture Substrate Preparation

The application of fibronectin, collagen or other cell matrix products to *in vitro* cell culture substrate can be achieved through using a previously-used substrate for second seeding or commercially supplied fibronectin or collagen, or a combination of both. Such substrate pre-treatment involves pouring a collagen or fibronectin solution over the substrate surface and allowing the excess to flow off. However, this procedure may result in detachment of collagen during cell culture. Thus, it is necessary to anchor the collagen to the substrate by crosslinking the collagen or fibronectin to the plastic substrate with carbodiimide (Freshney, 2010). Another method to overcome collagen detachment or insufficient substrate absorption was described in a study where it was found that insufficient cell adhesion on collagen treated PDMS substrate, due to poor collagen absorption, was improved by covalent bonding of collagen to the substrate (Ku et al., 2010). Another method applied to improve 2D cell culture substrates is the

application of an RGD tripeptide derivative which facilitates substrate interaction with cell surface integrins. N. Zanina and his team (2013) have studied the effect of fibronectin or collagen IV on adhesion of Caco-2 tumoral cells on polyelectrolyte film- functionalized surfaces. They found that collagen enhanced cell motility and proliferation (Zanina et al., 2013). In another study, human dental pulp stem cells were seeded on a chitosan scaffold coated with either RGD or fibronectin molecules to support cellular attachment. It was found that chitosan scaffolds and chitosan- RGD did not support stem cell attachment while fibronectin-immobilized chitosan scaffolds strongly enhanced cellular attachment but not the differentiation process (Asghari Sana et al., 2017). Also, PC12 cell adherence on different surfaces coated with collagen I, collagen IV, fibronectin and laminin. Results showed that PC12 cells attached poorly to uncoated glass surfaces, whereas glass surfaces with adsorbed proteins supported a significant increase in adherence (Cooke et al., 2008). Substrate surface pre-treatment is therefore necessary to enhance cell proliferation and adhesion in a 2D culture. Cell culture models that provide an environment resembling *in vivo* morphology are important to advance understanding of human physiology. However, in the two dimensional cultivation of cells, histological characteristics are generally lost, which affects cells behaviour (**Figure 1-7**). For example, cells of the thyroid gland lose their follicular organization when they are cultured in a monolayer. This leads to a decrease in the cell's ability to transport iodine (Khoruzhenko, 2011). Furthermore, the conventional 2D monolayer cell culture of oviduct epithelium cells (OVECs) does not reflect morphologic characteristics of OVECs *in vivo* (Miessen et al., 2011). Bovine OVECs grown in monolayer lost most of the critical morphological characteristics that play an important role in reproductive processes. These characteristics include a reduction of cell height, flattening on the culture surface, and loss of cilia and secretory granules (Palma-Vera et al., 2014). It can therefore be concluded that 2D culture cannot mimic the oviduct environment (Rottmayer et al., 2006). Therefore, reproductive researchers have attempted to develop novel methods of cell culture that more closely represent the *in vivo* tissue environment and morphology (Edmondson et al., 2014) (Lv et al., 2017). Characteristics of 2D and 3D cell culture system are described in appendix. 5.

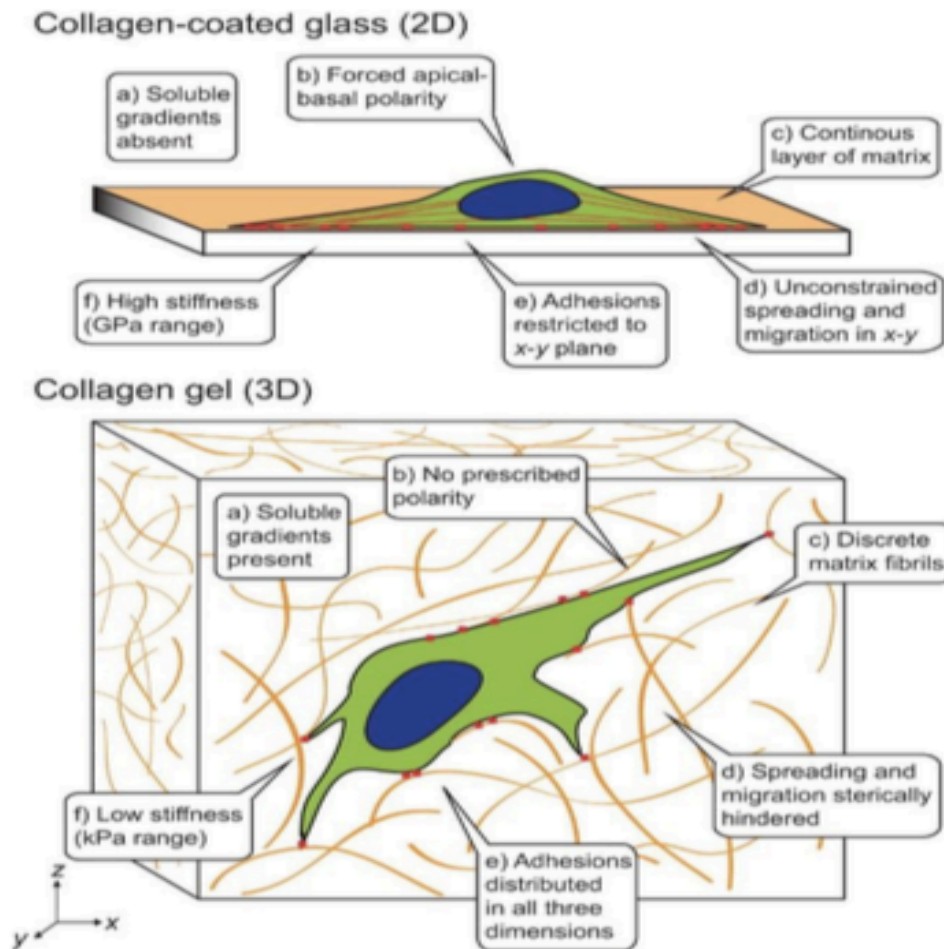


Figure 1-7 The difference between cells growing in 2D and 3D environment (Edmondson et al., 2014)

## 1.4 Cell viability assays

There are a number of cell viability assays that can be used to determine quantity of viable eukaryotic cells following an experiment (Stoddart, 2011). These assays often involve incubation of cells with substrate reagent that viable cells convert to a product that can be analysed using a plate reader. As only living cells can convert substrate to product, the proportion of substrate converted is a measurement of viable cells (Riss and Moravec, 2004).

### 1.4.1 Trypan blue exclusion assay

The number of viable cells present in a cell suspension can be determined by dye exclusion assay. Trypan blue exclusion assay is a simple and rapid method usually taking only 5-10 mins to quantify cell viability (Avelar-Freitas et al., 2014). This cell viability assay uses coloration

of dead cells that absorb trypan blue, in contrast to viable cells that have an intact cell membrane and exclude trypan blue (Strober, 2015). Thus, this technique relies on the membranes of dead cells being unable to restrict the entry of macromolecules. The assay requires cells to be in a single cell suspension which is visualised under a microscope to determine whether cells have taken up the dye or excluded it (Cook and Mitchell, 1989). Viable cells with clear cytoplasm (no blue coloration) are counted under a magnifying lens utilizing a hemocytometer. From these tallies, it is generally easy to ascertain the aggregate number of cells and percent of viable cells in a population (Stoddart, 2011).

The major disadvantage of the trypan blue reduction assay is that it is based on membrane integrity. It is possible for trypan blue dye to enter cells with an injured cell membrane, however, these cells may undergo repair and remain viable cells. Nonetheless, all cells staining blue, regardless of cell death or injury, are deemed as non-viable cells (Cook and Mitchell, 1989).

#### **1.4.2 Tetrazolium reduction assays**

Tetrazolium reduction assays provide a more accurate cell viability method, as compared to trypan blue assay. This type of assay utilises high throughput screening, rather than reliance on technician counting, to quantify cell viability. There are two categories of tetrazolium compounds that are commonly used in tetrazolium reduction assays: positively charged MTT which penetrates viable cells, and negatively charged compounds (MTS, XTT and WST-1) which do not penetrate cells, viable or non-viable. For the latter to function as a cell viability assay, an intermediate electron acceptor is required to facilitate tetrazolium reduction to produce the coloured formazan product (Riss and Moravec, 2004).

##### *1.4.2.1 MTT assay*

The principal behind the MTT assay is that mitochondrial activity is constant in viable cells and therefore increases or decreases in number of viable cells are linearly related to mitochondrial activity (van Meerloo et al., 2011). For determination of cell viability in drug screening protocols the hydrogen acceptor 3-(4,5-dimethylthiazol-2-yl)-2,5-diphenyltetrazolium bromide (MTT) is used. This enzyme-based assay utilizes the mitochondrial dehydrogenases, to determine the viable cells using calorimetric assay. During this assay, tetrazolium MTT is changed into purple formazan crystal by NADH due to mitochondrial activity of the viable cell (**Figure 1-8**). Purple formazan needle like crystal are solubilized before measuring the absorbance (Vistica et al., 1991).



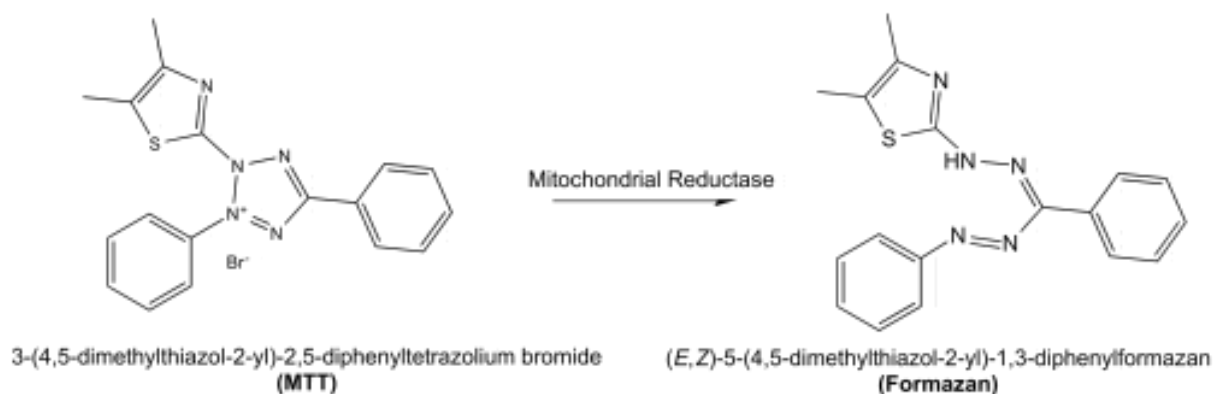


Figure 1-8 Principal of MTT assay, reaction in mitochondria, reaction of MTT change into formazan (46).

#### 1.4.2.2 MTS assay

Viable cells reduce the tetrazolium salt MTS to its soluble formazan product whose absorbance is measured by spectrophotometer. MTS is used with phenazine methyl sulfate (PMS) or phenazine ethyl sulfate (PES). These intermediate electron acceptors become reduced in the cytoplasm or at the cell surface. Their reduced form leaves the cell and accumulates on the surface, where it changes tetrazolium in the culture medium into soluble formazan and hence avoids the need for solubilization of formazan product. The major disadvantage is its use of highly toxic intermediate electron acceptor (Berridge et al., 2005). MTS must be used in a narrow concentration range that must be optimized for each cell line (Riss et al., 2016).

These assays (trypan blue, MTT and MTS measure the viability of the cells but not the functionality of treated cells. There are many types of assays that evaluate the cell function based on their type and the purpose of the experiment such as measuring antibodies present and hormone production. One of the most popular is the enzyme-linked immunosorbent assay (ELISA) (Casadevall et al., 1992).

#### 1.4.3 ELISA:

ELISAs are quantitative immunological assays used to measure different elements in biological samples such as antibodies and glycoproteins. The basis of this assay is that specific antibodies bind the target antigen in the sample (**Figure 1-9**). The ability to coat the plate of the assay with high-affinity antibodies gives this assay highest sensitivity and specificity than other assays. There are a large number of commercially available ELISAs for different purposes, that

have been utilized in many studies to support the finding of the experiments(Althouse and Hixon, 1999).

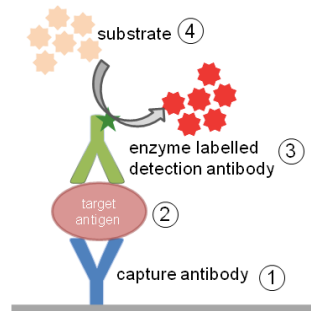


Figure 1-9 The main principle of ELISA assay

## 1.5 3D-BioPrinting

3D printers have traditionally been used with materials such plastic, metal, or food, to create an object with a 3-dimensional shape. These non-biological products vary from jewellery and clothing, to high-end manufactured items (Australian Academy of Science, 2016). Similarly, 3D bio-printers can be utilised to form 3-dimensional structures using biomaterials such as ECM and living cells. The process is auto-mated, using computer technology as computer-aided design (CAD) software to deposit these living cells on the matrix (Ventola, 2014, Australian Academy of Science, 2016). The aim of 3D bio-printing is to create complex 3D tissue structures that mimic the same organs present in living bodies with multiple cell types, similar quantities of each cell type and comparable tissue structure architecture. Researchers from the ARC Centre of Excellence for Electro-materials Science (ACES) used 3D bio-printing to develop what has been referred to as a ‘benchtop brain’. This structure has been developed from neural cells that comprise six-layers, in order to simulate features of brain tissue (Australian Academy of Science, 2016).

3D-bioprinting techniques can differ with the three major categories defined as inkjet-based bio-printing, extrusion bio-printing and laser-assisted bio-printing (Li et al., 2016a). Of these methods, extrusion-based has the ability to produce tissues with superior structural integrity. This is due to the focus on printing living cells by extruding continuous filaments rather than

in drops as with other methods. Cells are extruded under constant pressure in the form of a continuous filament, through a microscale nozzle orifice or microneedle onto a substrate. These cells are applied in layers through a computer-controlled motion, to construct the final 3-dimensional tissue structure. The pressure in this system is supplied by either pneumatic, piston-driven or screw-driven force. This method relies on the use of polymer of hydrogel to be combined with the living cells and loaded in syringes, then dispensed onto the substrate (Pati et al., 2015). There are parameters that can influence the resolution of the bio-printing, such as high-pressure, small nozzle diameters and speed of the printer head (“feed rate”) as these factors can cause damage to cells and effect the line width of the structure. Despite the increased cell viability that results from the use of low pressure and a bigger nozzle, the final construct may lack shape and have limited resolution. This is an important consideration when optimising the ideal conditions for 3D bio-printing using the extrusion method (Pati et al., 2015).

The key elements required for bio-printing are the cells and biomaterial. The choice of biomaterial is based on the properties of the desired cells, as the stiffness, functional groups and surface morphology of biomaterial can affect cellular behaviour (Li et al., 2016a). The cells are encapsulated within the biomaterials, which are chosen because they will provide an environment similar to the native tissue conditions. When combined together, this mixture is referred to as the “bio-ink”. The biomaterials support and stabilise the cells to attach and grow in the desired 3D structure (Li et al., 2016a). In this manner, one of the primary difficulties in the 3D bioprinting field has been to discover materials that are not just compatible with cells, but also give the coveted mechanical and functional properties for tissue constructs (Murphy and Atala, 2014b). Achieving this is dependent upon the development of optimised cellular matrices.

### **1.5.1 Matrix in 3D bio-printer:**

The ECM can be replicated in 3D-bioprinting using biomaterial, or called matrices (Lee et al., 2008). Biomaterials can be defined as being any material that interacts with biological systems, hence the affinity of cells to any type of substrate is an important consideration in biomaterial development (Khalili and Ahmad, 2015). Properties that need to be considered are surface chemistry, surface reaction, surface roughness, surface charge, contact angle, and rigidity. These characteristics determine the cell-biomaterial and cell-cell interactions. Therefore, cell attachment, viability, and differentiation are achieved (Jammalamadaka and Tappa, 2018).

Optimization of matrices as ideal scaffolds for a specific cell type requires a better understanding of the impact of substrate properties on these cells (A.P. Balgude, 2001). Since biomaterials used in 3D bioprinting should represent ECM within a specific tissue *in vivo* and there are different types of cells with their own specialized ECM, the physical chemical aspects of these materials should be considered (Forget et al., 2017). Hence, the biomaterials with adjustable properties are highly valuable because it gives the researchers a chance to reproduce biomaterial that mimics the native ECM (Forget et al., 2017). The balance between ideal structure and functionality of a biomaterial is hard to achieve. Chemical and physical reactions occur between cell and biomaterial, and affects cell behaviour (Santos et al., 2017). Some important biomaterial properties are described in appendix. 6.

#### *1.5.1.1 Viability of encapsulated cells.*

It is important that biomaterials preserve encapsulated cell viability for longer periods of time, and this property called “biocompatibility”. In 2005, CHO and embryonic motoneuron cells were first successfully deposited into a pre-defined pattern. Less than 8 % cell death was observed and that was satisfactory (Li et al., 2016b). Since then Researchers (Bertassoni et al., 2014) successfully built HepG2-loaded GelMA hydrogels presenting high cell viability, more than 95 %, for 8 days. Maintaining post-bioprinted or encapsulated cell viability and functionality is an important step in biomaterial development (Li et al., 2016b).

### **1.5.2 Different Matrices in 3D bio-printing**

A general need for biomaterials is to provide an extracellular matrix environment for cells to grow outside of their native tissue. Hydrogels, three-dimensional polymers, are commonly used in 3D bioprinting because of the ability to adjust their chemical and physical properties. Natural and synthetic derivatives are two groups of polymers that used in 3D bio-printing. Synthetic polymers, such as polyethylene, have some advantages such as high versatility and good workability since they are tightly regulated (Haycock, 2011). However, lack of biological functionality of synthetic polymers is one of the main disadvantages of this group as they do not possess functional binding sites for living cells (Birla, 2014). Naturally derived polymer biomaterials like collagen, fibrin, chitosan, agarose, and alginates, and starch, are directly extracted from biological source such as plants, animals, or human. Unlike the synthetic group, natural polymers in general show a good biocompatibility and low toxicity for living cells (Haycock, 2011). However, they have some drawbacks such as variation in quality which leads to poor reproducibility, a complex or undefined structure, and also limitations to modifying mechanical properties such as viscoelasticity (Ruedinger et al., 2014).

As the main role of collagen is to provide mechanical support to tissue, collagen has become a commonly used natural biomaterial in 3D cell culture. Chitosan, another natural polymer, is a polysaccharide commonly derived from the exoskeleton of crustaceans and insects. Chitosan can be shaped into 3D structures by ionic bonding or covalent crosslinking. Hepatocyte cells were cultured on chitosan scaffolds maintained their cells morphology and metabolic activity. Other examples of natural polymers are Glycosaminoglycan (GAGs), Silk Fibroin and Starch (Haycock, 2011).

Native Agarose (NA) is a natural polysaccharide that has 1,3-linked- beta-d-galactose and 1,4-linked 3,6-anhydro alpha-l-galactose residue repeating units. It is extracted from marine red algae and it is abundant and commercially available (Yixue et al., 2013). Agarose is very soluble in water because of the high amount of hydroxyl groups (Haycock, 2011). It also has a helical secondary alpha structure. Helical content is responsible for viscosity (gelation). Therefore, controlling the density of helices by changing the concentration leads agarose gels with different viscosity. NA undergoes thermally reversible gelation. The process of transition from solution-to-gel ( $T_{sol-gel}$ ) in NA occurs at RT which is lower than the gel-to-solution transition ( $T_{gel-sol}$ ), about 90°C. This phenomena is called the hysteresis (Forget et al., 2017). Agarose has many desirable characteristics as a biomaterial including its non-toxic, inexpensive and readily-available nature, but this and other hydrogel do not support cell adhesion due to its high hydrophilicity (Yixue et al., 2013), and lack of cell adhesion domains (Ulrich et al., 2010) (Forget et al., 2017). Aizawa et al. therefore modified agarose with glycine–arginine–glycine–aspartic acid–serine (GRGDS) to create a cell-adhesive matrix (Aizawa et al., 2008). The limitation of this is that the rich biochemical and topological information encoded in full-length ECM proteins is not reproduced (Ulrich et al., 2010). Au et al. found that agarose covalently modified with collagen supported the attachment of primary-derived canine hepatocytes and human neoplastic hepatocellular carcinoma (HepG2) cells (Au et al., 2012).

Chemical modification of Agarose, such as carboxylation, is another way to improve properties of this gel. In Caroxylated Agarose (CA), the hydrogel chains are heterogeneous which means they have two secondary structures (a-helices and b-sheets). Because the modification of agarose by carboxylation reduces the number of helices that can interact in crosslinking points, a significant decrease in the mechanical properties is noticed with increasing carboxylation. Consequently, the viscosity of the gel could be decoupled from its mechanical properties which adds an advantage to the gel. This unique feature of CA reduces shear stress induced cell death during printing processes. Moreover, the  $T_{gel-sol}$  and  $T_{sol-gel}$  decrease by increasing the

carboxylation. human mesenchymal stem cells (hMSCs) were printed by using 2% w/v solutions of NA, and CA with different degree of carboxylation. Cells with Nonprinted NA hydrogel were used as a negative control to investigate print process effects. By comparing between MSC viability in printed and nonprinted NA hydrogel, it was found that the printed NA gels had lower cell viability (65%). However, negligible change in cells viability was found when the cells were printed in CA with different degree of carboxylation. In the same study, as CA and NA showed a limitation in cell adherence, both were modified with cell adhesion protein to promote cell adhesion. Interestingly, cell viability increased with both gel, CA and NA. However, there were slight differences in viable cell numbers with different amount of carboxylation degree (Forget et al., 2017).

## **1.6 Project Aims**

This research project aims to develop a biomaterial suitable for production of a 3D printed Oviduct by:

- Examining the viability and function of human ovarian carcinoma (OVCAR) cells in different types of matrices with or without of collagen and/or fibronectin.
- Applying the optimized biomaterial and culture conditions to primary-derived oviduct cells

## **1.7 Hypothesis**

Mixed cell suspension obtained from Oviduct will maintain viability and function for 48h when encapsulated in Carboxylated Agarose (CA) matrix mixed with 10 $\mu$ g/ml fibronectin.

## 2 Method

### Reagents

See Appendix. 1 for chemicals, reagents, tools, and instruments.

### 2.1 Cell Culture Reagents

Complete RPMI 1640 media was prepared by dissolving and filtering (0.22 µm Minisart® filter) foetal bovine serum (FBS; 10% v/v), Insulin-transferrin-selenium supplement(ITS; insulin(5µg/ml); transferrin(5µg/ml; selenium(5ng/ml) ) and penicillin-streptomycin (1%v/v of 10000 units/ml penicillin;10 mg/ml streptomycin ) in RMPI-1640 media. The complete media was stored at 4 °C and used within 2 weeks.

1x (0.1%)Trypsin-EDTA was stored at -20°C and used as required.

A 20× phosphate buffered saline (PBS) stock solution was prepared by dissolving sodium chloride (NaCl; 160 g), potassium chloride (KCl; 4 g), disodium hydrogen phosphate (Na<sub>2</sub>HPO<sub>4</sub>; 28.8 g), and monopotassium phosphate (KH<sub>2</sub>PO<sub>4</sub>; 4.8 g) in reverse osmosis (RO) water (900 mL). This was made up to 1 L with RO water. A 1× PBS solution was prepared by diluting the 20x stock solution in RO water and adjusting the pH to 7.2-7.4. The solution was autoclaved and stored at room temperature (RT) between 20 °C to 25 °C.

### 2.2 Oviduct Disaggregation Reagents

Complete Minimum Essential Medium Eagle (αMEM) was prepared by dissolving FBS (10% v/v), penicillin-streptomycin(1%v/v of 10000 units/ml penicillin;10 mg/ml streptomycin ), antibiotic antimycotic solution (1% v/v), ITS (insulin(5µg/ml); transferrin(5µg/ml; selenium(5ng/ml)), beta Estradiol (E2; .01mg/ml) obtained from Flinders Medical Centre, epidermal growth factor (EGF; 2µg/ml) and L-Glutamine solution (200 mM) in αMEM medium. Then complete media was filter sterilised (0.22 µm Minisart® filter) and stored at 4 °C and used within 2 weeks.

Collagenase from *Clostridium histolyticum* was prepared by dissolving collagenase (20 mg) in αMEM medium (2 mL) to obtain 1% . The enzyme was filter sterilised and stored -20 °C.

Complete Dulbecco's Modified Eagle's Medium/Nutrient Mixture F-12 Ham (DMEM F12) was prepared by dissolving and filtering (0.22 µm Minisart® filter) foetal bovine serum (FBS; 10% v/v) in DMEM F12 medium. It was used to transfer whole Oviduct from the animal house to the laboratory. The complete medium was stored at 4 °C and used within 2 weeks.

## **2.3 Cell Viability Assay Reagents**

### **2.3.1 Thiazolyl Blue Tetrazolium (MTT) Reagents**

MTT powder (150 mg) was dissolved in sterile 1× PBS solution (30 mL) for a final concentration of 5 mg/mL. These components were mixed using a magnetic stirrer and filtered through a 0.22 µm Minisart® filter. Aliquots (5 mL) were stored at -20°C in the dark. 12 M hydrochloric acid (HCl; 0.8333 mL) was added to a volumetric flask containing RO water (~400 mL), and made up to 500 mL to afford a 0.02 M HCl solution that was stored in the fume hood at RT. Sodium dodecyl sulphate (SDS; 40 g) was combined with 0.02 M HCl (100 mL) and stirred under low heat in the fume hood until dissolved. The SDS solution was decanted into a volumetric flask and made up to 200 mL with 0.02 M HCl solution. The solution was stored in fume hood.

### **2.3.2 Preparation of Trypan Blue Dye**

Trypan blue (0.2 g) was added to a solution of NaCl (0.9 g) dissolved in 100 mL of MilliQ water, and filtered through a 0.22 µm Minisart® filter. The trypan blue solution was stored at RT.

### **2.3.3 Preparation of Tetrazolium (MTS) Reagents:**

To prepare the MTS solution, MTS powder was dissolved in 1× PBS solution ( 2 mg/mL), producing a clear golden-yellow solution. Phenazine ethosulfate (PES) was dissolved in the MTS solution to give a concentration of 0.21 mg/mL. The pH was adjusted to between 6.0 and 6.5 using 1 M HCl, and the solution was filtered through a 0.22 µm filter into a sterile, light protected container. The MTS solution was stored at -20°C until required.

## **2.4 Matrix Preparation**

### **2.4.1 2%(w/v) Agarose Gel:**

Agarose powder (Bio-Rad Laboratories, Inc; 100 mg) was dissolved in distilled water (5 mL) in a water bath at 90°C for 20 min to achieve a 2% (w/v) agarose solution. The agarose solution was kept at 90°C until dispensed into appropriate containers and prepared on the day of experimental use.

### **2.4.2 2% (w/v) Carboxylated Agarose Gel:**

Carboxylated agarose powder (CA) (Applied Chemistry and Translational Biomaterials (ACTB) Group, (Forget et al., 2017)) was prepared using the same method described above for 2% (w/v) agarose gel, but water bath temperature was 85°C. The gel was prepared in the same day of the experiment.



### **2.4.3 Collagen Solution**

Collagen solution was prepared using hydrolysed bovine collagen (type I and III combined) by dissolving 5 and 25 mg in PBS (500  $\mu$ L), to obtain 1 and 5% w/v solutions, respectively. These solutions were prepared immediately prior to use.

### **2.4.4 Fibronectin Solution**

Fibronectin was dissolved in distilled water (1 mg/mL) at 37°C. Stock solution was stored at -20°C until required. Standard solutions were prepared by diluting 1 or 10  $\mu$ L fibronectin stock solution in 999 and 990  $\mu$ L of PBS, respectively, to produce concentrations of 1  $\mu$ g/mL and 10  $\mu$ g/mL, which were used immediately.

### **2.4.5 Matrix Preparation for Encapsulated Cells**

#### *2.4.5.1 Carboxylated Agarose Gel*

CA (20 mg) was dissolved in complete RPMI media (950  $\mu$ L) at 80°C for OVCAR cell encapsulation and in  $\alpha$ MEM (950  $\mu$ L) for primary-derived oviduct cell encapsulation. The solution was then transferred to a heating block set at 40°C and irradiated under UV light for 30 minutes. The solution was then used immediately to encapsulate cells.

#### *2.4.5.2 Carboxylated Agarose Gel with 5%w/v Collagen*

OVCAR cell encapsulation was repeated using the same method described above, with the following changes: CA (20 mg) was dissolved in 650  $\mu$ L complete RPMI media and cooled to 40°C to avoid temperature drop upon collagen addition. Collagen (50mg) solution prepared in complete RPMI media (300  $\mu$ L) was added to CA solution and sterilised.

#### *2.4.5.3 Carboxylated Agarose Gel with 10 $\mu$ g/mL Fibronectin*

OVCAR cell encapsulation was repeated with addition of fibronectin using the procedures described above, but CA (20 mg) was dissolved in 940  $\mu$ L complete RPMI media, and the solution was cooled to 40°C prior to addition of fibronectin (10  $\mu$ L) stock and sterilisation.

#### *2.4.5.4 Carboxylated Agarose Gel with 10 $\mu$ g/mL Fibronectin and 5% Collagen*

Encapsulation of OVCAR cells using CA gel with fibronectin and collagen followed procedures described above with 20 mg CA dissolved in 640  $\mu$ L complete RPMI media. A further 300  $\mu$ L complete RPMI media with dissolved collagen (50 mg) and fibronectin stock (10  $\mu$ L) were added to the gel solution prior to UV sterilisation. Encapsulation of primary-derived oviduct cells was achieved using the same method, but instead of RPMI media,  $\alpha$ MEM medium was used.

## 2.5 Cell Line Maintenance and Subculture

Human ovarian carcinoma epithelial (OVCAR-3) cells (ATCC®HTB-161™), with 96h as population doubling time(PDT), were maintained in complete growth RBMI-1640 media. The cells were incubated in a sterile tissue culture flask (T75 flask) at 37 °C in the presence of a humidified atmosphere of 5 % CO<sub>2</sub>. The medium was renewed every two to three days. The cells were sub-cultured when they reached 80 to 90 % confluence. In a biosafety cabinet, the old media that contained floating dead cells was aspirated by using vacuum aspiration and then the flask was washed with sterile 1xPBS (10 mL). The cells then were detached by incubating them at 37 °C with 10 % trypsin-EDTA (5 mL) for 10 to 15 min. When all of the cells were detached, complete media (4 mL) was added to stop trypsinisation and to flush down the floor of the flask. The detached cells were collected from the flask in a 50 mL tube and centrifuged at 259 g for 5 min. The supernatant was discarded and the pellet was resuspended in complete RBMI media (4 mL). Aliquots of the cell suspension (1 mL) were transferred to new T75 labelled flasks that contained complete RPMI media (20 mL). The flasks were then incubated in 37 °C and 5 % CO<sub>2</sub>.

## 2.6 Cell Viability Assays

### 2.6.1 Trypan Blue Exclusion Assay

This assay was used to determine cell viability of the OVCAR cell suspensions. Cell suspension (50 µL) was collected by trypsinization, and transferred to a 96-well plate and mixed with trypan blue dye solution (50 µL ) at RT. An aliquot of the mixture (10 µL ) was loaded onto a haemocytometer slide (Marienfeld; Germany) containing nine large squares to count the cells under a microscope (Leica WETZLAR microscope). The viable cells were golden while the non-viable cells were stained blue. The average number of viable cells was determined by counting the viable cells in four squares. The mean number of viable cells in 1 mL was calculated by multiplying the average number by the dilution factor (2) and by the correction factor (10<sup>4</sup>). The formula that was followed to count the viable cells/ml is:

(Number of viable cells) × 10<sup>4</sup> × 2 = cells/mL culture

### 2.6.2 MTT and MTS Assay Standard Curves

After calculating OVCAR cell number by using the trypan blue exclusion assay, a single cell suspension that had a cell density of 800,000 cells/mL was used prepare a standard curve of MTT and MTS in six replicate wells. A 96-well flat bottom plate had 100 µL of complete RPMI media added to wells 2 to 11. The cell suspension was diluted serially 1:2 in the wells

that were prepared starting with 40,000 cells to 0 cells that contained media only as the control (**Figure 2-1**). The plate was incubated for 24 h at 37 °C and 5% CO<sub>2</sub> to allow cell attachment to the wells.

	1	2	3	4	5	6	7	8	9	10	11	12
A												
B												
C												
D												
E		Media	156	313	625	1,250	2,500	5,000	10,000	20,000	40000	
F												
G												
H												

Figure 2-1 A 96-well plate layout for MTT and MTS Assay standard curve

#### 2.6.2.1 MTT Cell Viability Assay

After a 24-hr adherence period, the seeding media were removed from the wells and replaced with MTT solution (200 µL, 0.5 mg/mL). The cells were then incubated for 24 hrs at 37 °C and 5% CO<sub>2</sub>. Subsequently, 20 % SDS in 0.02 M HCL (80 µL ) was added to dissolve formazan crystals. The plate was then incubated for 18 hrs at RT in the dark. Reading of the plate was performed using a spectrophotometer (BioTek Quant Microplate; American Laboratory Trading) at 570 nm with background absorbance at 630 nm using the KCjunior™ software. This assay was repeated at three different time points (24, 48 and 72 hrs) (**Figure 2-2**).

#### 2.6.2.2 MTS Cell Viability Assay

After 24-hr adherence period, the plate was taken out of the incubator. MTS reagent (20 µL ) was added to the wells, then the plate was incubated at 37 °C in 5% CO<sub>2</sub> for 2 hrs. Reading of the plate was done by using spectrophotometer (Quant automatic spectrophotometer) at 490 nm with non-reference using KCjunior™ software. This assay was repeated at three different adherence periods (24, 48, and 72 hrs) (**Figure 2-2**).

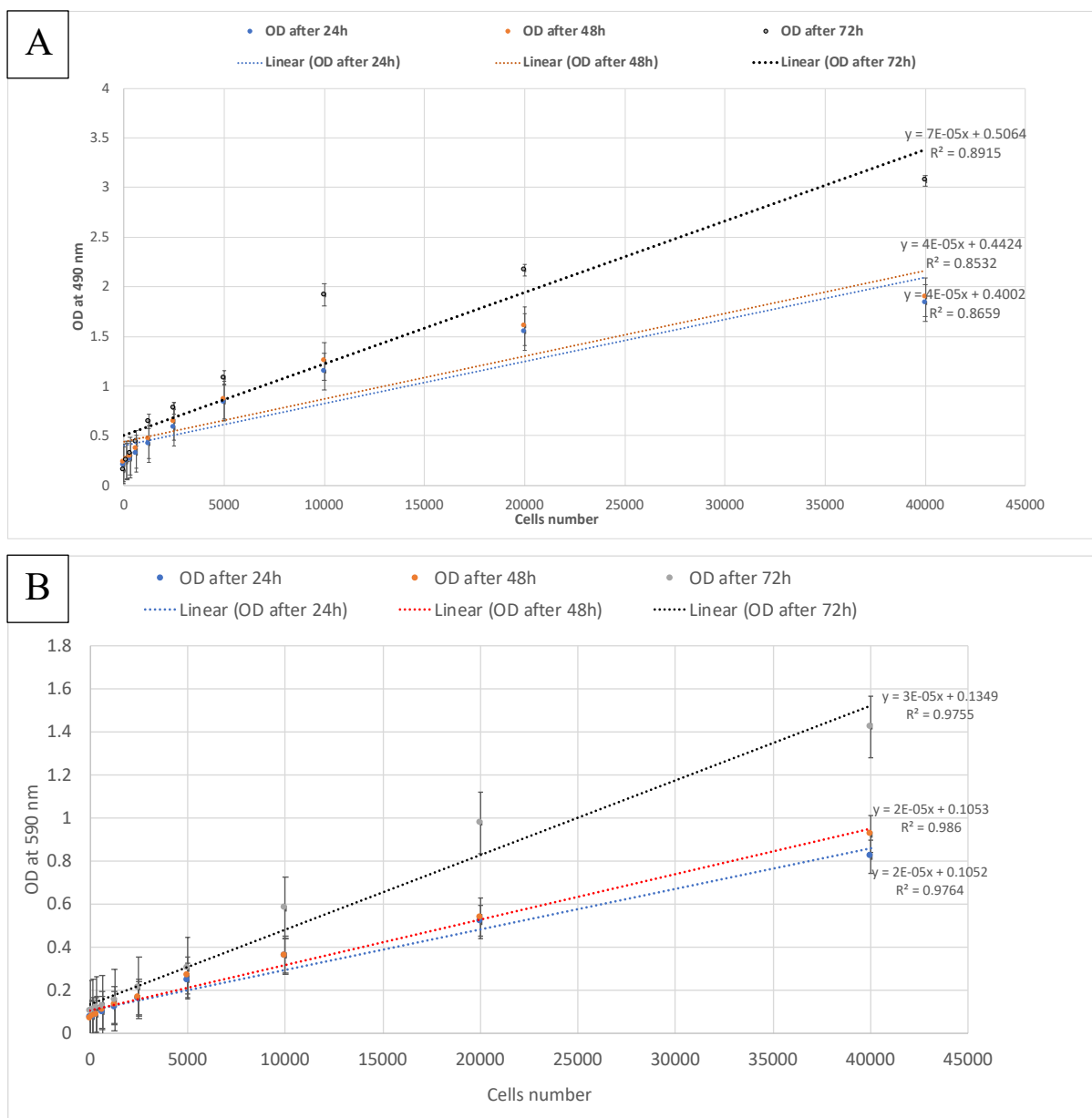


Figure 2-2 MTS(A) and MTT(B) standard curves for OVCAR cells. OVCAR cells were incubated for 24h to allow cell adherence in a 96-well plate. After incubation time MTT or MTS was applied as described in (MTT, 2.6.3 section; MTS, 2.6.4 section). Mean  $\pm$  standard deviation of optical density for 6 replicate wells/experiment (n=3) shown.

## 2.7 Matrix Interference with MTT Assay

This experiment was conducted to investigate whether 2% (w/v) agarose and CA gels interfered with the MTT assay. 2% (w/v) agarose and CA gels prepared as described in (section 2.4.1) and (section 2.4.2) (50  $\mu$ L per well) were added to a 96-well plate and kept at 4  $^{\circ}$ C for 2 hrs. Complete RPMI media (100  $\mu$ L) were added on top of these gels and wells with only complete RPMI media (100  $\mu$ L) were used as a negative control. MTT solution (200  $\mu$ L, 0.5 mg/mL) was then added to each well and the plate was incubated for 2h at 37 $^{\circ}$ C and 5 % CO<sub>2</sub>.

Subsequently, 80  $\mu$ L of 20% SDS in 0.02 M HCL was added to the wells and the assay completed as described above (section 2.6.2.1).

### 2.7.1 Matrix Interference with SDS Dissolution of Formazan Crystals in MTT Assay

The aim of this experiment was to investigate whether 2% (w/v) agarose and CA gels interfered with SDS dissolution of formazan crystals in MTT assay as indicated in (**Figure 2-4**) step (1). Trypsinized OVCAR cells ( $20 \times 10^3$ ) were seeded into a 96-well plate and incubated at 37°C and 5 % CO<sub>2</sub> for 24 h. MTT solution (200  $\mu$ L, 0.5 mg/mL) was added to the wells and the plate was incubated for 24 hrs at 37°C and 5 % CO<sub>2</sub>. Then, 80  $\mu$ L of 20 % SDS in 0.02 M HCl was added. In the same time, 2% (w/v) agarose gel and CA gel (50 all; prepared as described in section 2.4.1 and section 2.4.2) were added to the wells. Wells with cells only were used as positive control while wells with gel but without cells were used as negative control (see Fig. 2-4). The MTT assay was completed as described previously.

### 2.7.2 Matrix Interference Spectrophotometer Reading of 570 nm OD Readings

This experiment was conducted to demonstrate whether 2%(w/v) agarose and CA gels interfered with spectrophotometer reading in MTT assay. The same previous experiment in section (2.7.1) was conducted. The only difference was in which step the gels were added, here the gels were added immediately before reading as indicated in (**Figure 2-4**) step 2.

	1	2	3	4	5	6	7	8	9	10	11	12
A												
B		Cells only (positive control)					Compleat media only (negative control)					
C		Cells with 2 wt% Agarose Gel					2 wt% Agarose Gel only (negative control)					
D		Cells with 2 wt% Carboxylated Agarose Gel					2 wt% Carboxylated Agarose Gel only (negative control)					
E												
F												
G												
H												

Figure 2-3 A 96-well plate layout for Matrices interference with MTT/MTS Assay.

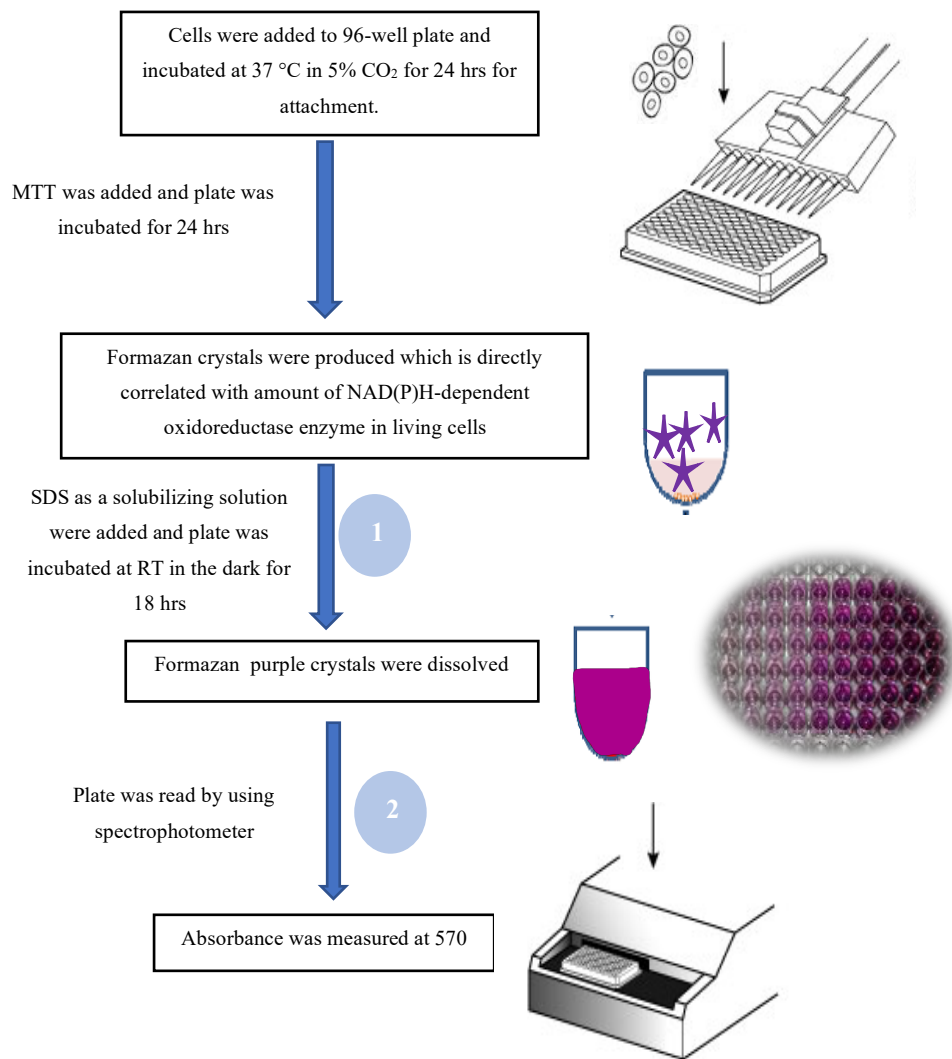


Figure 2-4 A scheme of MTT assay to explain at which stage the matrix was added

## **2.8 Matrix Interference with MTS Assay**

This experiment was conducted to investigate whether 2% (w/v) agarose and CA gels interfered with MTS reading. 2%(w/v) agarose gel and CA gel (prepared as described in section 2.4.1 and section 2.4.2; 50  $\mu$ L) were added to 96-well plate and kept at 4°C for 2 h to solidify. Complete RPMI media (100  $\mu$ L) was added. Complete RPMI media (100  $\mu$ L) wells without gels were used as a negative control. After 2 h incubation at 37°C and 5 % CO<sub>2</sub> , MTS assay was applied as described in (section 2.6.2.2). This experiment was repeated on three separate occasions (n=3).

### **2.8.1 Matrix Interference with MTS Includes Dissolution of Formazan Crystals**

The aim of this experiment was to investigate whether 2% (w/v) agarose and CA gels interfered with MTS Includes Dissolution of Formazan Crystals in MTS Assay as indicated in (**Figure 2-5**) step (1). OVCAR cells ( $20 \times 10^3$ ), collected by trypsinization, was seeded in 96-well plate and incubated at 37°C in 5% CO<sub>2</sub> for 24h. Then MTS reagent was added to the wells (0.33 mg/mL in the final concentration). In the same time, 2% (w/v) agarose gel and CA gel (prepared as described in section 2.4.1 and section 2.4.2; 50 all; 50  $\mu$ L) were added the wells as indicated in (**Figure 2-3**). The positive control was cells only without gel while wells with gels but without cells were used as negative control. The plate was incubated at 37 °C in 5% CO<sub>2</sub> for 2 h. Reading of the plate was done by using spectrophotometer (Quant automatic spectrophotometer) at 490 nm with non-reference using KCjunior™ software. This experiment was repeated on three separate occasions (n=3).

### **2.8.2 Matrix Interference Spectrophotometer Reading of 490 nm OD Readings**

This experiment was conducted to demonstrate whether 2% (w/v) agarose and CA gels interfered with spectrophotometer reading in MTS assay. The same previous experiment in section (2.8.1) was conducted. The only difference was in which step the gels were added, here the gels were added immediately before reading as indicated in (**Figure 2-5**) step 2. This experiment was repeated on three separate occasions (n=3).

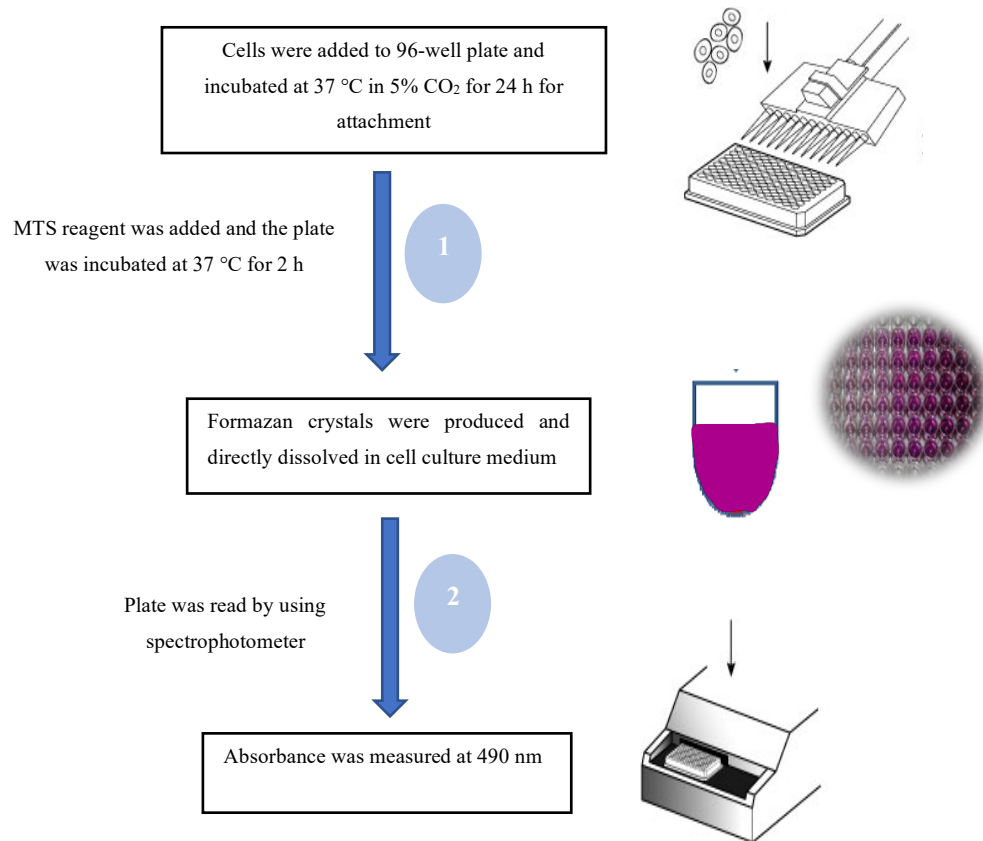


Figure 2-5 A scheme of MTS assay to explain at which stage the matrix was added.



## **2.9 Matrix Interference with ELISA**

This experiment was done to investigate whether Matrices interfered with ELISA assay. A 96-well plate was coated with 2 (w/v) % agarose gel and CA gel (prepared as described in section 2.4.1 and section 2.4.2; 50  $\mu$ L). Both gels solidified within 30 minutes at RT. Then complete RPMI media (100  $\mu$ L) was added on top of the matrices. The plate was incubated at 37 °C in 5% CO<sub>2</sub> for 24, 48 and 72h. After the designated incubation time, media from the top of each well (75  $\mu$ L) was collected and examined in ELISA (Commercial kit; Cayman Chemical NO. 582601) This experiment was repeated on three separate occasion (n=3).

## **2.10 OVCAR Cell Viability and Behaviour on Matrix Surface After 24-hr and 48-hr Incubation period**

2% (w/v) agarose gel and CA gel (prepared as described in section 2.4.1 and section 2.4.2; 50  $\mu$ L) were added to 96-well plates and kept at 4 °C for 2 hrs to solidify the gel. After 2h, gel surfaces were coated with collagen (prepared as described in 2.4.3; 1 or 5%; 30  $\mu$ L ) and fibronectin (prepared as described in 2.4.4; 1 or 10  $\mu$ g/mL; 30  $\mu$ L ) ( see **Figure 2-6** ). Then the plates were kept at 4 °C for 18 hrs. Prior to cell seeding, wells with collagen and fibronectin were washed three times with Complete RPMI media (80 $\mu$ L), then plates were sterilized under UV light while the cell suspension was prepared. OVCAR cells ( $20 \times 10^3$ ) were seeded into all wells and incubated for 24 and 48 h (see **Figure 2-7**). Before MTT or MTS assays were applied, cell morphology was monitored by using a microscope (NiKon eclipse Ts2R) and counted as described in (section 2-13). This was repeated with 48-hr incubation time. After 48 h, MTT and MTS assays were applied followed the method in section 2.6.2.1 and 2.6.2.2, respectively. This experiment was repeated on three separate occasions (n=3). Viable cell number were determined by comparison with a standard curve produced for each experiment.

plate (1)												
	1	2	3	4	5	6	7	8	9	10	11	12
A												
B		control(media only)										
C		2% agarose gel										
D		agarose+1%collagen										
E		agarose+5%collagen										
F		agarose+1ug/ml fibronectin										
G		agarose+ 10ug/ml fibronectin										
H												

plate (2)												
	1	2	3	4	5	6	7	8	9	10	11	12
A												
B		control(media only)										
C		2% carboxylated agarose gel										
D		carboxylated agarose+1%collagen										
E		carboxylated agarose+5%collagen										
F		carboxylated agarose+1ug/ml fibronectin										
G		carboxylated agarose+ 10ug/ml fibronectin										
H												

Figure 2-6 A 96-well plate layout for 2% agarose gel (plate 1) 2% Carboxylated Agarose gel (plate 2) coating with different proteins.

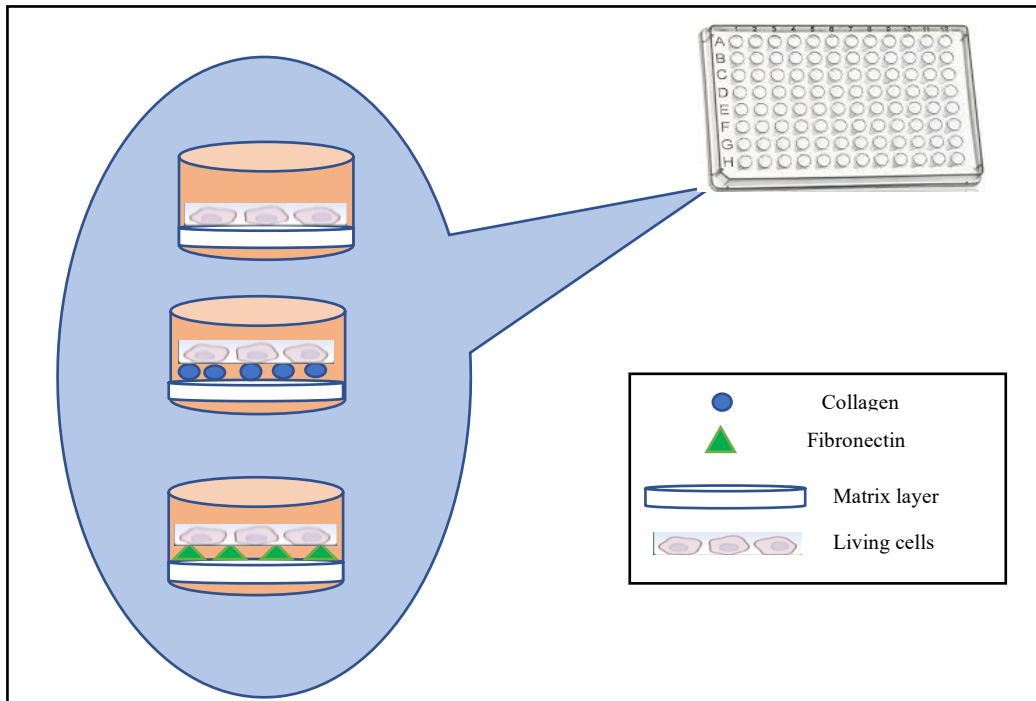


Figure 2-7 OVCAR cells were incubated on different surface substrates with/without adhesion protein.

## 2.11 Viability and Behaviour of Encapsulated OVCAR cells After 48-hr incubation

An OVCAR cell suspension (500,000/mL) was prepared and centrifuged at 340 g for 5 min. The supernatants were removed and complete RPMI media (50  $\mu$ L) was added to the pellet. The pellet was gently pipetted several times to mix and suspend the cells. Subsequently, the cell suspension (50  $\mu$ L) was added to sterilised CA matrix solution with or without adherence proteins(prepared as described in section 2.4.5). Cells with different matrices were mixed through gentle pipetting. Aliquots of the cells in matrix solutions (50  $\mu$ L) were added to wells (25  $\times$  10<sup>3</sup> cells/well) as indicated in (Fig. 2-8). The plate was kept at RT for 30 minutes to allow matrices solidified then complete RPMI media (100  $\mu$ L) was added. OVCAR cells were incubated at 37 °C and 5 % CO<sub>2</sub> for 48 h. Wells containing matrix but without cells were used as a negative control. Media from the top of each well (75  $\mu$ L) were collected, to use it in ELISA, and replaced with new complete RPMI media ( 75  $\mu$ L). After 48h, MTS assay was added to the wells and viable cell numbers determined 2h later followed the method in (section 2.6.2.2). Cell morphology was examined using a microscope (NiKon eclipse Ts2R) and counted as described in section 2.13. Viable cell number were determined by comparison with a standard curve produced for each experiment.

	1	2	3	4	5	6	7	8	9	10	11	12
A	OVCAR cells encapsulated in different matrices					Negative Control (without cells)						
B	Cells with media (positive control)					Compleat media						
C	2%(w/v) CA gel					2%(w/v) CA gel						
D	2%(w/v) CA gel + 5% Collagen					2%(w/v) CA gel + 5% Collagen						
E	2%(w/v) CA gel + 10ug/ml Fibronectin					2%(w/v) CA gel + 10ug/ml Fibronectin						
F	2%(w/v) CA gel + 10ug/ml Fibronectin+5%Collagen					2%(w/v) CA gel + 10ug/ml Fibronectin+5%Collagen						
G												
H												

Figure 2-8 A 96-well plate layout for 2% CA gel with or without adhesion proteins mixed with OVCAR cells.

### 2.11.1 ELISA to Measure Progesterone Secreted by Encapsulated OVCAR Cells:

A commercial ELISA kit (Cayman Chemical; No. 582601) was used to measure progesterone production by OVCAR cells after 48h encapsulated with the matrix. Complete RPMI media (75  $\mu$ L from the top of each well), collected from the previous experiment (section 2.11), was utilised in this assay. In this competitive progesterone EIA, a mouse monoclonal anti rabbit IgG, and an acetylcholinesterase progesterone tracer were used.

## 2.12 Viability and Morphology of Primary-Derived Oviduct Cells After 48hr Encapsulation

### 2.12.1 Isolation of Primary-Derived Oviduct Cells:

The oviduct from 6 female mice (BALB/c) with average age of 10 weeks and average weight of 20 g were dissected and transferred to warm DMEM F12 media (3 mL). Each oviduct was cut into three small pieces (approximately infundibulum and ampulla, excluding isthmus) with aid of a microscope. Each piece of oviduct, except isthmus, was incubated with collagenase I (1%; 150 $\mu$ L) at 37 °C with 5% CO<sub>2</sub> for 30 minutes, mixed by pipetting for 1 minute then vortexed at low speed for 30 seconds. The disaggregated tissue preparation was centrifuged at 340 g for 5 minutes. The resulting cell pellet was resuspended in complete  $\alpha$ MEM media (150  $\mu$ L) and cell viability assessed in a trypan blue exclusion assay as described in (section 2.6.1)

### 2.12.2 Encapsulation of Primary-Derived Oviduct Cells in Matrix:

An Oviduct cell suspension was centrifuged at 340 g for 5 min. The supernatant was removed and replaced with complete  $\alpha$ MEM medium (50  $\mu$ L). The cell pellet was gently pipetted several times to mix and suspend the cells. Subsequently, the cell suspension (50  $\mu$ L) was added to sterilised CA or CA gel with 10  $\mu$ g/mL fibronectin and 5% collagen (see description in section 2.4.5.1 and 2.4.5.4 respectively; dissolved in complete  $\alpha$ MEM medium instead of complete RPMI medium) and mixed thoroughly through gentle pipetting. Aliquots of the cells in matrix solutions (50  $\mu$ L) were added to wells (10  $\times$ 10<sup>3</sup> cells/well) as indicated in (**Figure 2-9**). The plate was kept at RT for 30 min to allow the solutions to set into gels, and then complete  $\alpha$ MEM medium (100  $\mu$ L) was added to each well. The plate was incubated at 37°C and 5 % CO<sub>2</sub> for 48 h. Wells with gel but without cells were used as a negative control. MTS assay was added to the wells and viable cell numbers determined 2h later followed the method in (section 2.6.2.2). Cell morphology was examined using a microscope (NiKon eclipse Ts2R).

	1	2	3	4	5	6	7	8	9	10	11	12
A	Primary-derived oviduct cells encapsulated in different matrices					Negative Control (without cells)						
B	Cells with media (positive control)					Compleat media						
C	2%(w/v) CA gel					2%(w/v) CA gel						
D	2%(w/v) CA gel + 10ug/ml Fibronectin+5%Collagen					2%(w/v) CA gel + 10ug/ml Fibronectin+5%Collagen						
E												
F												
G												
H												

Figure 2-9 A 96-well plate layout for 2% Carboxylated Agarose gel with or without adhesion proteins mixed with Oviduct cells.

### **2.13 Image analysis**

To analyse the photomicrographs that were obtained from experiment in (section 2.11), ImageJ software was used to manually mark each cell in a photomicrograph as a method to count the number of cells. For each experimental condition, the same experiment was conducted three times, on separate days. For each treatment, four photomicrographs from multiple areas were obtained from each well. The average number of cells across the four wells was calculated to get an average for that experiment. This method was repeated twice more to gain an average across the experiment triplicate. To estimate the total cell number for each experimental condition, the average of actual number of cells per each treatment was calculated following the equation, after adjusting for objective lens magnification:

$$\text{Total estimated number of cells per well} = \text{Average counted cell number in a well} \\ \times (\text{area of the well/ area of the image})$$

To analyse the photomicrographs that were obtained from encapsulation of OVCAR cells in CA mixed with 10 µg/ml fibronectin and 5% collagen, photomicrographs were taken from multiple areas on the gel, grouped and counted according to shape: flattened cells, rounded cells and cells of irregular shape by using ImageJ software. Again, four photomicrographs were analysed per well to obtain average number of cells/well as described above.

### **2.14 Statistical Analysis:**

GraphPad Prism software was used to conduct one-way ANOVA with the Tukey-Kramer post-hoc test and applied to MTT, MTS and P<sub>4</sub> ELISA data. Also, a two-way ANOVA with Bonferroni post-test was used with P<sub>4</sub> ELISA data. The P-value was judged to be statistically significant if it was less than 0.05.

### 3 Result

#### 3.1 Matrix Interference with Different Assays

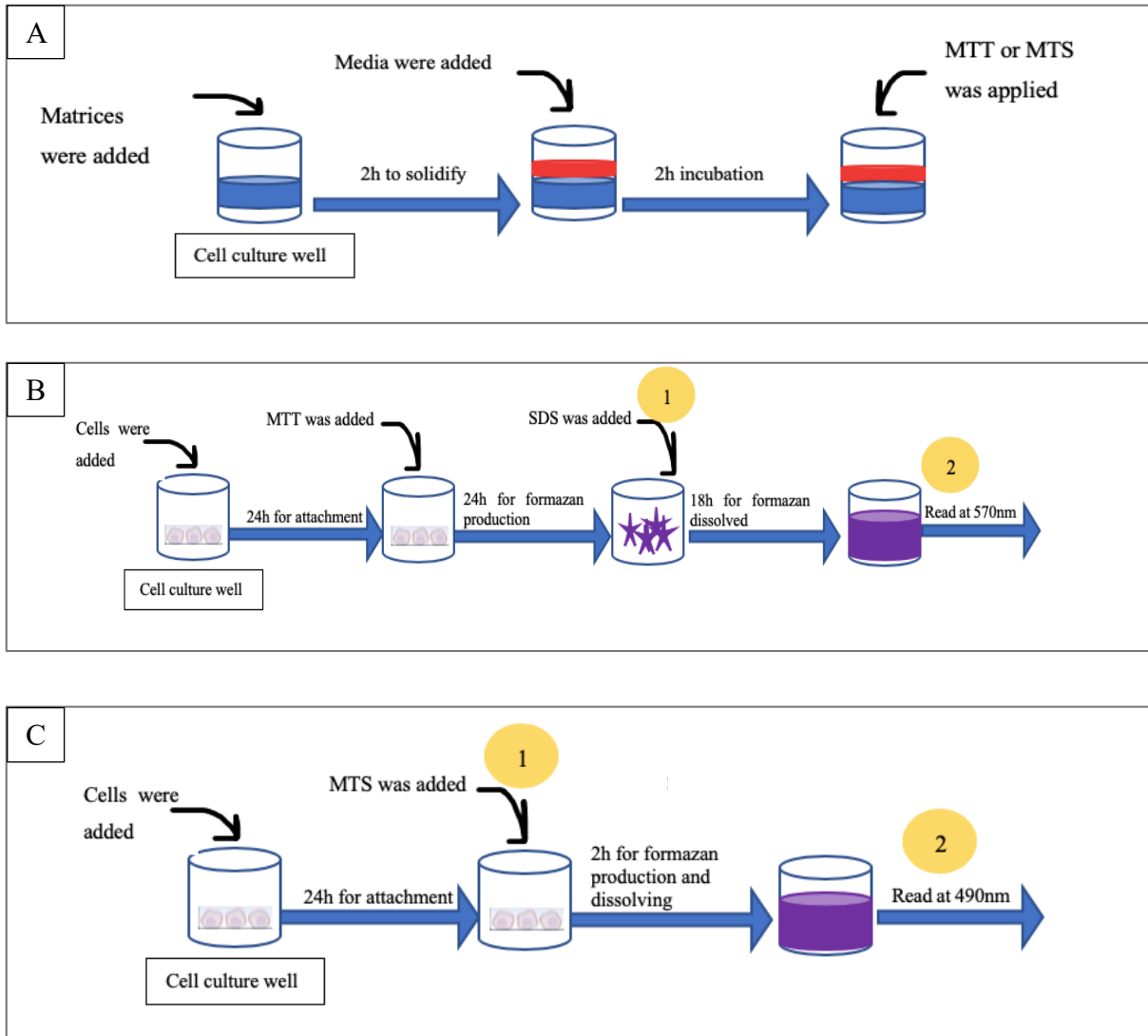


Figure 3-1 A scheme of MTT and MTS assays procedure to show at which stage the matrix was added in the Interference investigation. (A) Interference of matrices without cells with MTT or MTS assay (B) Interference of matrices with MTT assay in two steps (C) Interference of matrices with MTS assay in two steps.

### 3.1.1 Interference of Agarose gel and Carboxylated Agarose gel (CA) with MTT assay

The matrices were added at three different steps in the MTT assay process in three separate experiments. Agarose gel caused a significant increase in OD in MTT assay (**Figure 3-2**), whereas CA had a similar OD value when they were tested without cells (**Figure 3-1A**). However, when the matrices were added at the same time as SDS solution as shown in (**Figure 3-1B step 1**), both agarose gel and CA had similar OD value comparing to the media control after 24h (**Figure 3-3**). Moreover, when the matrices were added immediately before reading the OD (**Figure 3-1B step 2**), there was no significant change in OD value compared to the control (**Figure 3-4**).

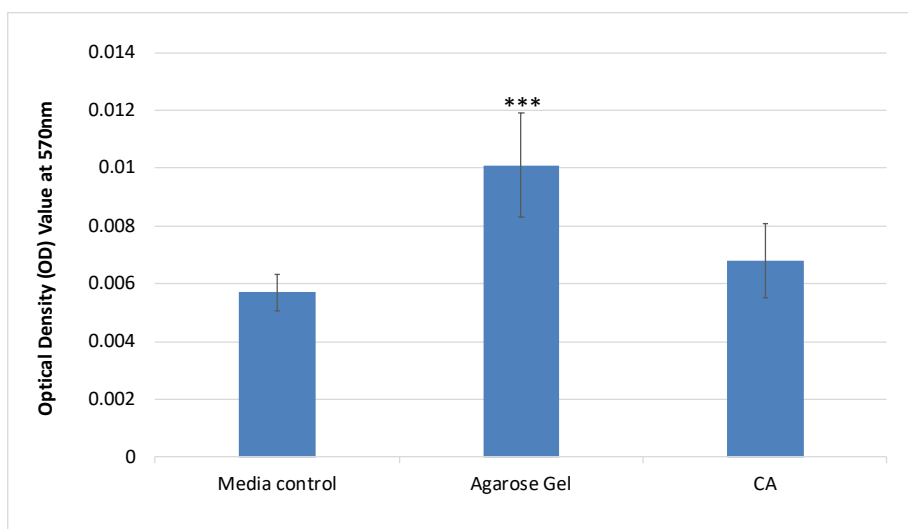


Figure 3-2 Interference of matrices without cells with MTT assay. Agarose gel and CA gel (50  $\mu\text{L}$ ) were plated in 96-well plate and solidified within 2h. Complete RPMI media (100  $\mu\text{L}$ ) was added on top of matrices, media only (150  $\mu\text{L}$ ) was used as a negative control. MTT was applied after 2 hrs of incubating the media with matrices. The experiment was repeated in three separate occasions ( $n=3$ ). Mean  $\pm$  standard deviation are shown. Analysing data was done by a one-way ANOVA with the Tukey-Kramer post-hoc test. The significant difference was assigned  $p < 0.0001$ (\*\*\*) and no significant difference ( $p > 0.05$ ).

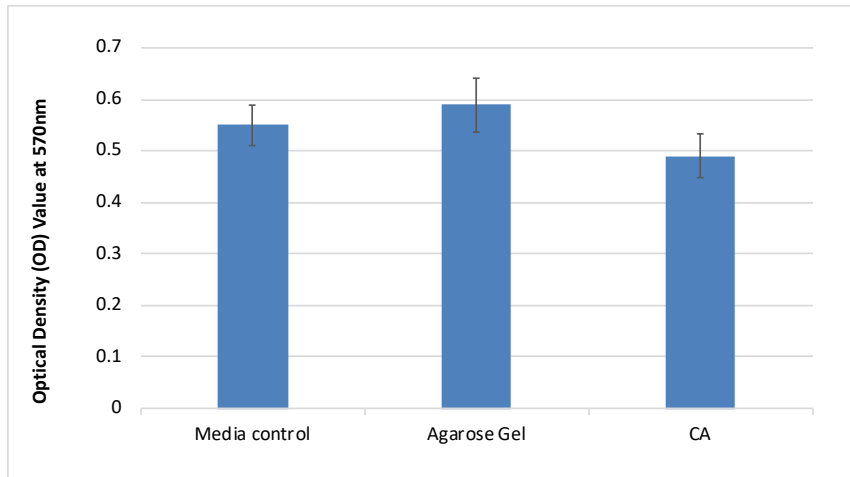


Figure 3-3 Interference of matrices with dissolving formazan crystals in MTT assay. A 96-well plate was seeded with  $20 \times 10^3$ /well of OVCAR cells and incubated for 24 hrs at 37 °C and 5 % CO<sub>2</sub> to allow cell adherence. MTT was added for 24h incubation, then SDS solution was added to dissolve formazan crystals and produce purple colour. Matrices (agarose gel and CA gel; 50 µL) were added in the same time as SDS solution. The experiment was replicated on three separate occasions (n=3). Mean ± standard deviation are shown. A one-way ANOVA with the Tukey-Kramer post-host test was used to analyse data. No sign indicates no significant difference ( $p > 0.05$ ).

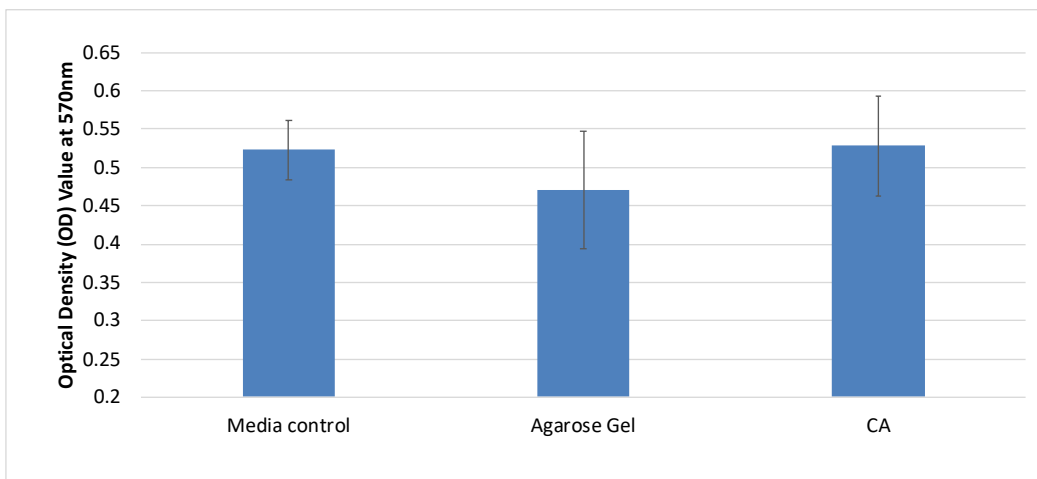


Figure 3-4 Interference of matrices with Spectrophotometer reading (at 570 nm). A 96-well plate was seeded with  $20 \times 10^3$ /well of OVCAR cells and incubated for 24h at 37 °C and 5 % CO<sub>2</sub> to allow cell adherence. MTT assay was applied and directly before reading, matrices (agarose gel and CA gel; 50 µL) were added. The experiment was replicated on three separate occasions (n=3). Mean ± standard deviation are presented. Data was analysed using a one-way ANOVA with the Tukey-Kramer post-host test. No sign at no significance difference ( $p > 0.05$ ).



### 3.1.2 Interference of Agarose gel and Carboxylated Agarose gel (CA) with MTS assay

In the absence of cells, both agarose and CA increased OD readings in MTS assay (Figure 3-5), but had no effect on the dissolution of cells and formazan crystals with SDS solution (Figure 3-6). Both agarose and CA also significantly increased spectrophotometer readings of OD (Figure 3-7). See Figure 3-1A and C for more explanation in the assay steps.

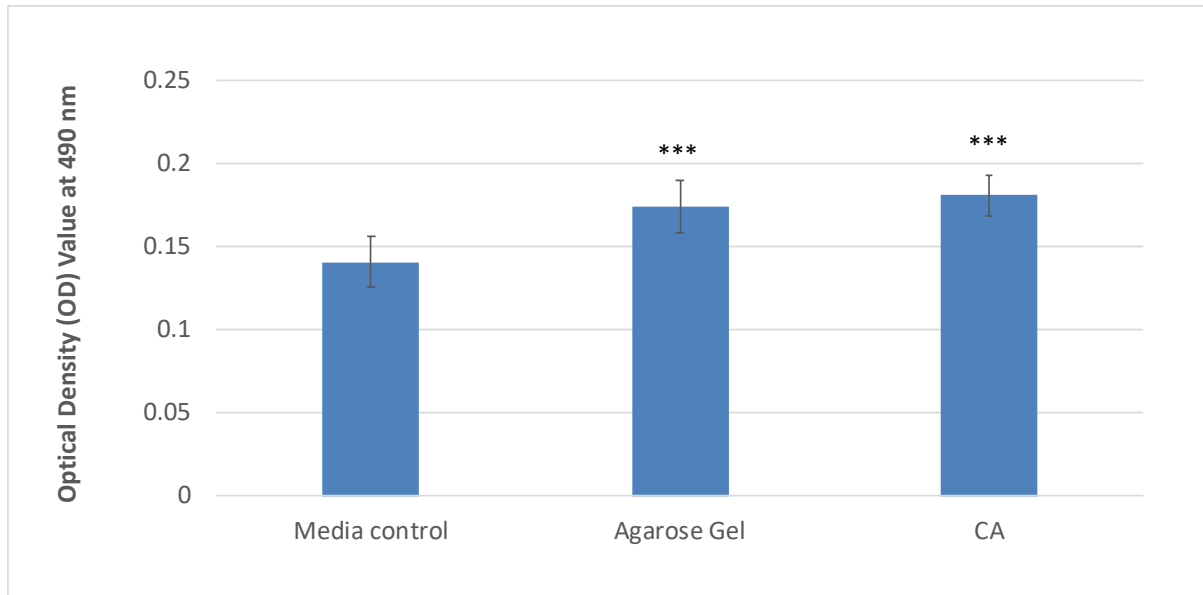


Figure 3-5 Interference of matrices without cells with MTS assay. Agarose gel and CA gel (50  $\mu\text{L}$ ) were plated in 96-well plate and solidified within 2h Complete RPMI media (100  $\mu\text{L}$ ) was added on top of matrices, media only (150  $\mu\text{L}$ ) was used as a negative control. MTS was applied after 2 hrs of incubating the media with matrices. The experiment was replicated on three separate occasions (n=3). Mean  $\pm$  standard deviation are presented. Data was analysed using a one-way ANOVA with the Tukey-Kramer post-hoc test. The significant difference was assigned at  $p < 0.0001$ (\*\*\*).

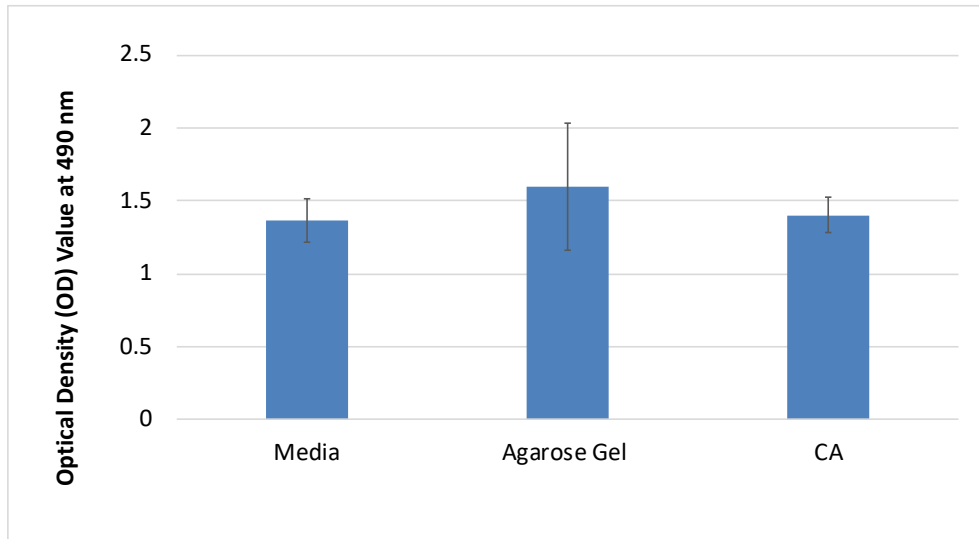


Figure 3-6 Interference of matrices with MTS Includes Dissolution of Formazan Crystals. A 96-well plate was seeded with  $20 \times 10^3$  cells/well of OVCAR cells and incubated for 24h at 37 °C and 5 % CO<sub>2</sub> to allow cell adherence. MTS reagent (30  $\mu$ L) was added to the wells and in the same time matrices (agarose gel and CA gel; 50  $\mu$ L) were added. Readings were obtained after 2h. Mean  $\pm$  standard deviation of three separated experimental replications (n=3) are presented. A one-way ANOVA with the Tukey-Kramer post-host test was used to analyse data. There was no significant difference ( $p > 0.05$ ) in OD of agarose gel and CA gel compared to negative control ( $20 \times 10^3$ /well of OVCAR cells with RPMI media only).

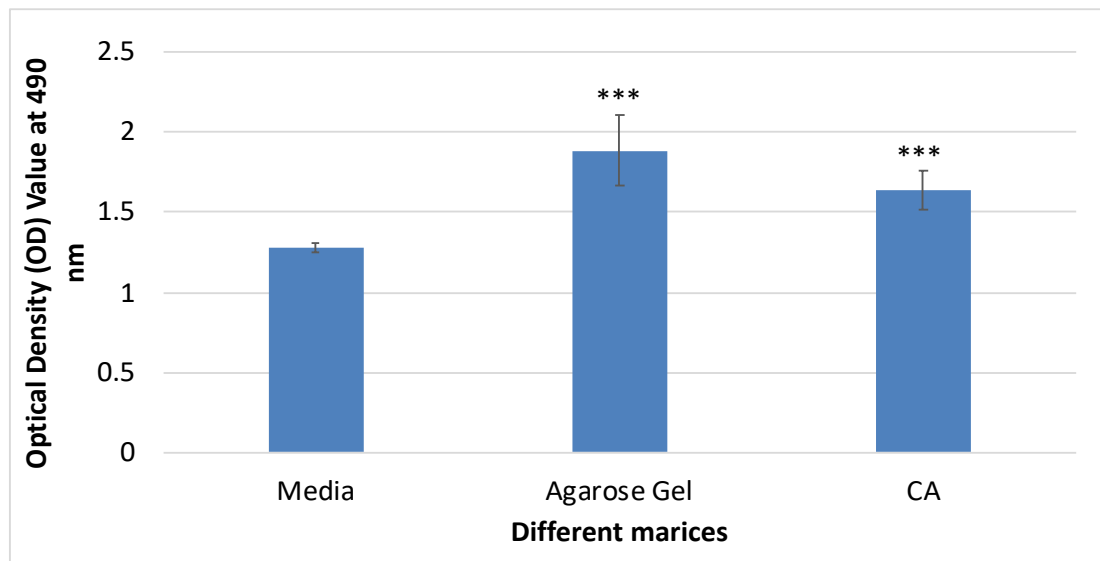


Figure 3-7 Interference of matrices with Spectrophotometer reading (at 490 nm). A 96-well plate was seeded with  $20 \times 10^3$ /well of OVCAR cells and incubated for 24h at 37 °C and 5 % CO<sub>2</sub> to allow cell adherence. MTS assay was applied and direct before reading, matrices (agarose gel and CA gel; 50  $\mu$ L) were added. Mean  $\pm$  standard deviation of three separated experimental replications (n=3) are represent. A one-way ANOVA with the Tukey-Kramer post-host test was used to analyse data. The significant difference was assigned at  $p < 0.0001$ (\*\*\*).

### 3.1.3 Interference of Agarose gel and Carboxylate Agarose gel (CA) with ELISA assay

In the absence of cells, 120 pg/mL P<sub>4</sub> was measured in control medium due to presence of 10% FCS in the medium (**Figure 3-8**), and this concentration did not change during 72h culture, indicating that the P<sub>4</sub> molecules was stable at 37 °C for 27h. the addition of agarose or CA to the culture wells did not affect the measurement in the ELISA.

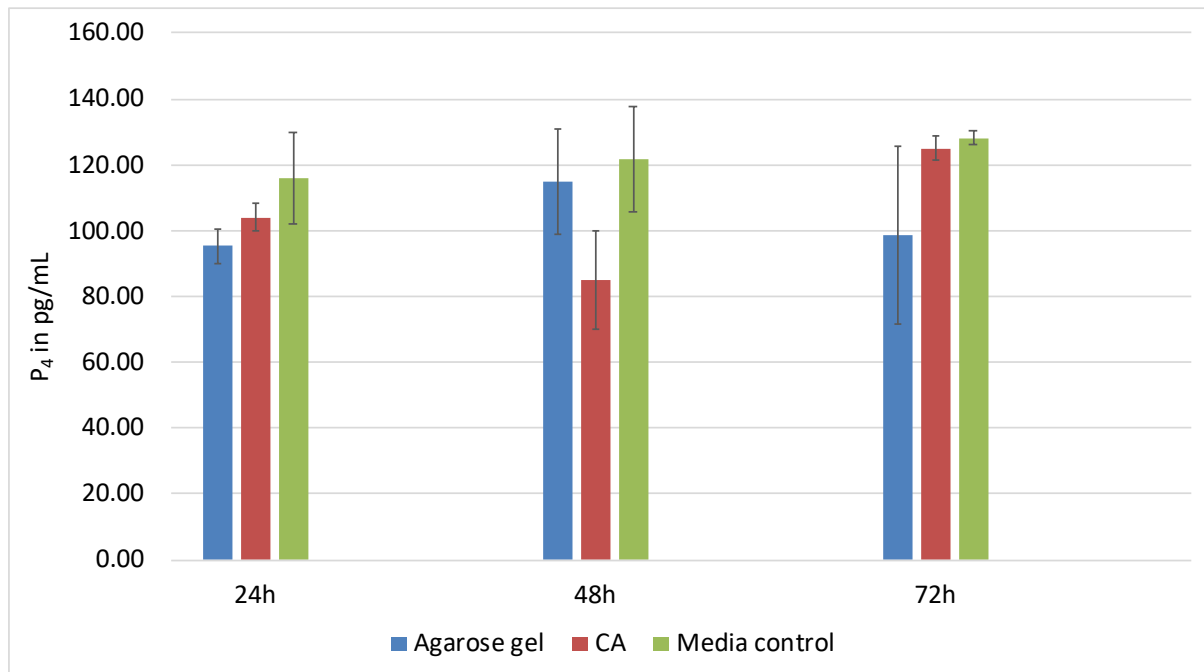


Figure 3-8 Matrices interference with P<sub>4</sub> ELISA assay. Triplicate wells of a 96 well plate was coated with 50  $\mu$ L matrices; RPMI media (control), agarose and CA and was incubated with 100  $\mu$ L media and conditioned media was collected after 24, 48 and 72 hours. Progesterone in the conditioned media was assessed in a competitive progesterone EIA in which progesterone concentration (pg/mL) was calculated by comparing with a standard curve ( $R^2=0.97$ ). Mean $\pm$ SD of three replicate experiments shown. Data were subjected to two-way ANOVA with Bonferroni post-test,  $p>0.05$  compared to control (media) at same incubation time.

### 3.2 Effect of different matrices on OVCAR cells viability

OVCAR cell viability was used to study the cytotoxicity of agarose gel and CA with or without adherence proteins (Collagen; 1 and 5%) and (fibronectin; 1 and 10 $\mu$ g/mL). OVCAR cells, cultured on the CA-coated 96-well plate after 24h and 48h, attached to the surface of the gel and keep their viability when examined in an MTT assay ( $90.2 \pm 11.1\%$ ; **Figure 3-9**) and in an MTS assay ( $89.3 \pm 7.4\%$ ; **Figure 3-10**). Adding adherence proteins to CA did not have any impact on cell attachment or viability. Microphotographs showed that OVCAR cells attached and formed a monolayer of epithelial-like cells on CA surface with or without adherence proteins(**Figure 3-11**).

In contrast, the percentage of cell viability after 24 and 48h on the agarose gel in the presence or absence of adherence proteins was significantly lower than the positive control with same culture duration(**Figure 3-9 and 3-10**). OVCAR cells accumulated in the centre of the agarose surface, forming loose cell aggregates(**Figure 3-11E**). These aggregated cells did not attach to the matrix even after coating the surface with adherence proteins (**Figure 3-11F**). The average numbers of viable cells on different surfaces were obtained by image analysis of photographs, MTT assay, and MTS assay. There was no significant differences in cell numbers after 24 and 48h culture on CA, CA+5% Collagen, CA+ 10  $\mu$ g/mL Fibronectin and agarose (**Table 3-1**). See appendix. 7 for data for some other substrates.

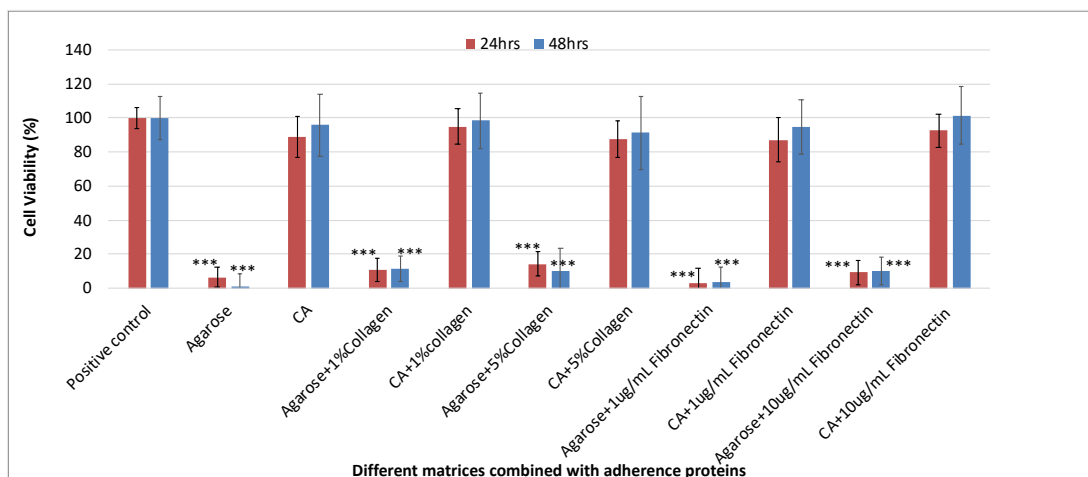


Figure 3-9 Comparison of the effect of different matrices with or without adherence proteins on OVCAR cells after 24 and 48h. Cell viability was assessed by MTT assay, in which cell number was obtained by using MTT standard curve and the matrices interference was removed by subtracting OD of matrices only. The experiment was replicated on three separate occasions (n=3). Mean  $\pm$  standard deviation are presented. Data was analysed using a one-way ANOVA with the Tukey-Kramer post-host test. The significant difference was assigned at  $p < 0.0001$ (\*\*\*) compared to positive control at the same incubation period.

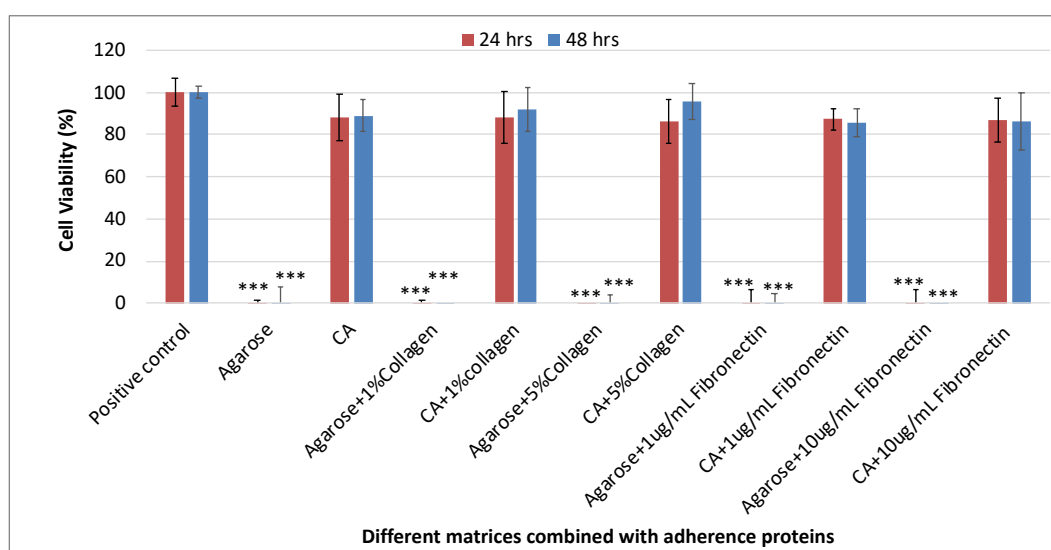


Figure 3-10 Comparison of the effect of different matrices with/without adherence proteins on OVCAR cells after 24 and 48h. Cell viability was assessed by MTS assay, in which cell number was obtained by using MTS standard curve the matrices interference was removed by subtracting OD of matrices only. The experiment was replicated on three separate occasions (n=3). Mean  $\pm$  standard deviation are presented. Data was analysed using a one-way ANOVA with the Tukey-Kramer post-host test. The significant difference was assigned at  $p < 0.0001$ (\*\*\*) compared to positive control at the same incubation period.

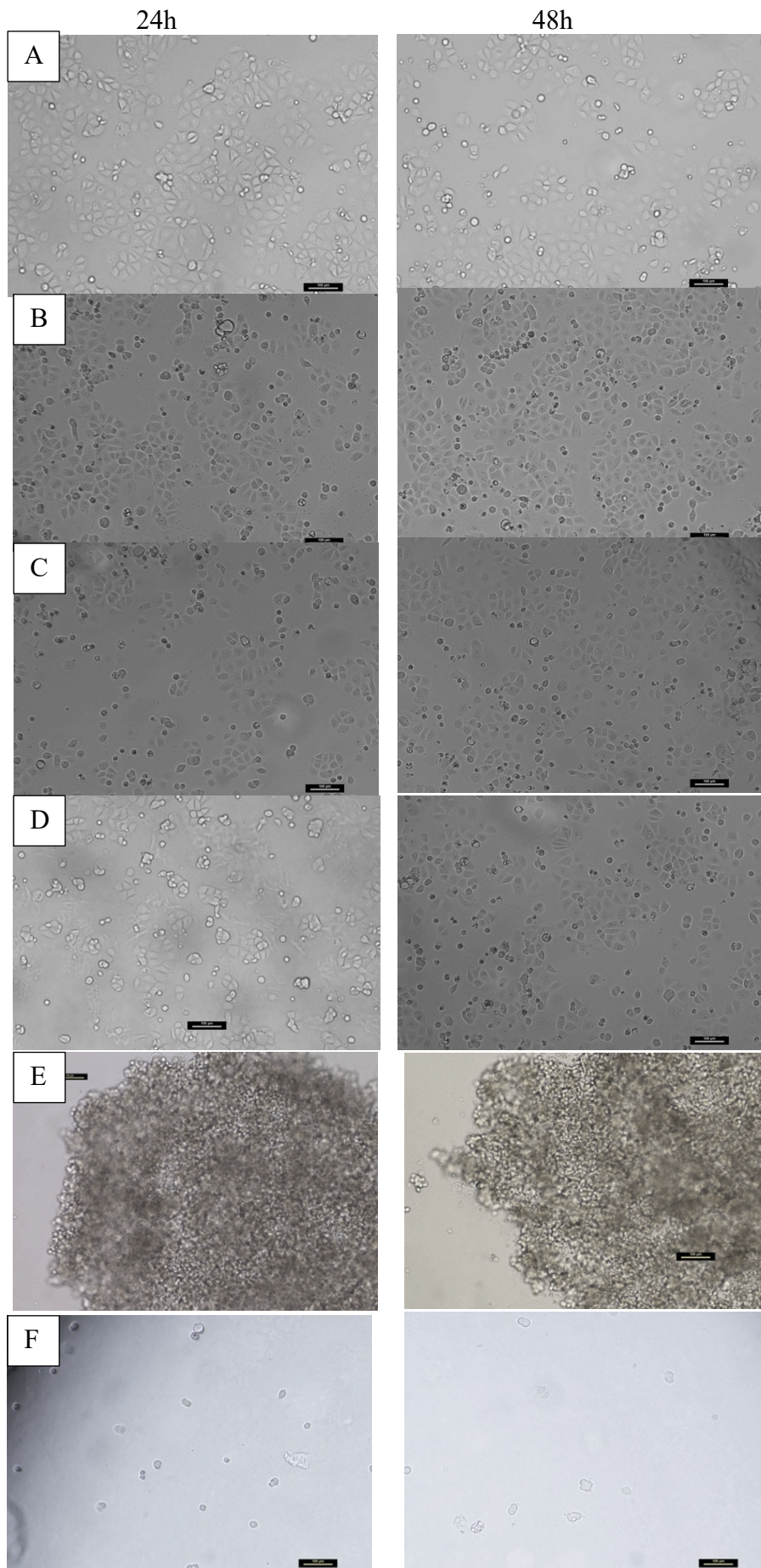


Figure 3-11 Morphology of OVCAR cells attached to surface of different matrices with/without adherence proteins. OVCAR cells ( $20 \times 10^3$ ) were cultured on 96-well plate or matrix-coated 96-well plate for 24 and 48 hrs at 37 °C and 5 % CO<sub>2</sub> (A) without matrix as a positive control, (B) CA, (C) CA+5% collagen, (D) CA+10µg/mL fibronectin, and (E) well containing agarose and unattached cells, (F) well containing agarose after aspiration of unattached cells. Images were taken using a light microscope. Represented is one of n=3 experiments at each time point. Scale bar =100 µm.

Table 3-1 numbers of viable cells determined by image analysis, MTT assay and MTS assay. After 24h and 48h incubation period at 37 °C and 5 % CO<sub>2</sub>, an ImageJ software was used to count the number of cells in 4 photos/well, then adjusted to indicate the total number of cells in the well. MTT and MTS assay were applied after 24h and 48h separately. Mean  $\pm$  standard deviation are shown. The experiment was repeated on three separate occasions (n=3). Data was analysed using a one-way ANOVA with the Tukey-Kramer post-hoc test. There was no significance difference between cell numbers obtained by image analysis, MTT and MTS assay at 24 and 48h for each substrate type (  $p > 0.05$ ).

<b>Substrates</b>	<b>Image analysis after 24h</b>	<b>MTT assay After 24h</b>	<b>MTS assay After 24h</b>	<b>Image analysis after 48h</b>	<b>MTT assay After 48h</b>	<b>MTS assay After 48h</b>
<b>Positive control</b>	17541 $\pm$ 2923	20923 $\pm$ 1290	20620 $\pm$ 1386	18100 $\pm$ 4332	19184 $\pm$ 2399	19270 $\pm$ 563
<b>CA</b>	18980 $\pm$ 5306	18551 $\pm$ 2500	18158 $\pm$ 2279	17230 $\pm$ 2414	18395 $\pm$ 3504	17120 $\pm$ 1447
<b>CA+ 5% collagen</b>	17393 $\pm$ 4433	18373 $\pm$ 2230	17808 $\pm$ 2139	19086 $\pm$ 4706	17528 $\pm$ 4095	18400 $\pm$ 1644
<b>CA+ 10<math>\mu</math>g/mL Fibronectin</b>	19046 $\pm$ 3956	19396 $\pm$ 2032	17931 $\pm$ 2160	18953 $\pm$ 4380	19467 $\pm$ 3233	16628 $\pm$ 2617
<b>Agarose</b>	ND	6.43 $\pm$ 5.841	0 $\pm$ 5356	ND	234.4 $\pm$ 1372	0 $\pm$ 2422

### 3.3 Encapsulation of OVCAR cells in Carboxylated Agarose gel (CA)

OVCAR cells were encapsulated in CA with or without adherence proteins for 48h and assessed by MTS assay. Figure. 11 shows that CA, CA+ 5% Collagen and CA+10 $\mu$ g/mL Fibronectin did not maintain cell viability for 48h ; killing 23, 28 and 24% of the cells respectively. Also, OVCAR cells had only one round morphology when they were capsulated

in the above matrices after 24h and 48h (Fig. 3-13). On the other hand, mixing 5% Collagen and 10µg/mL Fibronectin with CA supported OVCAR cells and maintained their viability ( up to 83%) after 48h (**Figure 3-12**). Within this matrix, cells with three different morphologies were distinguished (**Figure 3-13**); round , flattened , and irregular. Approximately half of the cells had a rounded morphology while the irregular shaped cells were the least frequent type (**Table 3-2**).

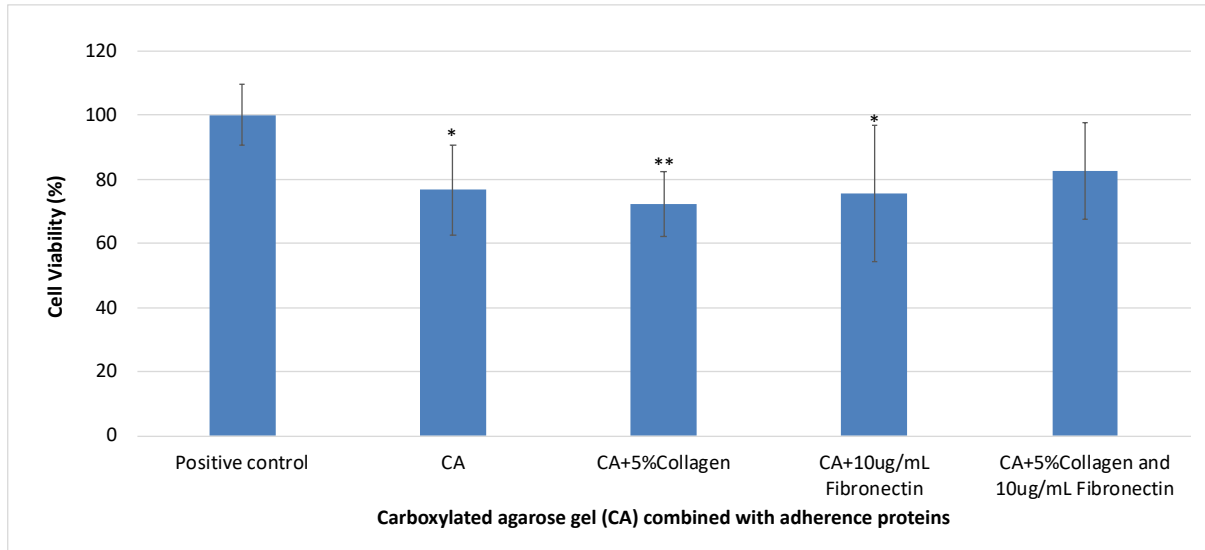


Figure 3-12 Viability of CA encapsulated OVCAR cell combined with adherence proteins. OVCAR cells ( $25 \times 10^3$ ) were encapsulated in CA with/without adherence proteins for 48 h at 37 °C and 5 % CO<sub>2</sub>. Cell viability was assessed by MTS assay, in which cell number was obtained by using MTS standard curve. The experiment was repeated three time separately (n=3). Mean  $\pm$  standard deviation are shown. A one-way ANOVA with the Tukey-Kramer post-host test was used to analyse the data. The significant difference was assigned at  $P \leq 0.05$  (\*)  $P \leq 0.01$  (\*\*) and  $p < 0.0001$ (\*\*\*).

Table 3-2 Comparison between the percentage of different cells encapsulated in CA+ adherence proteins based on morphology features. OVCAR cells ( $25 \times 10^3$ ) encapsulated in CA+5% collagen and 10µg/mL Fibronectin for 48 hrs at 37 °C and 5 %. Percentage of different cell morphology was calculated relatively to the total cells in one figure which were counted manually by using ImageJ. This data was obtained from the same experiments that done in previous figures (n=3). The Mean  $\pm$  standard deviation are shown (6 figures/ experiment).



<b>Cell morphology</b>	<b>Cell number (%)</b>
<b>Round cells</b>	49 ± 16 %
<b>Flattened cells</b>	39 ± 18 %
<b>Uncertain-shape cells</b>	12 ± 4 %

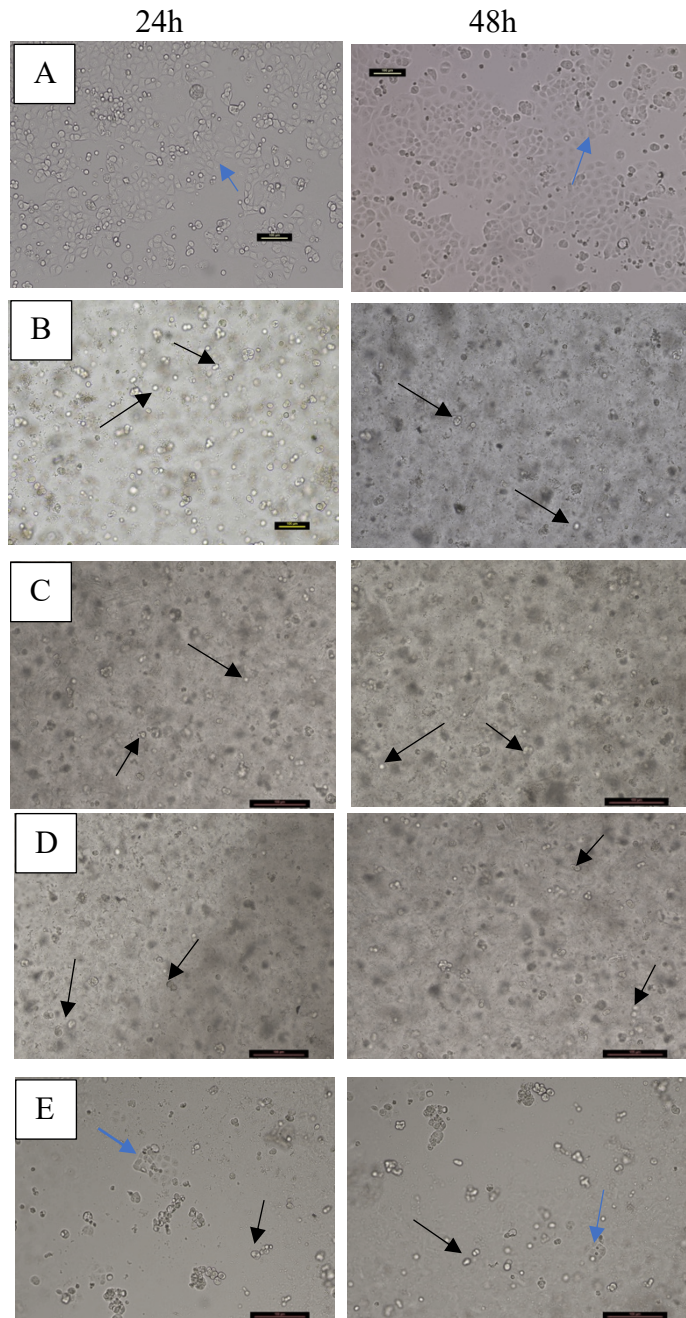


Figure 3-13 OVCAR cell morphology after encapsulation in CA matrix with or without adherence proteins. OVCAR cells ( $25 \times 10^3$ ) were encapsulated in (B) CA only, (C) CA+ 5%collagen, (D) CA+10 $\mu$ g/mL fibronectin (E) CA+ 5% Collagen and 10 $\mu$ g/mL Fibronectin and (A) positive control (cultured in 96-well plate) for 48h at 37 °C and 5 % CO<sub>2</sub>. Images were taken using a light microscope at 24h and 48h. Represented is one of experiments (n=3) at each time point. Scale bar =100  $\mu$ m. Blue arrow= flattened cells, Black arrow= round cells.

### 3.3.1 P<sub>4</sub> production by encapsulated OVCAR cells in matrices

Even though CA, CA+ 5% Collagen and CA+10µg/mL Fibronectin did not support OVCAR cell viability as well as CA+ 5% Collagen+10µg/mL Fibronectin (**Figure 3-12**), the ability of OVCAR cells to produce P<sub>4</sub> was not affected by 48h culture in the presence of any of the matrices (**Figure 3-14**).

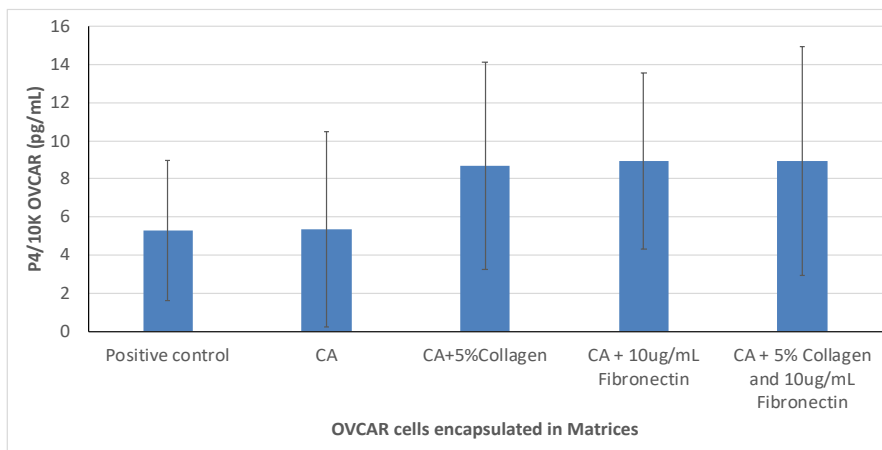


Figure 3-14 progesterone (P<sub>4</sub>) Produced by encapsulated OVCAR cells. OVCAR cells ( $25 \times 10^3$ ) were encapsulated in CA with/without adherence proteins for 48h at 37 °C and 5 % CO<sub>2</sub>. Conditioned media from three separate experiments (n=3) were then subjected to ELISA to measure Progesterone production per 10,000 OVCAR cells. The Mean  $\pm$  standard deviation are presented and one-way ANOVA with the Tukey-Kramer post-host test was applied.

## 3.4 Encapsulation of Oviduct cells in matrices:

### 3.4.1 Disaggregation of Primary-Derived Oviduct Cells

Oviduct from six mice were disaggregated using 1% Collagenase type1 and isthmus section was excluded. The average size of the oviduct was  $304 \pm 28 \mu\text{m}$  (Fig. 3-15). The highest yield was 7337 cells/10µm (**Table 3-3**).

Table 3-3 Oviduct cells yield. Oviducts from 2 mice/ experiment; n=6 animals were disaggregated by 1% collagenase type 1. Trypan blue assay was utilised to obtain cell yield for each oviduct

Mouse weight (g)	Mouse age (wks)	Oviduct size ( $\mu\text{m}$ ) (excluding isthmus)	Cell yield/10um
24.49	17	318	7337
24.23	16	294	
17.6 (swollen)	7	315	3828
17.5	6	312	
17.68	7	337	6826
18.67	8	249	

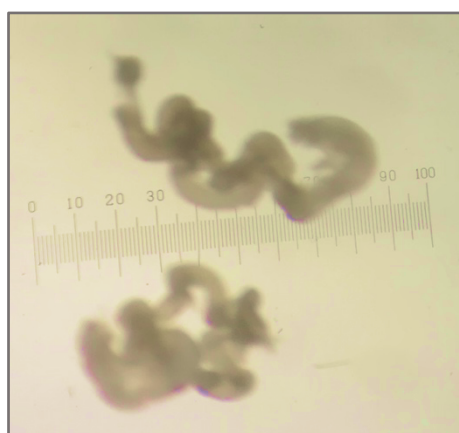


Figure 3-15 Dissected oviducts. Photo was taken directly after dissecting oviduct from female mouse. Representative of three separate experiments (n=3). Scale bar = 1.5  $\mu\text{m}$ .

### 3.4.2 Encapsulation of Primary-Derived Oviduct Cells in CA $\pm$ Adherence Proteins

By encapsulating primary-derived oviduct cells in CA and CA+ adherence proteins for 48h, it was found that the latter maintained the viability of primary-derived oviduct cells in comparison with the positive control, but CA did not (**Figure 3-16**).

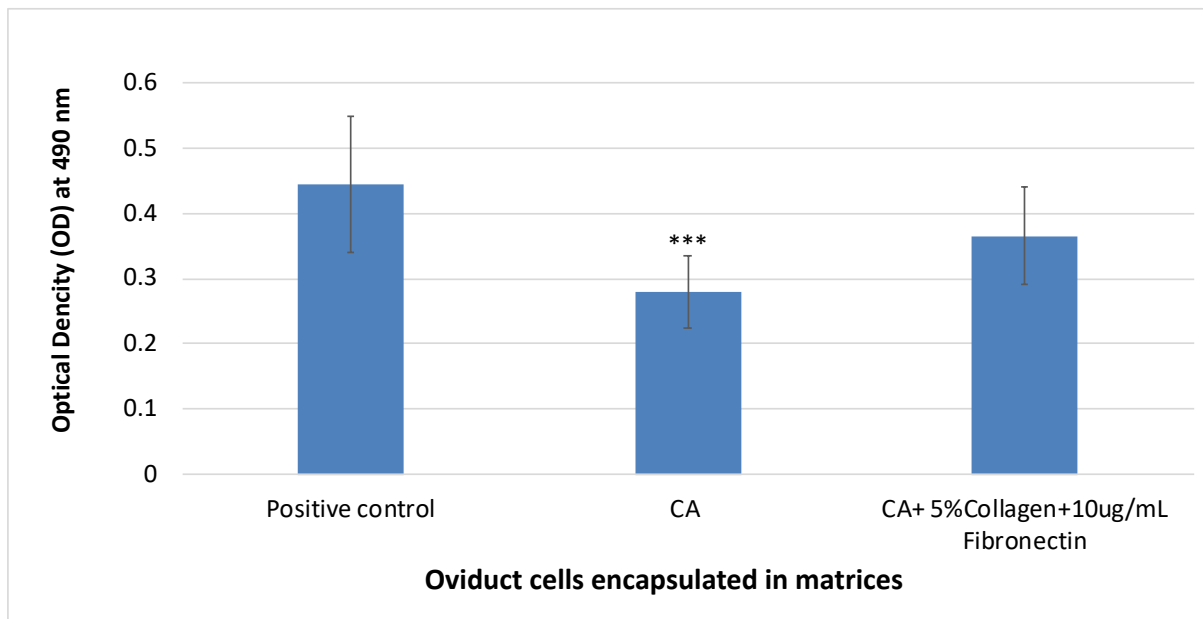


Figure 3-16 Cell viability of primary-derived oviduct cells encapsulated in different matrices. Primary-derived oviduct cells ( $10 \times 10^3$ ) were encapsulated in CA with/without adherence proteins for 48h at 37 °C and 5 % CO<sub>2</sub> before applying an MTS assay. A one-way ANOVA with the Tukey-Kramer post-host test was used to analyse the data. Mean  $\pm$  SD are shown (n=3);  $p < 0.0001$ (\*\*\*) compared with positive control.

Figure. 16 shows the presence of different cell types in positive control( 96-well plate without gel). Cells with two types of morphology were distinguished: ciliated cells (black arrows) and round cells (blue arrows). Furthermore, cells with the same morphologies were found inside CA in presence or absence of adherence proteins. Interestingly, cilia beating was noticed in the positive control as well as in CA+ adherence proteins matrix up to 48h but not found in CA only.

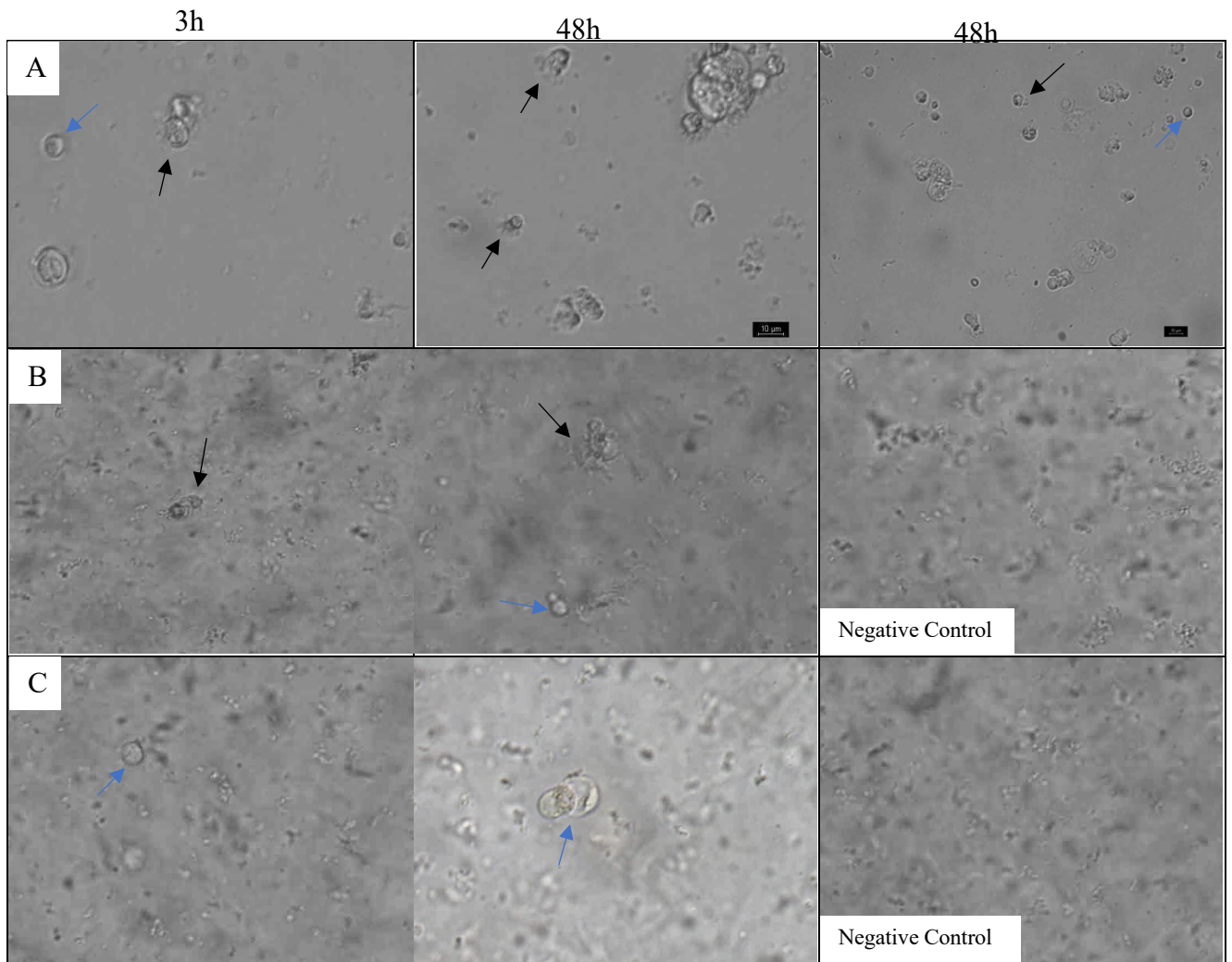


Figure 3-17 Morphological features of primary-derived oviduct cells encapsulated in CA matrix with or without adherence proteins. OVCAR cells ( $25 \times 10^3$ ) were encapsulated in (A) positive control (no matrix well), (B) CA only and (C) CA+ 5% Collagen and  $10\mu\text{g}/\text{mL}$  Fibronectin for 48 hrs at  $37^\circ\text{C}$  and 5%  $\text{CO}_2$ . Images were taken using a light microscope at 3 and 48h. Represented is one of the experiments ( $n=3$ ). Scale bar is written on the figures. Black arrow= ciliated cells, Blue arrow= round cells.

## 4 Discussion

Although the recent development of 3D-bioprinting has attracted attention, it needs a great deal of preparation, optimisation, and identification of suitable biomaterial that is compatible with mammalian cells. In this project, candidate biomaterials (agarose and carboxylated agarose gel) were tested for their ability to support primary-derived oviduct cells. Furthermore, the role of adherence proteins in improving the matrix properties was evaluated.

OVCAR cells did not attach on agarose gel surface, and adherence proteins made no difference with agarose gel. On other hand, CA supported OVCAR cells attachment. Also, the highest viability of encapsulated OVCAR cells was noticed in CA mixed with adherence proteins. Furthermore, CA mixed with adherence proteins maintained viability of encapsulated primary-derived oviduct cells for 48h, and some characteristics such as cilia beating also maintained.

### 4.1 Interference of Different Matrices with Different Assays

To determine the suitability of different matrices for 3D cell culture, the viability and functionality of the cells needs to be evaluated. Current methods for measuring cell viability; the MTT, MTS assays, have been designed for use with monolayer cell cultures and have not been optimised for 3D culture (Antoni et al., 2015). In this study, the interference of candidate gels in these assays was evaluated by the addition of gel solutions at various steps in each assay procedure. Inclusion of gels caused statistically significant differences in some steps of the MTT and MTS assays. In normal control medium without cells, there was a production of formazan crystals. It has been reported that common components such as L-glutamine in RPMI medium contribute to the amount of formazan produced (Huang et al., 2004). Another factor is pH because MTT forms formazan spontaneously when the  $\text{pH} > 5.5$  (Hansen et al., 1989). Chakrabarti et al. (Chakrabarti et al., 2001) stated that some serum components such as albumin influenced the tetrazolium assays by causing production of formazan products (Young et al., 2005) (Chakrabarti et al., 2001).

Agarose gel without cells (but not CA) significantly increased this non-specific background production of formazan in the MTT assay (Fig. 3-2). That could be because of the difference in the cross-linked networks between agarose and CA (Forget et al., 2017). This may cause light scattering; resulting in higher non-specific background value associated with the possible destruction of the gel network. Neither of the matrices, in presence of cells, affected dissolution of cells and formazan crystals with acidified SDS, and neither of them affected spectrophotometer reading of the homogenous solution in MTT assay (Fig. 3-3 and 3-4).

The effect of matrices on the MTS assay was similar to the MTT assay, although the MTS assay more sensitive to interference than the MTT assay. In the MTS assay, both agarose and CA increased production of formazan in the absence of the cells (Fig. 3-5) and that probably due to the same reasons that mentioned above. Neither matrices affected acidified SDS dissolution of formazan crystals, and unlike the MTT assay, both matrices increased OD values (Fig. 3-6 and 3-7). The MTS assay reading was obtained at 490 nm with non-reference in these experiments which means no background correction was applied. The goal of background correction is to remove the likelihood of any interference, and that did not happen here because the reading was taken without background correction (Wang et al., 2010).

Putting all together, these results necessitated that in further cell viability experiments (MTT and MTS assay), interference was measured by the use of a negative control (gel only or media only) at the specified absorbance for each assay, and subsequently subtracted from the treatment values obtained. This allows direct comparison with the positive control (cells), without spectrophotometric interference from the gel or media itself.

## **4.2 Effect of different matrices on OVCAR cells viability:**

Cell viability assays were initially performed to characterise the survival of OVCAR cells cultured on the surface of agarose and modified agarose gels with or without adherence proteins. Despite the use of adherence proteins, the OVCAR cells were not able to attach to the agarose cell surface. Instead, the cells aggregated above the gel and were lost following aspiration of the media. The MTT and MTS assays indicated the presence of a very low number of cells, however microscopy indicated that the viable cells were not attached to the agarose gel. Structurally, agarose contains a hydroxyl group and does not possess any ionised groups. As a consequence, the adherence proteins were not able to bind to the surface of the agarose molecules (Forget et al., 2017). It is possible that proteins generated by the OVCAR cells were also unable to bind to agarose because of the lack of adhesion domains. This incompatibility between cells and agarose has been noted for human umbilical vein endothelial cells (HUVECs), which attached weakly to agarose gels and were lost in the washing step performed prior to a Live/Dead assay (Benning et al., 2018). Weak attachment of the cells to this gel, as indicated by the rounded phenotype of endothelial cells (ECs), is caused by the absence of arginine-glycine-aspartate (RGD)-binding integrins in the agarose that are required for focal adhesion contacts. Furthermore, 3T3 fibroblasts cultured on glass substrates coated with agarose had abnormal morphology and formed aggregates of dead cells (Yixue et al., 2013). However, Au *et al.* showed that a combination of agarose and collagen allowed the covalent



attachment of both canine hepatocytes and human neoplastic hepatocellular carcinoma (HepG2) cells to a surface (Au et al., 2012). Although the use of adherence proteins to facilitate cell attachment in the presence of agarose has been reported (Aizawa et al., 2008), (Au et al., 2012) and (Connelly et al., 2011), in the current study the addition of collagen and fibronectin to agarose did not improve cell attachment to agarose. The procedure that followed in this study was pouring a collagen or fibronectin solution over the gel surface and washing the excess after 18h incubation. This procedure may result in detachment of collagen or fibronectin during the washing step. Thus, OVCAR cells did not attach to coated-agarose gel.

Since agarose gels were not able to support cell growth even in the presence of adherence proteins, a carboxylated agarose (CA) was evaluated as an alternative matrix in the viability assays. OVCAR cells were able to successfully attach to CA gels, in both the presence and absence of adherence proteins. This can be explained by the negatively charged ions of the carboxyl acid group in the CA, which interacts electrostatically with positively charged proteins (Yixue et al., 2013). These proteins can be either adherence proteins added to the surface, or the proteins in the extracellular matrix produced by the cells themselves. Carboxylation of agarose has been previously reported as an effective matrix for cell adhesion, with a well-ordered monolayer arrangement of 3T3 fibroblast cells observed on glass substrates coated with a synthesised CA (Yixue et al., 2013). Therefore, the addition of a functional carboxyl group to agarose is a way of successfully utilising agarose gels as a biomaterial. Furthermore, OVCAR cell numbers on surface of CA gel were as expected to be, seeding  $\approx 18 \times 10^3 \pm 2 \times 10^3$  and after 48h around same numbers were obtained. OVCAR cells has 69h doubling time so it was not expected for the cell number to increase after 48h (ATTC, 2016).

### **4.3 Encapsulation of OVCAR cells in CA with or without adherence proteins.**

CA with and without adherence proteins was used for the encapsulation of OVCAR cells, to determine the behaviour of cells within a 3D culture. OVCAR cells were viable (83%) when they were encapsulated in CA with collagen and fibronectin together, compared to the positive control (cells cultured on treated plastic without matrix or proteins). Additionally, flattened cells were observed with this matrix, indicating that the cells were attached to the 3D gel, whereas cells in CA, CA+collagen and CA+fibronectin possessed round morphology, signifying that they did not successfully attach within the fibres of the gel. Differences between

the CA+collagen+fibronectin and the other three groups are likely to be the result of collagen binding cells to the matrix, and fibronectin connecting collagen with the cells. In native tissue, fibronectin connects collagen fibres to cell surface via integrins that found in cell surface, which all together make the ECM (Mao and Schwarzbauer, 2005). Therefore, the addition of both fibronectin and collagen in the CA gel serves to enhance cell attachment and viability. CA, CA+collagen and CA+fibronectin groups demonstrated significantly ( $p < 0.05$ ) lower cell viability than in the positive control. The positive control contained cells in media only, which would facilitate the transportation of nutrients and the diffusion of oxygen to the cells. OVCAR cells encapsulated in the gel and proteins are were dependent upon slower diffusion of nutrients and oxygen from the matrix surface. Encapsulated OVCAR cells were assessed for progesterone production using an ELISA. The results of this assay indicated that there was no difference in the ability of the cells to produce this hormone within a 3D culture, using various CA and adherence protein matrices. From the encapsulation of OVCAR cells in combination of CA and adherence protein matrices, the findings indicate the use of CA mixed with fibronectin and collagen to be the most effective for 3D culture, and led to assessment of this matrix for use with primary-derived oviduct cells.

#### **4.4 Encapsulation of primary-derived oviduct cells in matrices:**

The primary-derived oviduct cells were first isolated from murine oviducts by enzymatic disaggregation. The cell morphology was monitored following 2D culture at 3, 6, 24 and 48 h using light microscopy, and there was no difference in cell morphology at any timepoints. Features such as ciliation, size and shape were noted, but it was not possible to distinguish further between cell types using light microscopy. A mixed population of cells was observed in the culture of disaggregated cells. Descriptions of cell morphology in the literature enabled basic identification of cell categories. Komatsu and Fujita (1978) identified the presence of both ciliated and secretory cells in the oviduct of at least 23 day old mice. In the present study, the age of mice ranged from 42 – 140 days, indicating that the differentiation of epithelial cells had been completed (Komatsu and Fujita, 1978) (Stewart and Behringer, 2012). Ciliated epithelial cells are characterised by the presence of beating cilia, which could be seen in the disaggregated primary-derived oviduct cells (Djahanbakhch et al., 1999). Cells without cilia were also found, but their classification is not straightforward as there are at least 3 types of rounded non-ciliated oviduct cells reported; secretory cells, basal cells and intercalated (peg) cells are all depicted as small and round non-ciliated cells of the oviduct (Ezzati et al., 2014) (Crow et al., 1994).

The mixed population of disaggregated primary-derived oviduct cells were encapsulated in both CA and CA+adherence proteins, to produce a tissue culture model partially representative of the native tissue. The addition of adherence proteins to the gel enhanced oviduct cell viability when cultured in the 3D form for the same reasons mentioned above about role of fibronectin and collagen in native tissue. Morphologically, the cell characteristics were maintained in the 3D culture, as the beating of cilia was observed in the CA+adherence protein group up to 48 h. Although beating cilia were not found in the CA, the ability of this matrix to support cilia beating should not be excluded. This is because of a limitation associated with the microscopy method, as not every plane of the gel can be viewed and therefore the ciliated cells beating may not be observed. The morphology of the 3D cultured cells was not examined after 48 h, because the viability assay was performed at this time point. Therefore, beating cilia could potentially be identified in the matrix after this designated period.

#### **4.5 Conclusion:**

To our knowledge, this is the first time that a mixed population of primary-derived oviduct cells have been cultured in 3D form. In this study, we found that encapsulation of primary-oviduct cells in carboxylated agarose mixed with adherence proteins maintained the viability and morphological characteristics of cells, such as cilia beating, relative to the non-encapsulated primary-oviduct cells.

#### **4.6 Future work:**

The biomaterial (CA and adherence protein matrix) that has been developed as a scaffold for 3D culture of oviduct cells in this project provides a basis for future development in the Bill and the Melinda Gates project. This wider project aims to 3D bio-print a complete and functional oviduct. For future work, it is key to confirm the identity of cells in the mixed population disaggregated from murine oviduct using immunohistochemistry. Knowledge of the secretions of cells in the matrix is also required to improve the functionality of the final 3D printed model.

## Appendix

### Appendix.1

#### Chemicals, reagents, tools, and instruments details

Materials	Supplier	Lot#	Cat#
NaCl	Merck		S3014
KCl	Sigma-Aldrich		A383-500g
Na <sub>2</sub> HPO <sub>4</sub>	Sigma-Aldrich	5921	
KH <sub>2</sub> PO <sub>4</sub>	Sigma-Aldrich		P0662-500g
Trypsin- EDTA	Sigma-Aldrich	SLBV0764	T4174
RMPI-1640 media	Sigma-Aldrich	RNBG4128	R8758
penicillin- streptomycin solution	Sigma-Aldrich	106M4809V	P4333
Liquid media supplement (ITS)	Sigma-Aldrich	SLBS7045	I3146
Foetal bovine serum (FBS)	Scientifix Life	60258A	Code FFBS-500
.22 µm filter	Minisart®		
Thiazolyl blue tetrazolium(MTT)	Sigma-Aldrich		M5665-1G
Hydrochloric acid (HCl)	BDH Chemicals		10125
Sodium dodecyl Sulphate (SDS)	Sigma-Aldrich		L4509
Trypan blue	Sigma-Aldrich		T0776
Agarose powder	Bio-Rad Labratoreies, Inc		161-3101
collagen (type I and III) bovine	PureBulk	2017080404	
Fibronectin bovine plasma	Sigma-Aldrich		F4759
T75 flask	Thermos scientific	154118	
Incubator	Thermos scientific	Model # 371	
Centrifuge	Eppendorf	Centrifuge 5804	
96-well plate	Costar	24215009	

Spectrophotometer	BioTek Microplate	Quant		
Microscope	Nikon		EclipseTs2R	Code 104174
MiliQ Water	Millipore			
MTS powder (tetrazolium reagents)	promega			Part # G111B
Phenazine ethosulfate (PES)	Sigma-Aldrich			P4544
Collagenase from Clostridium histolyticum	Sigma-Aldrich		SLBB0923V	C0374-100mg
Minimum Essential Medium Eagle	Sigma-Aldrich		RNBG0393	M4526-500ML
Dulbecco's Modified Eagle's Medium	Sigma-Aldrich		RNBG2219	D8437-500ML
Antibiotic antimycotic solution	Sigma-Aldrich		126M4750V	A5955-100ML
L-Glutamine solution	Sigma-Aldrich		RNBF8553	G7513-100ML
Epidermal growth factor (EGF) from mouse	Sigma-Aldrich			SRP3196

## Appendix. 2

### **Sperm capacitation:**

The ability of mammalian sperm to fertilise an oocyte, known as 'fertilisation capacity' has to be acquired through time spent in the female reproductive tract. During process of 'capacitation', sperm undergo changes that allow it to achieve the acrosome reaction and penetrate the oocyte (De Jonge, 2005, Suarez, 2016). an acrosome is a cap-like structure full of enzymes that covers the sperm head. In term of making penetrating the egg hard shell easier, sperm use the enzymes that are inside the acrosome to fuse with the egg (Okabe, 2018).The capacitation process and the acrosome reaction are proposed to be separate and distinct processes, with the acrosome reaction marking the completion of capacitation (De Jonge, 2005)

## Appendix. 3

### **Role of oviduct in sperm capacitation**

The oviductal conditions are crucial for ensuring prolonged sperm survival, until the optimal time of fertilisation. The oviduct also comprises one part of a larger strategy that aims to select the fittest sperm for fertilisation. Particularly, sperm are required to overcome many stages of passage through the reproductive tract and interactions with the oviduct environment in order to reach and fertilise the oocyte. Sperm interact with the oviduct in either physical or molecular ways. Physical interactions refer to movement of sperm in response to the cellular architecture of the oviduct walls and the flow of fluid, which has been measured in a mouse oviduct at  $18 \pm 1.6 \mu\text{m/s}$ . Molecular interactions are typified by communications between molecules on the sperm surface and oviductal receptors lining the epithelium. Specifically, the oviductal surface possesses carbohydrate molecules, specifically a glycosylated receptor at sperm binding sites that are of importance to interactions with sperm. The structure and characteristics of the epithelial receptor carbohydrates vary between species. The molecular interactions between oviductal epithelium and sperm facilitate the attachment of sperm to the epithelium (Suarez, 2016).

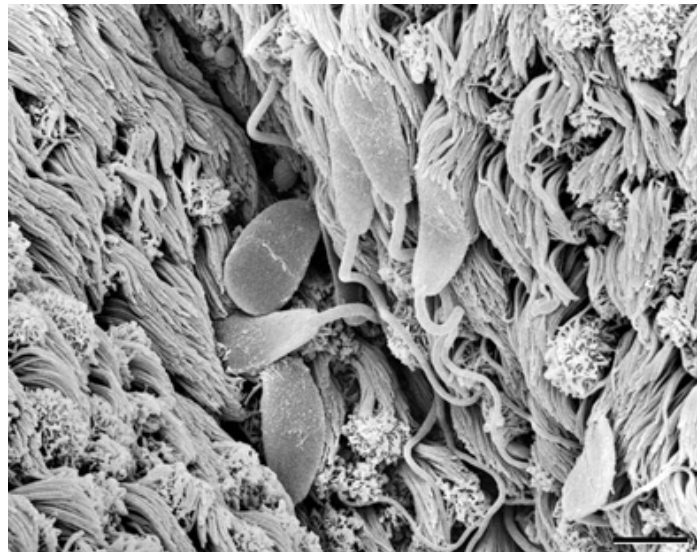


Figure 4-1 Scanning electron micrograph of sperm bound to cilia on the epithelium of the oviductal isthmus.(*bar* = 10  $\mu\text{m}$ ; (Lefebvre et al., 1997))

For capacitation and fertilisation to occur, sperm are required to attach and detach from the oviduct epithelium(Fig. 1-5). Despite previous reports of a singular attachment and detachment process, Chang and Suarez (Chang and Suarez, 2012b) have determined that an individual sperm can instead attach and detach several times during its' passage through the oviduct (Suarez, 2016). Sperm attachment to the oviduct epithelium has been used to explain the role of the oviduct in facilitating the development of a sperm reservoir (De Jonge, 2005).

Maintaining a sperm reservoir in the lower portion of the oviduct as serves as a strategy to prevent poly-spermic fertilisation, as fewer sperm will reach the oocyte at the same time (Suarez, 2016)(Fig. 1-6). It had been initially proposed that the sperm reservoir only occurred in the isthmus region of the oviduct, although sperm binding receptors were identified in the ampulla also. Recent research has confirmed that the presence of binding receptors in the ampulla also promotes sperm binding in the upper region of the oviduct. In this study, mutant Acr-EGFP male mice that produce sperm with a fluorescent acrosome were mated with peri-ovulatory wild type mice. The oviducts were examined 3 hours later to evaluate the fluorescence and determine the movement and location of the sperm. Of the few sperm found in the ampulla, most were bound to the epithelium and attached for a few minutes, which suggests that sperm continue to bind to the oviductal epithelium as they move up the tract. Comparisons between free-swimming sperm and attached sperm, in regards to morphology and DNA fragmentation, have identified the attached sperm as of superior quality(Chang and Suarez, 2012a). Despite the ability of sperm to bind to oviductal explants *in vitro*, Williams et al., (Chang and Suarez, 2012b) failed to demonstrate that sperm were bound to the epithelium of surgically excised oviducts post-insemination (De Jonge, 2005).

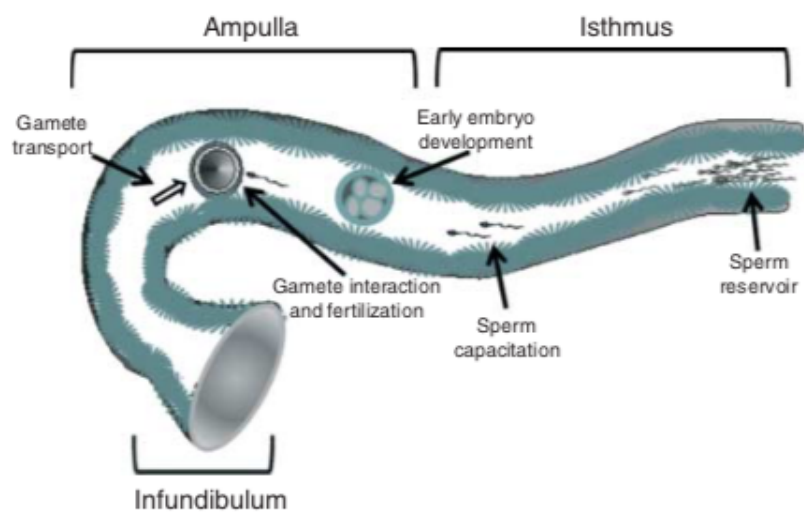


Figure 4-2 Schematic view of the oviduct and sperm journey inside it.

Sperm detachment from the oviduct epithelium occurs through either modifications of cell surface proteins, or hyperactivation of motility. The role of each of these mechanisms in cell detachment is likely to be species specific. A change in the proteins on the sperm surface may reduce binding affinity for epithelial receptors. This has been demonstrated using the capacitated sperm of hamsters, where the fetuin ligand was no longer detected in the acrosomal

region of the sperm, preventing sperm binding again to the oviduct epithelium receptor sialic acid after capacitation. Hyperactivation of motility causes an increase in force that allows the sperm to pull away from the oviduct epithelium (Suarez, 2016). In particular, the sperm use a rocking motion to tear themselves away from the cilia (Coy et al., 2012). The oviduct environment may contribute to the detachment of sperm through triggering hyperactivation, caused by factors secreted from the epithelium, hormonal signals that induce ovulation or signals from preovulatory follicle. Sperm that are bound to oviduct membrane vesicles have also demonstrated lower levels of cytoplasmic  $Ca^{2+}$ , compared with free swimming sperm. Sperm break free from oviductal epithelium, through alteration of receptors on the epithelium, or loss or alteration of ligands on the sperm. The  $Ca^{2+}$  present in the sperm cytoplasm is associated with the sperm capacitation process. Catalase that is present in the oviduct protects sperm against peroxidative damage, which has been proposed as a way of increasing sperm permeability to  $Ca^{2+}$  for completion of capacitation (Suarez, 2016).

The stimulation of capacitation in an *in vitro* co-culture of sperm and oviductal cells has not been consistently demonstrated. The use of hyperactivation as the marker for capacitation has been used by Kervancioglu et al. (2000) to indicate the importance of oviductal cells to the capacitation process. Conversely, the use of the acrosome reaction as a marker for the end-point of capacitation has yielded varied results, with both stimulation and stabilisation of the acrosome reaction demonstrated when sperm are co-cultured with oviductal cells (De Jonge, 2005). It is generally accepted that incubation of sperm with oviduct epithelium prolongs sperm viability when compared with incubation in sperm media alone. Additionally, Pollard and colleagues (Pollard et al., 1991) have demonstrated that even incubation in similarly ciliated tracheal epithelium results in decreased sperm viability, compared with oviduct epithelial cells. These findings infer that there are other factors present in oviduct epithelium that are more crucial to sperm survival. It should be noted that sperm viability can be extended by incubation in vesicles derived from apical membranes of oviductal epithelium, indicating that it is the binding between sperm and oviductal epithelial cells that is important to improved viability, rather than just the cell secretions (Suarez, 2016)(Fig. 1-7).



The amount of sperm entering the oviduct can number hundreds of millions, however for successful fertilisation only one sperm and one oocyte are required. At each stage of the sperm's passage through the reproductive tract, there will be some loss of sperm numbers. For successful transport, sperm need to be vigorously motile, with normal morphology and a functioning plasma membrane. Sperm loss can be attributable to a premature and degenerative acrosome reaction, or leukocyte-produced reactive oxygen molecules that cause deleterious effects to sperm, rendering them inviable. Sperm demonstrate a preferential attraction to the ampullary region of the ovulatory side of the oviduct, where the ovulatory follicle is located. This difference in sperm quantity between the contralateral sides of the oviduct has not been noted for the isthmic regions (De Jonge, 2005). Those sperm that eventually enter the ovulatory oviduct and attach to the oviduct epithelium may be only a few hundred in number, although not all of these sperm will be able to detach successfully. The cumulus complex and zona surrounding the oocyte serve as a final barrier for sperm, through which 10-20 sperm may reach the zona surface, with penetration of the oocyte occurring from a single sperm (De Jonge, 2005).

#### Appendix. 4

##### **Passive *in Vitro* Cell Adhesion**

Passive *in-vitro* cell adhesion process is takes place in a static medium culture. For example, culture flasks, petri dishes etc. In the process of static *in-vitro* matrix attachment and spreading, cells encounter morphologic modifications driven by passive changes and dynamic redesign of the cytoskeleton. The cell adhesion and spreading is maintained by Integrin receptors and heterodimeric transmembrane proteins. The integrin binding initiates mechanical linkage between the intracellular actin cytoskeleton and extracellular cell matrix. It also provides pathways for bidirectional transmembrane signalling (Geiger et al., 2001). Integrins allow soluble ligands and insoluble extracellular cell matrix multi-proteins. The interaction between soluble ligands and extracellular matrix proteins develop cytoskeleton. The linkage of integrins with their ECM proteins actuates the Rho GTPase family that includes Rho, Rac, and Cdc42. The Rho family of small signalling G protein which is actively involved in spreading and migration of cells. Rho regulates the mechanical stresses and cluster of focal adhesions (Khalili and Ahmad, 2015).

The procedure of static *in-vitro* cell adhesions is portrayed by three phases. The first stage is the attachment of the cell body to its substrate. Next stage is the spreading of cell body. The

final stage includes the organisation of the actin skeletal framework with development of focal adhesion in the cells. After the process of cell spreading, actin organises itself into microfilaments clusters. When the cell bonds with another cell or substrate, the strength of adherence increases gradually. The initial adhesion between the cells and the substrate are regulated by the particular integrin-interceded attachment and begins with the linkage of single receptor-ligand sets (Hong et al., 2006). This process activates the consequent receptor-ligand bonds and rapidly upgrade in number, subsequently expanding the aggregate adhesion strength (Taubenberger et al., 2007).

The adhesion mechanisms and properties between cells or their substrates could be determined by studying the different cell-substrate interaction durations. After the initial stage of adhesion, cells continue spreading on the substrate; and consequently decreases the cell height and increases the contact area (Phase I) (Huang et al., 2003). Following that, the cell spreads past the anticipated area of the un-spread round cell (Phase II) (Hong et al., 2006). The spreading procedure is the blend of proceeding with attachment with the redesign and circulation of the actin skeleton around the cell's body edge (Huang et al., 2003). Finally, cells will achieve their greatest spread area through development and adhesive characteristics become greater (Phase III) (Khalili and Ahmad, 2015)(Fig. 1-8).

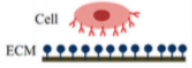
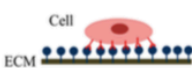
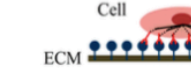



Cell Adhesion Phases	Phase I	Phase II	Phase III
Schematic diagram of cell adhesion			
Schematic diagram of the transformation of cell shape	 Initial attachment	 Flattening	 Fully spreading and structural organization
Cell adhesion intervention	Electrostatic interaction	Integrin bonding	Focal adhesion
Adhesion stages	Sedimentation	Cell attachment	Cell spreading and stable adhesion

Figure 4-3 Passive *in vitro* cell adhesion stages (Khalili and Ahmad, 2015).

## Appendix. 5

### Comparison between 2D and 3D Cultures

*In vitro* 2D cell culture systems do not provide an adequate platform for studying native cell behaviour due to inability to represent *in vivo* cell responses. However, behaviour of cells *in vivo* can be studied using three dimensional (3D) cell culture. The properties and capabilities of 3D cell culture have resulted in this method becoming increasingly popular over the past two decades. While high-throughput *in vitro* 2D cell culture has been widely applied to study novel therapeutic agents, the advantage of *in vitro* 3D cell culture is closer simulation of the *in vivo* environment(Edmondson et al., 2014) (Lv et al., 2017).. Previous studies have shown that 2D and 3D cell cultures are very different environments that influence bio-chemical and mechanical cell growth differently. A major difference is that 2D cell cultures interact with substrate on the basal surface only, whereas in 3D cell culture proteins are globally expressed across cell surfaces. Therefore, 2D and 3D cell cultures display very different cell growth in terms of morphology, migration and gene expression(Lv et al., 2017).

A major mechanical difference between 2D and 3D is that 2D cell culture is influenced by substrate rigidity, which is static as substrate consists of plastic or glass. However, in 3D cell culture the substrate is a gel and rigidity of the gel can be experimentally manipulated to achieve a biologically relevant composition. Resultant cell morphology of 2D and 3D cell cultures differ significantly(Lv et al., 2017). Importantly, 2D cell cultures produce cells that are polarised and flattened across the substrate, while 3D cell cultures produce cells that are spherical or highly branched, as would appear in native tissue. The impact of this difference in cellular shape is that 3D cell cultures promote cell-cell interactions that determine cell behaviour, as occur *in vivo*, but 2D cell cultures restrict cellular cross-talk and cannot replicate *in vivo* cell behaviour(Haycock, 2011).

The minimal effort and rapid of testing have influenced 2D cell culture to be a key part of medicinal programs. Monolayer 2D cell cultures are usually associated with flat plastic dishes. The cells are paced on the coated surfaces which let them expand. The response of the cells in 2D culture can be studied in a stable *in vitro* environment (Birla, 2014). One of the main advantages of monolayer cell culture is that the ability to investigate the cause and effect relationships of regulated stimuli without interference of confounding systematic variations *in vivo* systems (Birla, 2014). However, the limitations of 2D cell culture have turned out to be progressively perceived. Due to the profoundly unnatural geometric and mechanical limitations forced on cells, 2D cell cultures does not provide a true representation of native tissue. That is constantly restricted to single cell composes and does not consider the effect of multiple cell populations and the surrounding environment (Edmondson et al., 2014). One of the main concerns with 2D is that they represents pseudo-environment since the flat surface is not

suitable for studying the growth of cells. In the human body these cells are on enclosed surface surrounded by many other cells. With some problems, it can be hard to extrapolate information from 2D *in vitro* investigations and utilize that information to foresee how cells may act in their native tissue settings. Therefore, most current medication testing techniques utilizing 2D cell culture keep on giving unsatisfactorily deceptive and non-prescient information for *in vivo* reactions (Edmondson et al., 2014). Even though the importance 2D cell culture techniques cannot be overstated and they continue to be one of the main tools in many investigation areas, improving these techniques is an essential requirement to overcome their limitations.

3D cell cultures is a response to the flaws revealed in the 2D culture. It is a better modelling system that represents *in vivo* physiological conditions intently.

Appendix. 6

### **Properties of biomaterial**

**Rigidity.** Matrix stiffness or rigidity plays an important role in many cell behaviour such as gene expression , cytoskeletal architecture (Ruedinger et al., 2014). Rigidity of matrix is determined based on the cells type that are embedded in this matrix. For example, to design a biomaterial for peripheral nerve, it should be soft enough to mimic a soft uniaxially aligned lipoprotein myelin sheath that surrounded axons *in vivo*. In contrast, osteoblasts need more rigid surface that mimic bone surface. This factor could be controlled by increase the matrix concentration or mix two different types of matrices to achieve the desired stiffness. Consequently, providing appropriate surface in term of rigidity is preferred for the cells so it will enhance cell attachment beside to other factors (Haycock, 2011)

**Porosity.** Scaffold porosity is one of the fundamental characteristics to build a suitable biomaterial. Porosity provides available space for cells to migrate and proliferate and it also allows to transport nutrients effectively when cells into the scaffold. The optimum porosity is directly related to the tissue and cells type. For example, fibroblast and endothelial cells were investigated in term of growing in different pore sizes of scaffold. It was demonstrated that fibroblasts spread over the closest cells able to fill large pores by using a bridging mechanism, while endothelial cells cannot build bridging system so they prefer a smaller pore size (Haycock, 2011). Domingos et al. demonstrated the same previous results when the effects of pore size on hMSC was investigated. Interestingly, they added that pore topology did not affect the cell morphology (Domingos et al., 2013).

**Surface chemistry.** The surface chemical characteristics of a biomaterial are essential for dictating the cell adhesion and spreading. Charge and polarity usually control the surface chemistry, which then control the diffusion and adsorption of adherence proteins at the surface. There is a relationship between the surface charge and the amount of adsorbed proteins. By then, the tendency of cells to adhere to a biomaterial increase since the cell adhere to an adsorbed protein layer, rather than the biomaterial surface (Haycock, 2011). Biomaterials' surfaces are predominantly modified to promote cell adhesion by chemical modification and surface coatings. Chemical modifications are achieved by addition of several functional groups or change the chemical nature of the material which then result in promote cell adhesion, proliferation, and function. Surface coating of scaffolds could be done by using adhesion proteins leading to better cell-biomaterial interactions (Jammalamadaka and Tappa, 2018). Attachment of Schwann cell to aligned PLA microfibres, as a biomaterial, was enhanced by coating the surface with a plasma acrylic acid layer cell attachment and proliferation increase as the negative surface charge increases. On the contrary, the deposition of allyl amine prevents Schwann cell attachment. Even though both layers give surface charges, adhesion proteins react differently with them result in changing the conformation of the protein. This change determines if the adsorbed protein introduces adhesive ligands on the surface side allowing binding to receptors in cell membrane such as integrins (Murray-Dunning et al., 2011). Also, using RGD has shown significantly improvement in cell adhesion and functionality within matrix. Biomaterials can be functionalized by chemically linking the RGD sequence to the surface. This provides a binding site for cells by linking RGD sequence to the  $\alpha 5 \beta 1$  integrin. Linking (Birla, 2014). There are many different ways to alter the chemical surface of the biomaterial, however, there is no universal technique to use for all type of biomaterial. (Santos et al., 2017)

**Printability.** An important feature of a suitable biomaterial is that it can be accurately and precisely printed and maintains the desired shape. Also, the candidate biomaterial should have the ability to protect cell viability during the printing process. For example, some types of printers involve heating the biomaterial to deposit cells. In this case, using low thermal conductivity material can be preferred to increase cell viability and function after printing (Murphy and Atala, 2014a).

## Appendix. 7

Numbers of viable cells determined by image analysis (n=1), MTT assay and MTS assay. After 24h and 48h incubation period at 37 °C and 5 % CO<sub>2</sub>, an ImageJ software was used to count the number of cells in 4 photos/well, then adjusted to indicate the total number of cells in the well. MTT and MTS assay were applied after 24h and 48h separately. Mean ± standard deviation are shown . The experiment was repeated on three separate occasions (n=3). Data was analysed using a one-way ANOVA with the Tukey-Kramer post-hoc test. There was no significance difference between cell numbers obtained by image analysis, MTT and MTS assay at 24 and 48h for each substrate type ( p > 0.05).

<b>Substrates</b>	<b>Image analysis after 24h</b>	<b>MTT assay After 24h</b>	<b>MTS assay After 24h</b>	<b>Image analysis after 48h</b>	<b>MTT assay After 48h</b>	<b>MTS assay After 48h</b>
<b>CA+ 1% collagen</b>	18521 ± 1943	20722 ± 1570	19610 ± 1246	17100 ± 3132	19281 ± 1899	18270 ± 2503
<b>CA+ 1µg/mL Fibronectin</b>	17920 ± 4307	18650 ± 2419	19178 ± 1679	16230 ± 4414	19390 ± 1045	20040 ± 447
<b>Agarose + 1% collagen</b>	ND	8.83 ± 5.54	0	ND	0 ± 493	0
<b>Agarose + 5% collagen</b>	ND	8.2 ± 6.3	0	ND	0	0 ± 3256
<b>Agarose + 10µg/mL Fibronectin</b>	ND	2.4 ± 2	0	ND	0	0
<b>Agarose + 1µg/mL Fibronectin</b>	ND	6.02 ± 3	0	ND	0	0 ± 2956

## Reference

- A.P. BALGUDE, X. Y., A. SZYMANSKI, R.V. BELLAMKONDA 2001. Agarose gel stiffness determines rate of DRG neurite extension in 3D cultures. *Elsevier Science Ltd.*
- ABE, H. & OIKAWA, T. 1991. Regional differences in the ultrastructural features of secretory cells in the golden hamster (*Mesocricetus auratus*) oviductal epithelium. *Journal of anatomy*, 175, 147.
- AIZAWA, Y., LEIPZIG, N., ZAHIR, T. & SHOICHET, M. 2008. The effect of immobilized platelet derived growth factor AA on neural stem/progenitor cell differentiation on cell-adhesive hydrogels. *Biomaterials*, 29, 4676-4683.
- ALTHOUSE, G. C. & HIXON, J. E. 1999. Use of commercially available ELISAs to help determine estrous status in female swine. *Swine Health and Production*, 7, 65-68.
- ANTONI, D., BURCKEL, H., JOSSET, E. & NOEL, G. 2015. Three-dimensional cell culture: a breakthrough *in vivo*. *International journal of molecular sciences*, 16, 5517-5527.
- ASGHARI SANA, F., CAPKIN YURTSEVER, M., KAYNAK BAYRAK, G., TUNCAY, E. O., KIREMITCI, A. S. & GUMUSDERELIOGLU, M. 2017. Spreading, proliferation and differentiation of human dental pulp stem cells on chitosan scaffolds immobilized with RGD or fibronectin. *Cytotechnology*, 69, 617-630.
- ATTC. 2016. *the essentials of life science research* [Online]. Available: <https://www.atcc.org/Products/All/HTB-161.aspx> [Accessed].
- AU, A. Y., HASENWINKEL, J. M. & FRONDOZA, C. G. 2012. Micropatterned agarose scaffolds covalently modified with collagen for culture of normal and neoplastic hepatocytes. *Journal of biomedical materials research Part A*, 100, 342-352.
- AUSTRALIAN ACADEMY OF SCIENCE. 2016. *Printing the future: 3D bioprinters and their uses* [Online]. Available: <https://www.science.org.au/curious/people-medicine/bioprinting> [Accessed].
- AVELAR-FREITAS, B., ALMEIDA, V. G., PINTO, M. C. X., MOURÃO, F. A. G., MASSENSINI, A. R., MARTINS-FILHO, O. A., ROCHA-VIEIRA, E. & BRITOMELO, G. 2014. Trypan blue exclusion assay by flow cytometry. *Brazilian journal of medical and biological research*, 47, 307-315.
- AVILÉS, M., COY, P. & RIZOS, D. 2015. The oviduct: A key organ for the success of early reproductive events. *Animal Frontiers*, 5, 25-31.
- BENNING, L., GUTZWEILER, L., TRONDLE, K., RIBA, J., ZENGERLE, R., KOLTAY, P., ZIMMERMANN, S., STARK, G. B. & FINKENZELLER, G. 2018. Assessment of hydrogels for bioprinting of endothelial cells. *J Biomed Mater Res A*, 106, 935-947.
- BERRIDGE, M. V., HERST, P. M. & TAN, A. S. 2005. Tetrazolium dyes as tools in cell biology: new insights into their cellular reduction. *Biotechnology annual review*, 11, 127-152.
- BERTASSONI, L. E., CARDOSO, J. C., MANOHARAN, V., CRISTINO, A. L., BHISE, N. S., ARAUJO, W. A., ZORLUTUNA, P., VRANA, N. E., GHAEMMAGHAMI, A. M. & DOKMECI, M. R. 2014. Direct-write bioprinting of cell-laden methacrylated gelatin hydrogels. *Biofabrication*, 6, 024105.
- BESENFELDER, U., HAVLICEK, V. & BREM, G. 2012. Role of the oviduct in early embryo development. *Reproduction in domestic animals*, 47, 156-163.
- BILL & MELINDA GATES FOUNDATION 2018. *healthcare*
- BIRLA, R. 2014. *BIOMATERIALS FOR TISSUE ENGINEERING. Introduction to Tissue Engineering: Applications and Challenges*. John Wiley & Sons, Inc.
- BUHI, W., ALVAREZ, I. & KOUBA, A. 2000. Secreted proteins of the oviduct. *Cells Tissues Organs*, 166, 165-179.

- CASADEVALL, A., MUKHERJEE, J. & SCHARFF, M. D. 1992. Monoclonal antibody based ELISAs for cryptococcal polysaccharide. *Journal of immunological methods*, 154, 27-35.
- CHAKRABARTI, R., KUNDU, S., KUMAR, S. & CHAKRABARTI, R. 2001. Vitamin A as an enzyme that catalyzes the reduction of MTT to formazan by vitamin C. *Journal of Cellular Biochemistry*, 80, 133-138.
- CHANG, H. & SUAREZ, S. S. 2012a. Unexpected flagellar movement patterns and epithelial binding behavior of mouse sperm in the oviduct. *Biol Reprod*, 86, 140, 1-8.
- CHANG, H. & SUAREZ, S. S. 2012b. Unexpected flagellar movement patterns and epithelial binding behavior of mouse sperm in the oviduct. *Biology of reproduction*, 86, 140, 1-8.
- CONNELLY, J., PETRIE, T., GARCÍA, A. & LEVENSTON, M. 2011. Fibronectin-and Collagen-Mimetic Ligands Regulate BMSC Chondrogenesis in 3D Hydrogels. *European cells & materials*, 22, 168.
- CONSERVE ENERGY FUTURE. 2018. *What is overpopulation?* [Online]. Available: <https://www.conserve-energy-future.com/causes-effects-solutions-of-overpopulation.php> [Accessed].
- COOK, J. A. & MITCHELL, J. B. 1989. Viability measurements in mammalian cell systems. *Analytical biochemistry*, 179, 1-7.
- COOKE, M. J., PHILLIPS, S. R., SHAH, D. S. H., ATHEY, D., LAKEY, J. H. & PRZYBORSKI, S. A. 2008. Enhanced cell attachment using a novel cell culture surface presenting functional domains from extracellular matrix proteins. *Cytotechnology*, 56, 71-79.
- COY, P., GARCIA-VÁZQUEZ, F. A., VISCONTI, P. E. & AVILÉS, M. 2012. Roles of the oviduct in mammalian fertilization. *Reproduction*, 144, 649-660.
- CROW, J., AMSO, N. N., LEWIN, J. & SHAW, R. W. 1994. Physiology: Morphology and ultrastructure of Fallopian tube epithelium at different stages of the menstrual cycle and menopause. *Human Reproduction*, 9, 2224-2233.
- DE JONGE, C. 2005. Biological basis for human capacitation. *Human Reproduction Update*, 11, 205-214.
- DIRKSEN, E. R. 1974. Ciliogenesis in the mouse oviduct: A scanning electron microscope study. *The Journal of cell biology*, 62, 899.
- DJAHANBAKHCH, O., SARIDOGAN, E., KERVANCIOGLU, M. E., MAHMOOD, T., LI, L. & GRUDZINSKAS, J. G. 1999. Secretory function of the fallopian tube epithelial cells *in vitro*: A review. *Placenta*, 20, 87-104.
- DOMINGOS, M., INTRANUOVO, F., RUSSO, T., DE SANTIS, R., GLORIA, A., AMBROSIO, L., CIURANA, J. & BARTOLO, P. 2013. The first systematic analysis of 3D rapid prototyped poly ( $\epsilon$ -caprolactone) scaffolds manufactured through BioCell printing: the effect of pore size and geometry on compressive mechanical behaviour and *in vitro* hMSC viability. *Biofabrication*, 5, 045004.
- EDMONDSON, R., BROGLIE, J. J., ADCOCK, A. F. & YANG, L. 2014. Three-dimensional cell culture systems and their applications in drug discovery and cell-based biosensors. *Assay and drug development technologies*, 12, 207-218.
- EVEN-RAM, S. & YAMADA, K. M. 2005. Cell migration in 3D matrix. *Current opinion in cell biology*, 17, 524-532.
- EZZATI, M., DJAHANBAKHCH, O., ARIAN, S. & CARR, B. R. 2014. Tubal transport of gametes and embryos: a review of physiology and pathophysiology. *Journal of assisted reproduction and genetics*, 31, 1337.
- FERRAZ, M. A. M. M., HENNING, H. H. W., STOUT, T. A. E., VOS, P. L. A. M. & GADELLA, B. M. 2016. Designing 3-Dimensional *In Vitro* Oviduct Culture Systems to Study Mammalian Fertilization and Embryo Production. *Annals of Biomedical Engineering*, 45, 1731-1744.



- FORGET, A., BLAESER, A., MIESSMER, F., KOPF, M., CAMPOS, D. F. D., VOELCKER, N. H., BLENCOWE, A., FISCHER, H. & SHASTRI, V. P. 2017. Mechanically Tunable Bioink for 3D Bioprinting of Human Cells. *Adv Healthc Mater*, 6.
- FRANTZ, C., STEWART, K. M. & WEAVER, V. M. 2010. The extracellular matrix at a glance. *J Cell Sci*, 123, 4195-200.
- FRESHNEY, R. I. 2010. Culture of animal cells. . NJ: John Wiley & Sons, Inc.
- GEIGER, B., BERSHADSKY, A., PANKOV, R. & YAMADA, K. M. 2001. Transmembrane crosstalk between the extracellular matrix and the cytoskeleton. *Nature reviews Molecular cell biology*, 2, 793.
- HANSEN, M. B., NIELSEN, S. E. & BERG, K. 1989. Re-examination and further development of a precise and rapid dye method for measuring cell growth/cell kill. *Journal of immunological methods*, 119, 203-210.
- HAYCOCK, J. W. 2011. *3D cell culture methods and protocols*, springer protocols.
- HONG, S., ERGEZEN, E., LEC, R. & BARBEE, K. A. 2006. Real-time analysis of cell–surface adhesive interactions using thickness shear mode resonator. *Biomaterials*, 27, 5813-5820.
- HUANG, K. T., CHEN, Y. H. & WALKER, A. M. 2004. Inaccuracies in MTS assays: major distorting effects of medium, serum albumin, and fatty acids. *Biotechniques*, 37, 406-412.
- HUANG, W., ANVARI, B., TORRES, J. H., LEBARON, R. G. & ATHANASIOU, K. A. 2003. Temporal effects of cell adhesion on mechanical characteristics of the single chondrocyte. *Journal of orthopaedic research*, 21, 88-95.
- HYNES, R. O. 1990. *Fibronectins*.
- JAMMALAMADAKA, U. & TAPPA, K. 2018. Recent Advances in Biomaterials for 3D Printing and Tissue Engineering. *J Funct Biomater*, 9.
- KERVANCIOGLU, M. E., SARIDOGAN, E., AITKEN, R. J. & DJAHANBAKHCH, O. 2000. Importance of sperm-to-epithelial cell contact for the capacitation of human spermatozoa in fallopian tube epithelial cell cocultures. *Fertility and sterility*, 74, 780-784.
- KHALILI, A. A. & AHMAD, M. R. 2015. A Review of Cell Adhesion Studies for Biomedical and Biological Applications. *Int J Mol Sci*, 16, 18149-84.
- KHORUZHENKO, A. 2011. 2D-and 3D-cell culture. *Biopolymers and Cell*, 27, 17-24.
- KOMATSU, M. & FUJITA, H. 1978. Electron-microscopic studies on the development and aging of the oviduct epithelium of mice. *Anatomy and embryology*, 152, 243-259.
- KU, S. H., RYU, J., HONG, S. K., LEE, H. & PARK, C. B. 2010. General functionalization route for cell adhesion on non-wetting surfaces. *Biomaterials*, 31, 2535-2541.
- LEE, J., CUDDIHY, M. J. & KOTOV, N. A. 2008. Three-dimensional cell culture matrices: state of the art. *Tissue Engineering Part B: Reviews*, 14, 61-86.
- LEESE, H. 1988. The formation and function of oviduct fluid. *Journal of reproduction and fertility*, 82, 843-856.
- LEFEBVRE, R., LO, M. C. & SUAREZ, S. S. 1997. Bovine sperm binding to oviductal epithelium involves fucose recognition. *Biology of Reproduction*, 56, 1198-1204.
- LI, J., CHEN, M., FAN, X. & ZHOU, H. 2016a. Recent advances in bioprinting techniques: approaches, applications and future prospects. *Journal of translational medicine*, 14, 271.
- LI, J., CHEN, M., FAN, X. & ZHOU, H. 2016b. Recent advances in bioprinting techniques: approaches, applications and future prospects. *Journal of Translational Medicine*, 14.
- LI, S. & WINUTHAYANON, W. 2017. Oviduct: roles in fertilization and early embryo development. *Journal of Endocrinology*, 232, R1-R26.
- LI, Y. & KILIAN, K. A. 2015. Bridging the gap: from 2D cell culture to 3D microengineered extracellular matrices. *Advanced healthcare materials*, 4, 2780-2796.

- LV, D., HU, Z., LU, L., LU, H. & XU, X. 2017. Three-dimensional cell culture: A powerful tool in tumor research and drug discovery. *Oncology letters*, 14, 6999-7010.
- MAO, Y. & SCHWARZBAUER, J. E. 2005. Fibronectin fibrillogenesis, a cell-mediated matrix assembly process. *Matrix biology*, 24, 389-399.
- MIESSEN, K., SHARBATI, S., EINSPANIER, R. & SCHOEN, J. 2011. Modelling the porcine oviduct epithelium: a polarized *in vitro* system suitable for long-term cultivation. *Theriogenology*, 76, 900-910.
- MURPHY, S. V. & ATALA, A. 2014a. 3D bioprinting of tissues and organs. *Nat Biotechnol*, 32, 773-85.
- MURPHY, S. V. & ATALA, A. 2014b. 3D bioprinting of tissues and organs. *Nature biotechnology*, 32, 773.
- MURRAY-DUNNING, C., MCARTHUR, S. L., SUN, T., MCKEAN, R., RYAN, A. J. & HAYCOCK, J. W. 2011. Three-dimensional alignment of schwann cells using hydrolysable microfiber scaffolds: strategies for peripheral nerve repair. *3D Cell Culture*. Springer.
- NIELSEN, M. S., NYGAARD AXELSEN, L., SORGEN, P. L., VERMA, V., DELMAR, M. & HOLSTEIN-RATHLOU, N. H. 2012. Gap junctions. *Comprehensive Physiology*.
- OKABE, M. 2018. Sperm-egg interaction and fertilization: past, present, and future. *Biology of reproduction*.
- PALMA-VERA, S., EINSPANIER, R. & SCHOEN, J. 2014. Bovine oviductal epithelial cells: long term culture characterization and impact of insulin on cell morphology. *Reproductive biology*, 14, 206-212.
- PATI, F., JANG, J., LEE, J. W. & CHO, D.-W. 2015. Extrusion bioprinting. *Essentials of 3D Biofabrication and Translation*. Elsevier.
- POLLARD, J. W., PLANTE, C., ALLAN KING, W., HANSEN, P. J., BETTERIDGE, K. J. & SUAREZ, S. S. 1991. Fertilizing capacity of bovine sperm may be maintained by binding to oviductal epithelial cells. *Biology of reproduction*, 44, 102-107.
- RISS, T. L. & MORAVEC, R. A. 2004. Use of multiple assay endpoints to investigate the effects of incubation time, dose of toxin, and plating density in cell-based cytotoxicity assays. *Assay and drug development technologies*, 2, 51-62.
- RISS, T. L., MORAVEC, R. A., NILES, A. L., DUELLMAN, S., BENINK, H. A., WORZELLA, T. J. & MINOR, L. 2016. Cell viability assays.
- ROTTMAYER, R., ULBRICH, S. E., KÖLLE, S., PRELLE, K., NEUMUELLER, C., SINOWATZ, F., MEYER, H. H., WOLF, E. & HIENDLEDER, S. 2006. A bovine oviduct epithelial cell suspension culture system suitable for studying embryo-maternal interactions: morphological and functional characterization. *Reproduction*, 132, 637-648.
- RUEDINGER, F., LAVRENTIEVA, A., BLUME, C., PEPELANOVA, I. & SCHEPER, T. 2014. Hydrogels for 3D mammalian cell culture: a starting guide for laboratory practice. *Applied Microbiology and Biotechnology*, 99, 623-636.
- SANTOS, D., VENINA, BRANDALISE, NICHELE, R. & MICHELE, S. 2017. *Engineering of Biomaterials*, Springer International Publishing AG.
- STEWART, C. A. & BEHRINGER, R. R. 2012. Mouse oviduct development. *Mouse Development*. Springer.
- STODDART, M. J. 2011. Cell viability assays: introduction. *Mammalian Cell Viability*. Springer.
- STROBER, W. 2015. Trypan blue exclusion test of cell viability. *Current protocols in immunology*, 111, A3. B. 1-A3. B. 3.
- SUAREZ, S. S. 2016. Mammalian sperm interactions with the female reproductive tract. *Cell and tissue research*, 363, 185-194.
- TASIOPOULOS, C. P., WIDHE, M. & HEDHAMMAR, M. 2018. Recombinant Spider Silk Functionalized with a Motif from Fibronectin Mediates Cell Adhesion and Growth on

- Polymeric Substrates by Entrapping Cells During Self-Assembly. *ACS Appl Mater Interfaces*, 10, 14531-14539.
- TAUBENBERGER, A., CISNEROS, D. A., FRIEDRICH, J., PUECH, P.-H., MULLER, D. J. & FRANZ, C. M. 2007. Revealing early steps of  $\alpha 2\beta 1$  integrin-mediated adhesion to collagen type I by using single-cell force spectroscopy. *Molecular biology of the cell*, 18, 1634-1644.
- THEOCHARIS, A. D., SKANDALIS, S. S., GIALELI, C. & KARAMANOS, N. K. 2016. Extracellular matrix structure. *Adv Drug Deliv Rev*, 97, 4-27.
- TREUTING, P. M., DINTZIS, S. M., LIGGITT, D. & FREVERT, C. W. 2011. *Comparative anatomy and histology: a mouse and human atlas (expert consult)*, Academic Press.
- ULRICH, T. A., JAIN, A., TANNER, K., MACKAY, J. L. & KUMAR, S. 2010. Probing cellular mechanobiology in three-dimensional culture with collagen-agarose matrices. *Biomaterials*, 31, 1875-84.
- VAN MEERLOO, J., KASPERS, G. J. & CLOOS, J. 2011. Cell sensitivity assays: the MTT assay. *Cancer cell culture*. Springer.
- VENTOLA, C. L. 2014. Medical applications for 3D printing: current and projected uses. *Pharmacy and Therapeutics*, 39, 704.
- VISTICA, D. T., SKEHAN, P., SCUDIERO, D., MONKS, A., PITTMAN, A. & BOYD, M. R. 1991. Tetrazolium-based assays for cellular viability: a critical examination of selected parameters affecting formazan production. *Cancer research*, 51, 2515-2520.
- WANG, P., HENNING, S. M. & HEBER, D. 2010. Limitations of MTT and MTS-based assays for measurement of antiproliferative activity of green tea polyphenols. *PLoS one*, 5, e10202.
- WORLD HEALTH ORGANIZATION. 2018. *Family planning/contraception* [Online]. Available: <http://www.who.int/mediacentre/factsheets/fs351/en/> [Accessed].
- YIXUE, S., BIN, C., YUAN, G., CHAOXI, W., LINGMIN, Z., PENG, C., XIAOYING, W. & SHUNQING, T. 2013. Modification of agarose with carboxylation and grafting dopamine for promotion of its cell-adhesiveness. *Carbohydrate Polymers*, 92, 2245-2251.
- YOUNG, F. M., PHUNGTAMDET, W. & SANDERSON, B. J. 2005. Modification of MTT assay conditions to examine the cytotoxic effects of amitraz on the human lymphoblastoid cell line, WIL2NS. *Toxicology in vitro*, 19, 1051-1059.
- ZANINA, N., MORA, L., OTHMANE, A., BÉNARD, M., DUNCAN, A., JOUENNE, T., VAUDRY, D. & SOUIRI, M. 2013. Differences in Caco-2 cell attachment, migration on collagen and fibronectin coated polyelectrolyte surfaces. *Biotechnology and Bioprocess Engineering*, 18, 144-154.
- ZOLLINGER, A. J. & SMITH, M. L. 2017. Fibronectin, the extracellular glue. *Matrix Biology*, 60-61, 27-37.